

The Next Level in Pole Vaulting

A mechanical model based exploration

27-05-2016

Marco M. Reijne

Master of Science Thesis
Faculty of Aerospace Engineering

The Next Level in Pole Vaulting

A mechanical model based exploration

MASTER OF SCIENCE THESIS

For obtaining the degree of Master of Science in Aerospace
Engineering at Delft University of Technology

Marco M. Reijne

27-05-2016



Copyright © Marco M. Reijne
All rights reserved.

DELFT UNIVERSITY OF TECHNOLOGY
DEPARTMENT OF
AEROSPACE STRUCTURES AND MATERIALS

The undersigned hereby certify that they have read and recommend to the Faculty of Aerospace Engineering for acceptance a thesis entitled “**The Next Level in Pole Vaulting**” by **Marco M. Reijne** in partial fulfillment of the requirements for the degree of **Master of Science**.

Dated: 27-05-2016

Head of department:

dr. C. Kassapoglou

Supervisor:

dr.ir. O.K. Bergsma

Reader:

dr.ir. A.L. Schwab

Reader:

dr. D.J.J. Bregman

Summary

This thesis aims to improve pole vaulting performance. For the last twenty years the seasonal maximum height reached by top vaulters is approximately 6.00 [m] which indicates that the current strategies to improve pole vaulting performance have reached their limit. Looking ahead to the Summer Olympics of 2020 in Tokyo, the Dutch decathletes want to improve their pole vaulting performance by approximately 15 [cm] to increase their chance of winning an Olympic medal. As the current strategies have reached their limit, the coach of the top Dutch decathletes and NOC*NSF asked the TU Delft Sports Engineering Institute to identify possibilities from an engineering point of view that can improve pole vaulting performance. This MSc thesis addresses their question through a model based exploration of the pole vault. The exploration is done in three steps. In the first step a literature study is performed that generates a framework for the exploration and identifies two innovations. In the second step a mechanical model is developed that can explore, identify and assess the pole vault motion. In the third step the mechanical model developed in step two is to evaluate two innovations identified in step one.

In the literature study the pole vaulting performance is defined, a benchmark is established, important kinematic parameters are determined, current approaches to improve pole vaulting performance are examined, current models that describe the pole vault motion are compared and innovations that can improve pole vaulting performance are identified. The pole vaulting height can be defined by the maximum height the center of mass of the athlete reaches in a distance of 80 [cm] behind the planting box or by the energy efficiency ratio. These definitions are used to establish a benchmark. Currently the maximum height of the center of mass of the athlete during a vault is approximately 6.00 [m] and efficiency ratios between 0.85-0.92 are achieved. The initial velocity and maximum pole bend are important parameters that determine pole vaulting performance. The current approach aims to increase the initial velocity by reducing the mass of the pole. However, current initial velocity is limited by the arm swing restriction and not the weight of the pole. Another approach tries to improve the pole stiffness and length selection. Also here a limit is reached as the athlete are currently using poles close to these values. Based on the analysis of the important kinematic parameters and the evaluation of the current approaches two new potential innovations are identified. The first innovation reduces the

energy loss when the pole impacts with the planting box by adding a spring to the bottom end of the pole. This innovation has a lot of potential as the spring can also increase the return force of the pole and can be implemented before 2020. The second innovation aims at optimizing the pole vault motion. It is proven by several studies that the pole vaulting performance is highly sensitive to three sets of parameters: system properties, conditions at take-off and the motion coordination of the athlete. No optimization has been done for these three sets combined. Currently athletes use different techniques and motions, which indicates that at least some athletes perform sub-optimal. Hence optimizing the pole vault can significantly increase pole vaulting performance. Both innovations identified in the literature study are evaluated in step three.

The advantages and disadvantages of different models that can predict pole vaulting performance are also discussed in the literature study. The comparison demonstrates that the large deflection of the pole and the moment the athlete applies to the top end of the pole have a significant influence on the pole vault motion and shows how these can be accounted for in the model. These results are used to develop the mechanical model in the next step.

To explore, identify and assess different innovations, a model that describes the entire motion of the pole vault is necessary. The majority of this thesis is dedicated to developing, evaluating and applying this model. To model the motion of the pole vault, many simplifications and assumptions are needed. It is chosen to develop a mechanical model and simplify the pole vault motion into three bodies: a massless pole and a two-segment athlete. The motion is simplified to a two-dimensional motion. The impact of the pole with the take-off box and the pull-up action of the athlete are neglected. Also, the motion during the run-up phase and fly-away phase are simplified using an energetic approach. Finally, the inputs for the mechanical model are chosen to be the physical properties of the athlete and the pole properties, the conditions at take-off and the moments the athlete applies in his joint and to the top end of the pole. The moments the athlete applies are modeled using control torques. The control torque profile is determined from a starting value that prescribed the body orientation of the athlete.

The next step is to derive the equations of motion for the model defined above. The equations of motion for the pole vault are derived using the TMT-method. The complete body position of the athlete and the motion of the top end of the pole can be determined from four state variables. The pole forces and pole deformation are determined using an iterative numerical solution that is based on the elastica solution of a slender pole subjected to a compressive force. This solution can also be used to analyze the stiffness behavior of the pole and determine the internal forces and moments during a vault. The equations of motions are solved numerically using the fourth order Runge-Kutta integration scheme.

The quality of the model is examined by comparing it to results available in literature. The results for trajectory, motion of the athlete, pole forces and energies are in line for magnitude and profile. Finally, the sensitivity of the model is demonstrated by varying the pole stiffness and initial horizontal velocity. The maximum vault height is significantly influenced by tiny variations of both parameters. This makes it difficult to analyze the influence of individual parameters on pole vaulting performance.

The two innovations that were identified in the literature study are evaluated using this

mechanical model. First the innovation of adding a spring to the bottom end of the pole is examined. It is decided to add a spring in series to the pole and aligned with the pole chord axis. Results of the mechanical model demonstrate that the motion of the athlete and pole remain similar to a vault when the athlete uses a regular pole. This indicates that it should be feasible for the top Dutch decathletes to adapt to a pole with a spring in time for the Summer Olympics of 2020 in Tokyo. The increase in pole return force does not seem to have a significant influence on pole vaulting performance, while the reduction in energy loss cannot be determined by the mechanical model. Results of the literature study suggested that the energy loss can be in the order of ten percent and hence significantly influence pole vaulting performance. A critical remark has been placed at these results. The spring compresses one meter and the choice of aligning the spring with the pole chord axis results in a significant different deformation of the pole than that of reality.

The mechanical model developed is also used to examine the second innovation. The sensitivity of the motion coordination on pole vaulting performance is demonstrated and shown to be significant. Tiny adaptations to the athletes technique that can be made before the Summer Olympics of 2020 can already result in a significant increase in pole vaulting performance. Also an optimization formulation is developed. The mechanical model developed can be used for this optimization.

To recapitulate, first a literature study is performed that establishes a benchmark and identifies two innovations that can improve pole vaulting performance. Second, a mechanical model is developed that can be used to evaluate and assess the innovations. And third, the two innovations identified are evaluated using this model. The evaluation of the two innovations shows that both innovations are feasible within the period to the Summer Olympics of 2020 and have the potential to improve pole vaulting performance. The improvement in pole vaulting performance for the pole with spring cannot be determined accurately yet, but the improvement in pole vaulting performance by optimizing the pole vault motion can be significant and in the order of the required 15 [cm].

Acknowledgements

I enjoyed working on this MSc thesis very much. It combined my study with my passion for sports. It was very satisfying to see that all the courses I learned throughout my study (including structural analysis, dynamics and control theory) are all present in this project. This confirmed that my choice for Aerospace Engineering was good choice to accomplish my ambition of working in the field of sports engineering and I am keen to continue in this field after I graduate.

The pole vault motion is very interesting. It is amazing to see how horizontal motion can be transformed so efficiently in height by only using a flexible pole. The heights the athlete can reach are incredible. The interaction between the pole and the athlete offer a range of possible strategies and techniques that cannot be seen in any other athletic event. This project really made me appreciate the beauty and complexity of the sport.

I wish to thank my supervisors Otto Bergsma and Arend Schwab for their weekly support and enthusiasm for my MSc thesis project. I wish to thank Vince de Lange for initiating this project and giving me insight in the pole vault event. I hope this project continues and will help increase the performance of his athletes. Further I wish to thank Minke Remmerswaal, Jan Remmerswaal and Sjoerd Reijne for helping me write my report and proofreading.

Delft, The Netherlands
27-05-2016

Marco M. Reijne

Contents

Summary	V
Acknowledgements	IX
List of Figures	XVIII
List of Tables	XIX
Nomenclature	XXI
1 Introduction	1
2 Research Objective	5
2.1 Literature Study	5
2.2 Model	6
2.3 Model Elaboration of Two Potential Innovations	7
3 Literature Study	9
3.1 Pole Vault Motion	9
3.2 Definition of Pole Vaulting Performance	11
3.3 Current Vaulting Performance	12
3.4 Kinematic Parameters	12
3.5 Current Approach to Improve Pole Vaulting Performance	16
3.5.1 Pole Length and Pole Stiffness	17
3.5.2 Weight Minimization of the Pole	18
3.6 Pole Vault Models	19
3.6.1 Analytical Models	19
3.6.2 Finite Element Models	20
3.7 Potential Innovations to Increase Pole Vaulting Performance	21
3.7.1 Innovation 1	21
3.7.2 Innovation 2	23
3.8 Summary	24

4 Pole Vault Model	25
4.1 Mechanical Model	25
4.2 Choices, Assumptions and Simplifications	27
4.3 Athlete Sub-Model Outline	29
4.3.1 Athlete Body Discretization	29
4.3.2 Muscle Model	32
4.3.3 Schematics of the Athlete	32
4.4 Equations of Motion	34
4.5 Pole Sub-Model	39
4.5.1 Elastica Solution for a Slender Pole under Compression	40
4.5.2 Numerical Iterative Solution for Combined Load	48
4.6 Runge-Kutta	50
4.7 Fly-Away Phase	52
4.8 Summary	53
5 Pole Stiffness and Internal Forces	55
5.1 Along the Chord Stiffness	55
5.2 Bending Stiffness	57
5.3 Envelope of Maximum Internal Forces and Moments	58
5.4 Summary	60
6 Validation	61
6.1 Illustrative Example	61
6.2 Inputs	62
6.2.1 System Properties, Initial Conditions	62
6.2.2 Motion Coordination of the Athlete	63
6.3 Comparison with Literature	66
6.3.1 Motion of the Athlete and Pole, Trajectory and Peak Height	67
6.3.2 Pole Forces	69
6.3.3 Energy Transformations	70
6.4 Sensitivity of the Model	73
6.5 Summary	75
7 Innovation 1: A Pole with a Spring	77
7.1 Deformation of the Pole with Spring	77
7.2 Inputs of the Mechanical Model	80
7.3 Influence on Pole Vaulting Performance	81
7.3.1 Motion of the Athlete and Pole, Trajectory and Peak Height	82
7.3.2 Pole Forces	84
7.3.3 Energy Transformations	85
7.4 Implementation	87
7.5 Summary	87

8 Innovation 2: Optimization of the Pole Vault Motion	89
8.1 Motion Coordination of the Athlete	89
8.2 Sensitivity	90
8.3 Optimization	91
8.4 Summary	94
9 Conclusions and Recommendations	95
References	99
References	99
A Convective Acceleration	101
B Trigonometry	103
C Elastica Shapes	105
D MATLAB Script	107
E Small Angle Theorem Solutions for Pole Forces	109
F Reversed Inputs Pole Sub-Model	115
G Inertia Properties of the Athlete	119
H Maximum Internal Stress	123
I Inputs for Spring Added to Pole Results	125

List of Figures

1.1	Timeline of world record height in the men’s pole vault event (IAAF website).	2
1.2	Timeline of season’s best performance in the men’s pole vault event (IAAF website).	2
3.1	A jump of Eelco Sint-Nicolaas, filmed at a training at the 18th of November 2013 (Abram et al., 2013). Position 1 is during the run-up phase, position 2 is at take-off, position 3 is during pole bending phase, position 4 is the start of the pole straightening phase, position 5 is at the time of pole release, position 6 is during the fly-away phase and position 7 is when the athlete falls back to the landing cushion.	10
3.2	Mechanical energy transformations of the pole vault (Arampatzis et al., 2004). Take-off phase is from 0 sec to dashed line A. Bending phase is from dashed line A to dashed line B. Straightening phase is from dashed line B to dashed line C. Free flight phase is from dashed line C onwards. The total mechanical energy of the athlete $E_{athlete}$ consists out of the potential energy, translational kinetic energy, rotational kinetic energy and the work done by the athlete. $E_{kin,athl.}$ is the translational kinetic energy of the athlete and hence a fraction of the total mechanical energy of the athlete as well. The fractions E_{pole1} and E_{pole2} should be neglected. They represent the pole strain energy components of bending and axial displacement. Arampatzis uses an unconventional definition and we believe the components cannot be viewed as such. However, the total pole strain energy E_{pole} is correct.	14
3.3	Three force components of the pole force during a vault measured using a force plate fixed under the planting box. The forces shown are opposite to those measured by the force plate. The x -axis is aligned with the direction of the run-way (positive axis moving away from the planting box), the z -axis is the vertical axis (positive pointing upwards) and y -axis complies with the right hand rule. The origin is defined at the back of the planting box. (Morlier & Cid, 1996)	22
3.4	Transversal moment component of the moment applied to the top end of the pole by the athlete during a vault. The results are shown for seven different athletes. The time starts right after the take-off phase and ends when the athlete releases the pole. (Morlier & Mesnard, 2007).	24

4.1	Schematic diagram of the pole vault	26
4.2	The four important body orientations during the pole support phase. (a) take-off position, (b) rock-back position, (c) inverted position, (d) fly-away position.	30
4.3	Schematic diagram of the athlete	33
4.4	Schematic diagram of the pole	39
4.5	Schematic of a slender subjected to a compressive load	41
4.6	Definition of ϕ	42
4.7	Schematic diagram of the pole and fictitious pole	49
5.1	The normal force component R_n versus the chord shortening percentage δ/L a range of values of the input variables M and l	56
5.2	The normalized applied moment versus the angle between the pole tangent at the top end and pole chord for various values of the normal force component N	57
5.3	Maximum internal normal and tangential force during a vault along the pole length.	59
5.4	Maximum internal moment during a vault along the pole length.	59
6.1	The orientation angle ϕ of the first segment of the athlete and the orientation angle θ of the second segment of the athlete during a vault. The time is defined from take-off until pole release.	64
6.2	The control torques M_1 (wrists) and M_2 (shoulder) during a vault for an illustrative example (system properties of table 6.1 and initial conditions of table 6.2) and prescribed motion of a two segment athlete (figure 6.1). The time is defined from take-off until pole release.	66
6.3	The final control torques M_1 (wrists) and M_2 (shoulder) during a vault for an illustrative example (system properties of table 6.1 and initial conditions of table 6.2) that resulted in a realistic vault for the mechanical model of a massless pole and two segment athlete. The time is defined from take-off until pole release.	67
6.4	Diagram showing the deformation of the pole, body orientation of the two segment athlete and the velocity vector of the total center of mass of the athlete for every time interval of 0.2 [s] starting from take-off until pole release. The final position is shown as well. The trajectory of the total center of mass of the athlete is shown for every time increment of 0.02 [s]. The grey area indicates the area in which the cross bar can be placed. The results are for the system properties of table 6.1, initial conditions of table 6.2 and torque control profile shown in figure 6.3.	68
6.5	The horizontal ground reaction force component F_x and the vertical ground reaction force component F_y . The continuous lines are the forces predicted by the mechanical model. The dashed lines are the average forces measured during the experiments of Arampatzis et al. (2004), Morlier and Mesnard (2007) and Schade et al. (2006). The forces are the ground reaction forces and thus have the opposite direction of the forces acting on the bottom end of the spring. The forces predicted by the mechanical model start after 0.1 [s] as the mechanical model does not take into account the impact process of the pole with the planting box.	69
6.6	Schematic diagram of pole with angle definitions.	71

6.7	The mechanical energy transformation of the pole vault during the pole support phase. The continuous lines are the mechanical energies predicted by the mechanical model. The dashed lines are the energies predicted by Arampatzis et al. (2004). The potential energy E_{pot} and kinetic energy E_{kin} are both of the athlete only and are also a fraction of the total mechanical energy of the athlete. E_{pole} is the pole strain energy. The total mechanical energy of the athlete $E_{tot,ath}$ consists out of the potential energy, translational kinetic energy, rotational kinetic energy and work done by the athlete.	72
6.8	Sensitivity of the trajectory of the athlete to variations in pole stiffness. (a) $B = 2222$ [Nm ²], (b) $B = 2522$ [Nm ²], (c) $B = 2822$ [Nm ²].	74
6.9	Sensitivity of the trajectory of the athlete to variations in initial horizontal velocity. (a) $v_x = 7.7$ [m/s], (b) $v_x = 8.7$ [m/s], (c) $v_x = 9.7$ [m/s].	76
7.1	Schematic diagram of pole with a spring at its bottom end.	78
7.2	Diagram showing the deformation of the pole with a spring, body orientation of the two segment athlete and the velocity vector of the total center of mass of the athlete for every time interval of 0.2 [s] starting from take-off until pole release. The final position is shown as well. The trajectory of the total center of mass of the athlete is shown for every time increment of 0.02 [s]. The spring is visualized at the bottom end of the pole. The grey area indicates the area in which the cross bar can be placed. The results are for the system properties of table 6.1, initial conditions of table 6.2 and torque control profile shown in figure 6.3.	80
7.3	Diagram showing the deformation of the pole with a spring, body orientation of the two segment athlete and the velocity vector of the total center of mass of the athlete for every time interval of 0.2 [s] starting from take-off until pole release. The final position is shown as well. The trajectory of the total center of mass of the athlete is shown for every time increment of 0.02 [s]. The grey area indicates the area in which the cross bar can be placed. The results are for the system properties of table 7.1, initial conditions of table 7.2 and torque control profile shown in figure 6.3.	82
7.4	Diagram showing the deformation of the pole where a spring is added to the length ($L = 5.47$ [m]), body orientation of the two segment athlete and the velocity vector of the total center of mass of the athlete for every time interval of 0.2 [s] starting from take-off until pole release. The final position is shown as well. The trajectory of the total center of mass of the athlete is shown for every time increment of 0.02 [s]. The grey area indicates the area in which the cross bar can be placed. The results are for the system properties of table 6.1, initial conditions of table 6.2 and torque control profile shown in figure 6.3.	83
7.5	The horizontal F_x and vertical F_y ground reaction force component of the pole with a spring inserted and with a spring added to the pole length. The values for the pole with spring are compared to the results of the regular pole presented in chapter 6.	84
7.6	The different mechanical energies of the athlete and the pole. The values estimated by the model are compared to the energy transformations for the regular pole presented in chapter 6.	85
7.7	Work done by the wrists M_1 and hips M_2 during the vault for a pole with a spring inserted.	86
8.1	Work done by wrist M_1 and hips M_2 during the vault of the illustrative example.	90

8.2	Trajectory of the pole vault for the control torques shown in figure 8.3.	92
8.3	The control torques M_1 (wrists) and M_2 (shoulder) for the vault shown in figure 8.2.	92
8.4	Trajectory of the pole vault for the control torques shown in figure 8.5.	93
8.5	The control torques M_1 (wrists) and M_2 (shoulder) for the vault shown in figure 8.4.	93
C.0	Various deformed shapes of the pole for huge deflections.	106
E.1	Schematic diagram of a simply supported beam subjected to a compressive force and an applied moment at one end.	109
F.1	Schematic diagram of the pole	115
G.1	Tin man	120
I.1	The control torques M_1 (wrists) and M_2 (shoulder) during a vault for the results of a vault using a pole to which a spring is added that resulted in a realistic vault for the mechanical model of a massless pole and two-segment athlete. The time is defined from take-off until pole release.	126

List of Tables

6.1	Athlete and Pole Properties	62
6.2	Initial Conditions	63
7.1	Athlete and Pole Properties	81
7.2	Initial Conditions	81
G.1	Athlete Anthropomorphic Measurements (Moore, 2009)	121
G.2	Body Mass and Segment Mass (Moore, 2009)	121
I.1	Athlete and Pole Properties	125
I.2	Initial Conditions	125

Nomenclature

Latin Symbols

β	angle pole top end tangent relative to orientation of the arms segment
η	angle fictitious pole chord relative to horizontal
γ	slope of the pole tangent at origin relative to R -direction
λ	angle pole chord relative to horizontal
λ	ratio between compressive force and Euler buckling load
ω_1	angular velocity first segment
ω_2	angular velocity second segment
ϕ	amplitude elliptic integral
ϕ	arm angle relative to vertical
σ	direct stress
\mathbf{f}	force vector
\mathbf{g}	state transformation vector
\mathbf{M}	convective acceleration vector
\mathbf{M}	mass matrix
\mathbf{q}	generalized independent coordinates state vector
\mathbf{T}	kinematic transformation matrix
\mathbf{x}	state vector
θ	angle x' -axis relative to line tangent to central line of pole at cross-section
θ	torso angle relative to the arms
B	bending stiffness of the pole
d	diameter of the pole vaulting pole

E	Young's modulus
E	elliptic integral of the second kind
E_{kin}	translational kinetic energy
E_{pole}	pole strain energy
E_{pot}	potential energy
E_{rot}	rotational kinetic energy
$E_{tot,ath}$	total mechanical energy of the athlete
F	axial force on spring
h	height
h	step size
I_1	mass moment of inertia of the first segment of athlete
I_2	mass moment of inertia of the second segment of athlete
K	elliptic integral of the first kind
K	spring stiffness
k	modulus of elliptic integral
L	total pole length
l	compressed chord length
l_1	distance from center of mass first segment to hands
l_2	distance from the center of mass first segment to shoulder
l_3	distance from the shoulders to the center of mass of the second segment
$l_{0,spring}$	uncompressed length spring
l_{spring}	compressed length spring
M	applied end moment
m	mass of the athlete
M'	internal moment
M_1	applied moment at the top end of the pole applied by athlete
m_1	mass of the first segment of athlete
M_2	joint moment at the shoulder applied by athlete
m_2	mass of the second segment of athlete
N	internal normal force
R	compressive pole force
R_n	normal component of pole compressive force aligned with the chord axis
R_t	tangential component of the pole compressive force perpendicular to the chord axis
s	arclength measured from origin at bottom end pole
T	internal tangential force
t	thickness of the pole vaulting pole cross section
t	time
v_x	horizontal velocity

v_y	vertical velocity
W_1	work done by the wrists of the athlete
W_2	work done by the shoulder of the athlete
x', y'	local position coordinates fictitious pole
X, Y	global position coordinates
x, y	local position coordinates for the pole
X_{cm1}, Y_{cm1}	position coordinates of the center of mass of the first segment representing the arms
X_{cm2}, Y_{cm2}	position coordinates of the center of mass of the second segment representing the torso, head and legs
X_{top}, Y_{top}	position coordinates of the top end of the pole

Chapter 1

Introduction

Sergey Bubka broke the world record 35 times before he retired in 1994.¹ In the twenty years since no athlete has come close to his final world-record of 6.14 [m]. Still, this did not stop the French athlete Renaud Lavillenie from trying.² On the evening of February 15th 2014 he set the bar at a height of 6.16 [m]. His attempt that evening was even more special because Sergey Bubka himself was present in the stadium that night. Bubka did not seem to be worried about Lavillenie's attempt to take his world record and he seemed to have no reason to. Lavillenie needed already all three tries to clear the height of 6.01 [m].³ Bubka looked down relaxed to watch the attempt of Lavillenie.

Meanwhile Lavillenie focused on his jump. He rocked forwards and backwards to visualize the jump and get into the right rhythm. He held the pole upright, his body still relaxed. When he found the right rhythm, he straightened his back and launched himself forwards. He accelerated along the track and at the end of the run-up lowered the pole and dropped it into the take-off box. In the same movement he pushed the top end of the pole upward and away from his body. Just before the pole hits the back of the box, Lavillenie jumped upward. The pole started to bend under Lavillenie's momentum. Lavillenie rotated his body into a vertical upside down position, still close to the ground. His movements seemed to slow down. He seemed to stop.

Right at this moment the pole reached its maximum bending point and starts to straighten again. Lavillenie flew upwards and accelerated again. When the pole straightened, he pushed of the pole to gain maximum acceleration. After he released the pole, he again

¹Indoor and outdoor combined.

²A vault of Lavillenie is shown on the front cover (retrieved from: <http://www.diamondleague.com/fr/galleries/photos/2015>).

³An athlete can choose the height he wants to start with. He gets three attempts to clear this height. When he clears this height he again gets three attempts to clear a higher height. An athlete is finished after three consecutive misses. The maximum height the athlete successfully completed counts as his score. An athlete can also choose to pass a height after an unsuccessful jump and continue to a higher height. For example, if an athlete fails a height at the first attempt he can continue to a higher height. However, he will only have two tries at this height as otherwise he would have three consecutive misses and is finished.

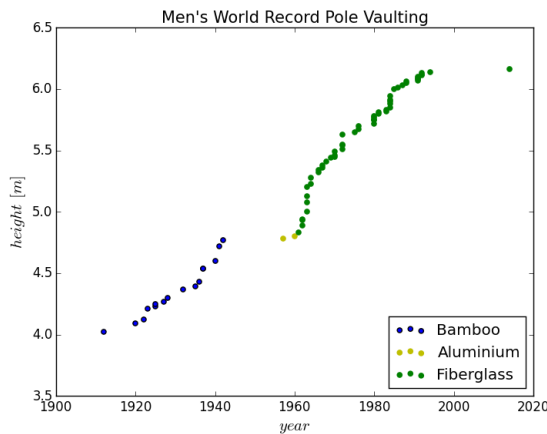


Figure 1.1: Timeline of world record height in the men's pole vault event (IAAF website).

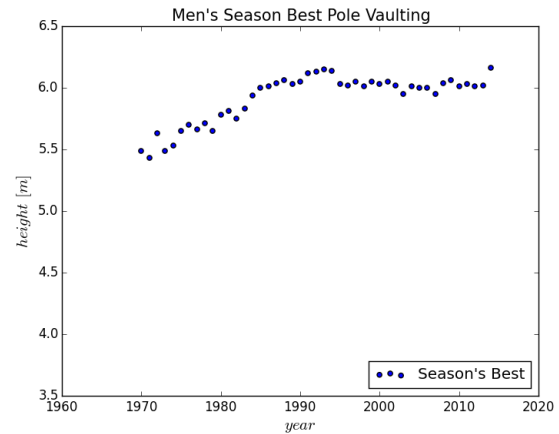


Figure 1.2: Timeline of season's best performance in the men's pole vault event (IAAF website).

seemed to slow down. The bar was close by. In his final movements he curled himself over the bar.

He had reached his point of maximum height and when he fell back to the landing cushion he looked up at the bar. It was still in place, resting at the 6.16 [m] Lavillenie just passed. He had done it. He had broken the 20 year old world record.

Although this is one of the greatest vaults in history, it is also one of the few top vaults of the last two decades. Since the introduction in the 1960's of glass-fibre composite poles, rapid improvements in vault heights have been achieved. The improvements accumulated in the world record height of 6.14 [m] in 1994 set by Sergey Bubka as is shown in figure 1.1 (retrieved from the website of the International Association of Athletics Federations (IAAF): <http://www.iaaf.org>). Figure 1.2 shows that after 1994 season's best performances have been for years significantly lower, the only exception being February 2014 when Lavillenie improved the world record to a height of 6.16 [m] (IAAF website).

The figures suggest that current pole vaulting performance has reached a limit. It is interesting to examine whether this limit is also the theoretical limit of the pole vault or whether further improvements are possible. A theoretical limit can be derived using an energetic approach. Consider the following scenario. An athlete has a mass of 72 [kg], takes off at 10 [m/s] with his center of gravity 1 [m] above the ground and he adds a further twenty percent to the energy input of the vault by muscular work (either bending the pole or by the motion coordination of his body).⁴ With these values, the energy the athlete puts into the system is approximately 5000 [J]. The theoretical maximum height the athlete can reach is when all this energy is converted into potential energy. The theoretical maximum the athlete can then reach is 8.3 [m]. The current world record in pole vaulting is still 2 [m] short of this. This simple analysis thus shows that further improvements in pole vaulting performance are possible.

The Netherlands currently have several world-class decathletes whose ambition it is to win

⁴Values are based on results of experimental research studies.

an Olympic medal. In preparation for the Summer Olympic Games of 2016 in Rio and 2020 in Tokyo, the coach of the Dutch top decathletes concluded that Eelco Sint-Nicolaas should increase his score with approximately 500 points in order to win an Olympic medal (on a total score of 8000). His conclusion is based on the results of the last Olympic Games of 2012 in London and the last IAAF world championship.

As proven, improvements in pole vaulting performance are still possible. This is especially the case for decathletes whose personal records in pole vaulting are in general lower than those of the specialized top vaulters. Eelco Sint-Nicolaas his personal record is for example 5.45 [m]. If the 500 point he should gain in order to win an Olympic medal are equally divided over the ten events of the decathlon, his pole vaulting score should increase with 50 points. Based on his result in the pole vault event at the Summer Olympics of 2012 this means an increase of approximately 15 [cm].⁵

Extra points can be gained by increasing the strength of the decathlete or improving his technique. Part of these extra points can also be acquired with innovations through engineering. For example, engineering innovations can improve the training feedback for the athlete. By improving his training feedback, he can train more efficient. Or a tool can be developed that can analyze the optimum technique for the athlete. The results might indicate that the athlete has a different (non-optimal) technique and the athlete can then adapt his technique on specific points to improve his pole vaulting performance. Or the pole can be improved such that the athlete can vault higher. These are just three examples.

The top decathletes already trained their strength and technique for many years and are already close to the limits of the athlete. Marginal improvements are expected for these. The examples given demonstrate that a larger increase in pole vaulting height can be accomplished by engineering innovations. Therefore, the TU Delft Sports Engineering Institute was contacted last year by the coach of the top Dutch decathletes and the Dutch Olympic Committee*Dutch Sports Federation (NOC*NSF). Their question was to identify what possibilities there are from an engineering point of view to improve the pole vaulting performance of the top Dutch decathletes for the Tokyo Summer Olympics of 2020. This MSc thesis addresses this question through a model based exploration of the pole vault

This MSc thesis report describes the process and the results of this model based exploration. In chapter 2 the research objective and questions are defined. The research is done in three steps. The first step is to perform a literature study. The results are presented in chapter 3. The literature study generates an overview of current pole vaulting performance, an overview of current design practice to improve pole vaulting performance and an overview of models that evaluate pole vaulting performance. The literature study also identifies two engineering innovations that can improve pole vaulting performance. The second step is to develop a model of the pole vault that can explore, identify and assess innovations. The choices, assumptions and simplifications made are presented in chapter 4, as well as the detailed derivations of the equations that describe the pole vault motion. The stiffness behavior of the pole and the internal forces and moments are determined in chapter 5. The quality of the model is discussed in chapter 6. The third

⁵The score grading of the decathlon for the pole vault event is: $\text{points} = 0.2979(h - 100)^{1.35}$ where h is the vault height in centimeters.

step is to evaluate the two engineering innovations identified by the literature study. The results are shown in the chapters 7 and 8. Finally, the conclusions and recommendations for future work are given on how the pole vault can best be improved.

Research Objective

Last year the coach of the top Dutch decathletes and the Dutch Olympic Committee*Dutch Sports Federation (NOC*NSF) contacted the TU Delft Sports Engineering Institute with the question to identify what possibilities there are from an engineering point of view to improve the pole vaulting performance of the top Dutch decathletes for the Tokyo Summer Olympics of 2020. They gave no direct focus or direction on how the improvement in performance should be achieved.

There exist numerous solutions to improve pole vaulting performance. Not all these solutions can be developed and applied in time for the Olympic Games of 2020 in Tokyo. It is therefore important to identify the solutions that have the most potential, such that the increase in vaulting performance is maximized. This MSc thesis therefore serves as an exploratory research and addresses the following research question:

What are the most promising engineering innovations that can improve the pole vaulting performance of the top Dutch decathletes at the Tokyo Summer Olympics of 2020?

The research question is answered in three steps. The first step consist out of a literature study and is presented in chapter 3. The literature study is performed to identify engineering innovations that can improve pole vaulting performance. The second step is to develop a model for the pole vault that can explore, identify and assess engineering innovations and is discussed in chapter 4 and chapter 6. The third step is use the model developed in step two to evaluate the engineering innovations found in step one and are discussed in chapters 7 and 8. The results of the third step will be used to answer the main research question.

2.1 Literature Study

A literature study is chosen as it is a tool to obtain a broad view of the main published work concerning pole vaulting and achieve insight what is currently the state-of-the-art technology. From literature, the current pole vaulting performance can be established.

This is required as a benchmark to evaluate the engineering innovations. The literature can also identify important parameters for pole vaulting performance and compare models that describe the pole vault motion. The important parameters can then again be used to identify innovations on how pole vaulting performance can be increased.

To recap, the literature study answers the following sub-questions:

- 1.1 What is pole vaulting performance and what determines pole vaulting performance?
- 1.2 What models have already been developed that describe the pole vault motion? What is the quality of these models? And what are the advantages and disadvantages of these models?
- 1.3 What is the current pole vault performance and is the current approach to improve pole vaulting performance?
- 1.4 What engineering innovations can improve pole vaulting performance?

2.2 Model

The second step is to develop a model that can be used to explore, identify and assess innovations for the pole vault. In order to assess the potential of an innovation, not only the increase in pole vaulting performance has to be estimated but also the feasibility of the innovation. The feasibility is a difficult aspect to evaluate. In order to do this accurately the complete motion of the pole vault has to be described. The complete motion is required as not only the maximum height (final conditions) of the vault is important but also the trajectory the athlete follows and his motion coordination during the vault. Along the complete trajectory the forces and movements of the athlete should remain within bounds. If the bounds are exceeded the vault is no longer feasible. For example, the pole forces may never exceed the maximum force the pole can sustain during the complete vault. Otherwise, the pole would break during the vault and the athlete will not reach the height predicted if only the final conditions are considered. Or in order to reach the maximum height the athlete should perform a somersault in one tenth of a second. He will not be able to do this and hence in reality not reach the predicted final height. Or the athlete has to deliver superhuman power (somewhere during the vault) in order to reach the maximum height. Again he will not be able to do this in reality. These examples illustrate that the complete motion is needed in order to evaluate that none of the bounds are violated and the new technological innovation is feasible.

Therefore, the second step is to develop a mechanical model that can predict the complete motions and forces of the pole vault. The pole vault is defined as the process that includes the motion of the athlete and the motion of the pole from the time when the athlete starts to run until the athlete falls on the landing mat. The results of the literature study carried out in the first step show different models that can predict the pole vault motion. These results are used to develop the model.

The motions of the pole vault consist out of the motions of the athlete and the motions of the pole. The equations of motions have to be derived for both type of motions. The

motions are related to the forces acting on the system. Therefore, the forces acting on the system also need to be identified. The external forces acting on the system are defined as control inputs and values need to be supplied for these. The internal forces are a result of the motion and external forces. The equations to determine these internal forces need to be derived as well. Also, the quality of the model has to be determined. Issues such as accuracy, sensitivity and applicability are important to understand how the models works and what conclusions and recommendations can be made based on the results of this model.

To recap, the following sub-questions have to be answered in the second step to develop a model that can be used to explore, identify and asses innovations for the pole vault:

- 2.1 What is the motion of the athlete during a vault? How can this be modeled?
- 2.2 What is the motion and deformation of the pole during a vault? How can this be modeled?
- 2.3 What are the control inputs for the athlete-pole system? How can this be modeled?
- 2.4 Which forces act on the system, and how can we calculate them?
- 2.5 How do the results compare with literature?
- 2.6 What is the robustness of the model?

2.3 Model Elaboration of Two Potential Innovations

The third step is to use the model developed in step two to evaluate the engineering innovations found in step one. In hindsight, the literature study performed in step one identified two engineering innovations to be the most promising. Only these two innovations will be explored and assessed. However, the model has been developed to relatively easily evaluate other options as well.

The promising innovations resulting from the literature study is adding a spring to the bottom end of the pole and optimization of the motion coordination of the athlete. The reasoning for this will be given in chapter 3.

In chapter 7 it is explained how the model developed in step two can be used to evaluate the innovation of adding a spring to the bottom end of the pole. The motions of the athlete and pole, the peak height, the trajectory, the forces and the energy transformations for a vault with such a pole are compared to a vault with a regular pole.

In chapter 8 it is explained how the model developed in step two can be used to optimize the motion of the pole vault. The parameters that need to be optimized are determined and an approach is given how the pole vault motion can be optimized. Also an estimation is given on how much the pole vaulting performance can be improved with this optimization.

To summarize, the sub-questions to be answered in step three are:

- 3.1 How can the model be used to describe the motion of a pole with a spring?

- 3.2 What is the deformation of such a pole during a vault?
- 3.3 What is the motion of the athlete during a vault?
- 3.4 What is the pole vaulting performance when using a pole with a spring? How does it compare with the regular pole?
- 3.5 What parameters need to be optimized? What are the sensitivities of these parameters with respect to pole vaulting performance?
- 3.6 How can the pole vault motion be optimized?
- 3.7 What is the improvement in pole vaulting performance?

Chapter 3

Literature Study

In this chapter the results of the literature study are presented. In order to analyze the pole vault, it is important to know what the pole vault motion looks like and how the different motions, phases and characteristics are called. With this information, it is not only easier to understand the pole vault motion but also easier to understand the literature on pole vaulting and the choices made for the model that will be developed in step two. Therefore the first section will describe the different pole vault motions and phases. In the next section two definitions for pole vaulting performance are given. This is followed by a section that identifies the most important kinematic parameters that determine pole vaulting performance. In the following section these parameters will be linked to the current vault performance and current approach to improve vault performance. It will be shown that innovation is necessary to further improve pole vaulting performance. In the last section relevant new research areas and engineering innovations will be presented that have the potential to improve pole vaulting performance. At the end of the chapter a recap is given of the results.

3.1 Pole Vault Motion

A description of the motion of the pole vault is given by [Frère et al. \(2010\)](#). The pole vault motion is shown in figure 3.1. The study of [Frère et al. \(2010\)](#) divides the pole vault in four phases. In the first phase the athlete runs towards the pole take-off box carrying the pole indicated with position one in figure 3.1. The second phase is occurs between the positions two and three in figure 3.1 and is a short phase. It starts just before the athlete jumps up and drops the pole into the take-off box. Simultaneously, he pushes the top end of the pole up, such that his arms are stretched. When the pole hits the back of the take-off box, the athlete jumps up. To initiate bending the upper arm pulls and the lower arm pushes (equivalent to an applied moment) on the pole. This ends the second phase, also called the take-off phase. Due to the impact and the moment applied by the athlete the pole starts to bend. The kinetic energy of the athlete is converted into pole strain energy. This starts the bending phase and takes place between position three and

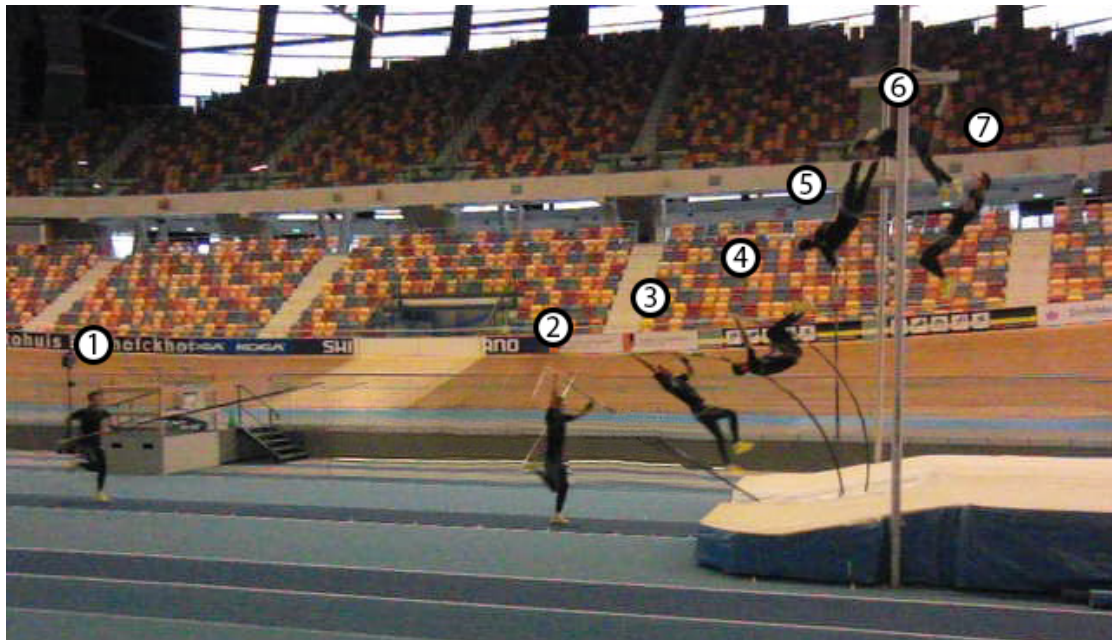


Figure 3.1: A jump of Eelco Sint-Nicolaas, filmed at a training at the 18th of November 2013 (Abram et al., 2013). Position 1 is during the run-up phase, position 2 is at take-off, position 3 is during pole bending phase, position 4 is the start of the pole straightening phase, position 5 is at the time of pole release, position 6 is during the fly-away phase and position 7 is when the athlete falls back to the landing cushion.

four. The bending phase ends at the time of maximum pole bend. During this phase the athlete rotates around his shoulder until his torso is horizontal. Just before maximum pole bend the legs are rotated upwards around the hips. In the next phase the pole starts to straighten again and happens between position four and five. The athlete quickly pulls himself up such that his body is in an upside down vertical position. Now, the pole returns the stored strain energy back to the athlete. As the athlete is in a vertical upside down position and has rotated the pole to vertical, the strain energy is almost completely converted into potential energy and vertical kinetic energy. The athlete only has to retain a small amount of horizontal kinetic energy to cross the bar. The pole bending and straightening phase combined is defined as phase three. Phase three is also defined as the pole support phase. Finally, the athlete releases the pole and continues in a parabolic trajectory over the bar as is illustrated by position five to seven. This fourth phase and is called the free flight phase or fly-away phase.

The different phases can also be identified by the different body positions of the athlete. After the run-up, the athlete moves through four body positions before he crosses the bar. First, after take-off, the athlete keeps his body in a straight line until his body is aligned with the pole chord (straight line connecting the two ends of the pole) and is shown by position three in figure 3.1. The second body position is called the rock-back position and is marked in figure 3.1 with the number four. The athlete is in this body position at approximately the time of maximum pole bend. The legs are pulled up and the back of the athlete is parallel to the ground. The third body position that can be identified is at pole release and is pointed out with number five. The athlete has his body again

almost in a straight line. His arms still point downwards while the rest of his body is in an inverted position. The fourth body position occurs when the athlete crosses the bar, referred to with number six. He has curled his body in an inverted U-shape facing downwards. In this position the center of mass of the athlete can pass underneath the cross bar while the body of the athlete passes over the cross bar. This maximizes pole vaulting performance.

The different phases and body positions are used throughout the rest of the report.

3.2 Definition of Pole Vaulting Performance

The simplest definition of pole vaulting performance is the maximum height the athlete achieves. However, this definition is ambiguous as the reference point for which the maximum height is measured is not defined. For example it is not defined if the maximum height is measured for the feet or for the arms. Usually, the location of the center of mass of the athlete is used. This is a better definition of pole vaulting performance but still has some limitations that have to be considered. First, as discussed above, the athlete curls his body over the cross bar such that his center of mass actually passes below the cross-bar. His vaulting height is thus higher than measured. However, if the off-set is consistently the same for each jump it can be easily corrected for. Second, if only the height of the center of mass is measured the body position of the athlete when he crosses the bar is not known. The height of for example the feet might be lower, hence the cross-bar should be placed lower. The pole vaulting performance will then be lower than determined for the location of the center of mass.

It is also important to not only measure the maximum height of the center of mass but also the horizontal location at which the maximum height is reached. The cross-bar can only be placed between any point directly above the back end of the planting box to a point 80 [cm] in the direction of the landing area (IAAF website). The athlete should thus reach his maximum height somewhere between these two points.

Another way to define the pole vaulting performance of an athlete is to determine the ratio between the height he reaches at the cross-bar and the theoretical maximum height he could have achieved (Ekevad & Lundberg, 1995, 1997). The ratio shows the efficiency of the vault and gives an indication of how much the athlete can improve his vault. It compensates for the difference in physique and style between athletes.

The efficiency ratio is defined using an energetic approach and is the ratio between the maximum potential energy of the athlete (equivalent to maximum height of his center of gravity) and the total energy the athlete has put into the system. The ratio shows how much of the energy put into the system is converted into potential energy. The ratio will never be equal to one, as the athlete has to keep some kinetic energy in order to cross the bar. The athlete with the highest ratio has made the best use of the energy he has put into the system. It can be considered he has maximized his performance given his potential. This is another definition that can be used to determine pole vaulting performance.

The drawback of efficiency ratio is that it does not give direct information on the height the athlete reaches at the cross-bar. The athlete with the highest energy efficiency does

not necessarily win the competition. He might even become last. However, if this is the case, the ratio does show that he should then focus on increasing his energy input.¹

For the exploratory research the athlete physique is kept constant. It is therefore preferred to assess the pole vaulting performance directly with vault height. In this report it was therefore chosen to use the following definition to assess pole vaulting performance: the maximum height of the center of mass of the athlete between the point placed directly above the back end of the planting box and the point 80 [cm] in the direction of the landing area. Furthermore the body position at pole release is checked to make sure the athlete can maneuver to an inverted u-shape to cross the bar and all his body parts can cross the bar.

3.3 Current Vaulting Performance

The definitions given for pole vaulting performance can now be used to determine current pole vaulting performance. As shown in the introduction, the current world record in pole vaulting was set in February 2014 by Lavillenie to a height of 6.16 [m]. However, the world-record can be seen as an outlier. Current seasonal best performances of elite vaulters are commonly around a height of 6.00 [m]. The seasonal best performances for decathletes are approximately 60 [cm] lower as these athletes do not specialize on the pole vault event and commonly perform six of the ten events before they start with the pole vault event. The maximum height of the centre of gravity of the athlete is just below these heights of the cross bar.

The current energy efficiency ratio can also be determined. Consider the world record vault of Lavillenie described in the introduction. His run-up velocity was approximately 9.5 [m/s], he weighs approximately 70 [kg] and his center of mass at take-off was approximately 1 [m] above the ground. Assuming he added a further twenty percent of energy by doing muscular work his total energy input was 4615 [joule]. He reached a height of 6.16 [m] which is equivalent to a potential energy of 4230 [joule]. His efficiency ratio for that vault was equal to 0.92. This was an exceptional vault and usually these values are around 0.85 for top vaulters and 0.80 for top decathletes.²

3.4 Kinematic Parameters

The brief description of the phases given in section 3.1 already showed the large number of actions the athlete performs during a pole vault jump. The actions themselves can be defined in kinematic parameters. The experimental research presented below shows that some kinematic parameters have more influence than others on pole vaulting performance.

The first experimental study on kinematic parameters is a paper by [Pikulsky \(1964\)](#). Pikulsky concludes that the maximum pole bend is strongly correlated with vault height.

¹We should keep in mind that the problem remains two-fold. Increasing his energy input might decrease his energy efficiency ratio. There exist an optimum between these. If the decrease in energy efficiency is high, the result might be that the height the athlete reaches at the cross-bar is lower than before.

²Based on the experimental data of [Angulo-Kinzler et al. \(1994\)](#).

His conclusions are based on experimental measurement results of a video analysis of 24 vaults of five college athletes. The work of Hay (1968) complements the work of Pikulsky (1964) and demonstrates that the horizontal take-off velocity in turn, is the main contributor to the pole bend. However, these first two studies are limited in the number of kinematic parameters that were measured.

The experimental study of Angulo-Kinzler et al. (1994) is the first to measure more kinematic parameters. The kinematic parameters are derived from measurement results of a video analysis of the top eight vaulters at the 1992 Summer Olympic Games in Barcelona. The main conclusions are that horizontal take-off velocity combined with well-timed angular momentum (rotation of the athlete's body) have the most influence on vault performance.³ This conclusion is different from the two previous experimental studies. However, the conclusion should be considered with caution, as these are only based on observations. The sample size of eight vaults is very small to determine strong correlations, nor does the study provide an argumentation on how the conclusions are established.

The three experimental studies of Zagorac et al. (2008), Gudelj et al. (2013) and Zagorac (2013) try to determine the relation between a large number of kinematic parameters and vault performance using a statistical regression analysis. The kinematic parameters are derived from the measurement results of a video analysis. The vaults measured were performed by junior vaulters (17-19 years old). The sample size of the three experiments varies between 13-30 vaults. This sample size seems to be too small for a statistical regression analysis as the results of the three experimental studies all differ. The regression coefficients calculated seem to be weak and care should be taken using the results. The study of Zagorac et al. (2008) determines that the maximum pole bend is the only main factor for vault performance. The take-off velocity also has a relatively high regression coefficient but Zagorac states it is not as statistically significant. The results of Gudelj et al. (2013)⁴ show that take-off velocity and trunk angle at pole release are the most significant contributors for vault performance.⁵ The results of Zagorac (2013) are again different and show that take-off velocity and the time at which maximum pole bend occurs have the most influence on vault performance.

Although the results of the experimental studies discussed differ and some results should be thought about critical, all studies either define maximum pole bend or take-off velocity as main contributor to vault height. This does seem to indicate the importance of these two parameters.

Another approach that underlines the importance of these two parameters are the mechanical energy transformations that happen during the pole vault. The energy transformation were already briefly discussed in section 3.2 to help define the pole vaulting performance. The energetic approach is very suitable to analyze the pole vault as it can also analyze the interaction between the pole and athlete. In total three experimental studies have measured the mechanical energy transformation of the pole vault.

The first experimental study was presented by Fletcher et al. (1960). He performed a slow-

³The maximum pole bend was also measured, but Angulo-Kinzler does not discuss it in the results. This implies that for her the maximum pole bend is not significant for pole vaulting performance.

⁴Zagorac is also co-author of this paper.

⁵Note that the maximum pole bend is measured similar to Zagorac et al. (2008) and Zagorac (2013).

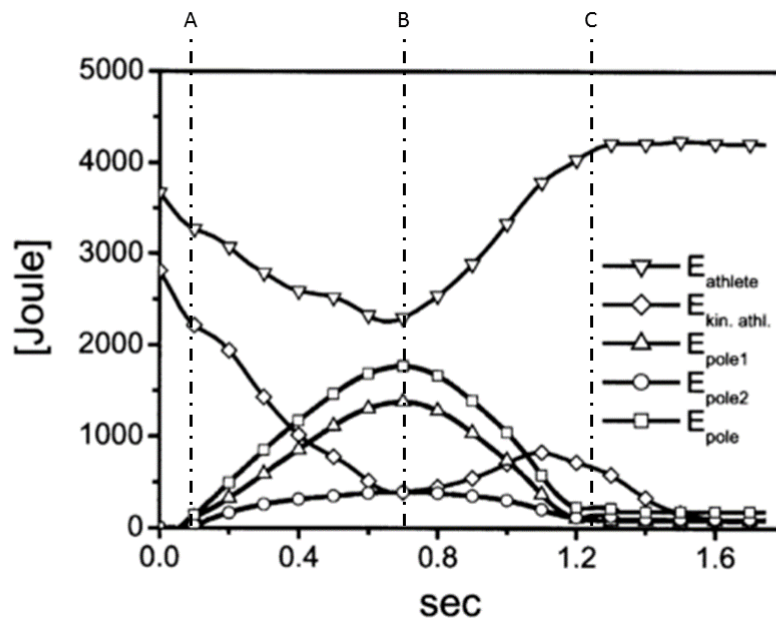


Figure 3.2: Mechanical energy transformations of the pole vault (Arampatzis et al., 2004). Take-off phase is from 0 sec to dashed line A. Bending phase is from dashed line A to dashed line B. Straightening phase is from dashed line B to dashed line C. Free flight phase is from dashed line C onwards. The total mechanical energy of the athlete $E_{athlete}$ consists out of the potential energy, translational kinetic energy, rotational kinetic energy and the work done by the athlete. $E_{kin, athl.}$ is the translational kinetic energy of the athlete and hence a fraction of the total mechanical energy of the athlete as well. The fractions E_{pole1} and E_{pole2} should be neglected. They represent the pole strain energy components of bending and axial displacement. Arampatzis uses an unconventional definition and we believe the components cannot be viewed as such. However, the total pole strain energy E_{pole} is correct.

motion video analysis of five male pole vaulters using a rigid pole. Mapping the trajectory of the centre of gravity during the pole vault, Fletcher could measure the potential and kinetic energy changes.

With the introduction of the flexible pole in the 1960's the mechanical energy transformation of the pole vault changed. Therefore Dillman and Nelson (1968) performed the same experiment as Fletcher et al. (1960). It is interesting to compare the final energy of the athlete as measured by both experiments. The vaults of the athletes using a flexible pole all show a net energy gain, while this was only the case for half the vaults of the athletes using a rigid pole. This indicates that more energy can be put into the system by actively bending the pole and the new motion coordination of the athlete or that less energy is lost during impact as the impact force is reduced. Or a combination of both.

However, both experiments are limited. They only measure the kinetic and potential energy of the athlete. The pole energy and the energy exchange between the athlete and the pole cannot be analysed. This aspect is solved in the third and final experimental

study on mechanical energy transformation by [Arampatzis et al. \(2004\)](#). He develops a test set-up that can measure the pole forces using a force plate. The pole forces can then be used to calculate the pole strain energy during the vault. This methodology provides insight in the energy exchange between the athlete and pole.

The measurements of the different energy types during the vault also show the phases of the vault. As the experimental study of [Arampatzis et al. \(2004\)](#) is the most complete it will be used to demonstrate this. The measurement results are shown in figure 3.2. The measurement starts just before the pole hits the back of the pole planting box. The energy at the moment the pole hits the back of the pole planting box is commonly called the initial energy of the athlete and pole system. From the figure it can be seen that about three quarters of the initial energy consists only out of the kinetic energy of the athlete. The initial kinetic energy is also almost two thirds of the final mechanical energy of the athlete. The pole energy is zero at the end of the vault.

At the end of the run-up phase some actions happen in fast occurrence, as described in section 3.1. The athlete jumps up, the pole hits the back of the pole planting box and the pole starts to bend. From the figure it can be seen that from this point on the pole energy starts to increase and the kinetic energy of the athlete decreases rapidly. The kinetic energy of the athlete is transferred to the pole as strain energy. It can also be seen that the potential energy of the athlete does not increase significantly in the beginning. In reality the athlete follows a convex trajectory. This is more energy efficient as the change in direction is small (change in momentum). Also the athlete rotates his body in vertical position such that the stored strain energy can be returned completely in the vertical plane. The time of maximum pole bend is when the pole strain energy reaches its maximum value. This also corresponds with the time the athlete has the minimum mechanical energy and minimum kinetic energy. The athlete thus slows down.

Next the pole starts to straighten. The kinetic and potential energy of the athlete start to increase, while the pole energy decreases. The pole strain energy is transferred back to the athlete. Also a small and short increase in kinetic energy of the athlete can be seen in the graph. The time of pole bending and pole straightening are approximately equal.

After the pole straightens the athlete releases the pole. This is commonly called the free flight phase. Maximum height is achieved in this phase. The athlete always maintains some kinetic energy to travel forward over the bar. No energy is stored in the pole for this phase.

The limitation of the experimental study of [Arampatzis et al. \(2004\)](#) is that the different energy losses and the muscular work performed by the athlete is not measured directly. As the final energy of the athlete is higher than the initial energy, the only conclusion that can be drawn is that muscular work is definitely present during the pole support phase (pole bending and pole straightening) and is larger than the energy losses during this phase. The energy losses are masked by the muscular work done.

The athlete does muscular work in two ways. First, he can bend the pole. This adds muscular work to the athlete-pole system as extra strain energy. Second, he can add muscular work to the athlete-pole system by applying action-reaction moments in his joints.

The initial run-up velocity and maximum pole bend were identified as the two most important pole vault performance indicators. These can now be linked to the mechanical

energy transformations. The initial run-up velocity is approximately equivalent to the initial kinetic energy of the athlete. As shown above, the initial kinetic energy contributes a very large portion of the final mechanical energy of the athlete. The run-up velocity is an indicator of the main energy input source. If the athlete has a higher initial kinetic energy it means that there is more energy available that can be converted into potential energy. This shows the importance of this kinematic parameter.

However, a higher initial kinetic energy does not necessarily result in an increase in performance. The increase in kinetic energy might result in higher energy losses that outweigh the gain in initial kinetic energy. The maximum pole bend is therefore an even better indicator.

The energy losses will be discussed later on, but for now it is reasonable to assume that most energy is lost during the impact of the pole with the take-off box and that almost no energy is lost during the pole straightening phase. Furthermore, the experimental study of [Frère et al. \(2012\)](#), which measures the muscular activation during the pole straightening phase and free flight phase, shows that little muscular work is done during these phases. So most of the muscular work performed is done during the pole bending phase. This makes sense as during this phase the athlete tries to bend the pole further and already rotates his body in a vertical upside down position.

Hence, during the pole straightening phase almost no more energy is lost or added to the athlete-pole system. Each body part has no rotation or a very small rotation. Essentially, the motion of the athlete during the pole straightening is completely in vertical direction. The energy measured at the time of maximum pole bend shows how much energy there is in the system that will be converted into potential energy. Compared to the initial energy at take-off, extra energy has been put into the system as the athlete has done muscular work and energy has been lost by the impact with the planting box. Now, at this point in the vault, no large changes will occur to the total energy of the athlete-pole system. Almost all of the energy in the system now will be converted into potential energy. As at this time most of the system energy is as strain energy in the pole (see figure 3.2), this explains why the maximum pole bend is even a better indicator for pole vault success.

To recap, the initial velocity and the maximum pole bend largely determine the pole vaulting performance. The energy loss during the impact of the pole with the planting box should be minimized and the muscular work performed during the pole support phase maximized.

3.5 Current Approach to Improve Pole Vaulting Performance

The current approach to improve pole vaulting performance through engineering innovations focuses on improving the design of the pole. Improving the pole design has led to great success in the past. The introduction of the flexible pole completely changed the game. Compared to the rigid pole used before it increased the energy efficiency ratio significantly by reducing the energy loss, increasing the energy input and increasing the conversion efficiency in general. The flexible pole has a lower impact force compared to the rigid pole because of the lower axial and bending stiffness and therefore less energy is

lost during the impact of the pole with the planting box. The flexible pole also allows the athlete to temporarily store his kinetic energy as strain energy. The strain energy is returned to the athlete during the pole straightening phase when he has maneuvered his body and the pole in a vertical position. This is an efficient way to transform the horizontal kinetic energy into potential energy and vertical kinetic energy. This increased the conversion efficiency in general. Finally, the flexible pole allows the athlete to add extra strain energy to the athlete-pole system by performing muscular work to further bend the pole during the pole support phase. Taking these aspects into account it is no surprise that after the introduction of the flexible pole rapid improvements in the pole vaulting world record height were achieved.

As illustrated above, the pole properties thus have a significant influence on the pole vaulting performance. Studies have proven the influence of pole length, stiffness, mass and pre-bend on pole vaulting performance (Hubbard, 1980a; Ekevad & Lundberg, 1995, 1997; Burgess, 1998; Ohshima et al., 2010; Davis et al., 2004). The pole length and stiffness determine the deformation of the pole and hence also the trajectory and duration of the vault. The pole stiffness is highly non-linear (among others because of the large deflections). This offers a lot of freedom for how the pole can deform and what trajectories the athlete can follow. Several researchers have tried to determine the optimal values for these. Their research is discussed in section 3.5.1. The pole mass has an influence on the run-up velocity and hence the energy input for the athlete-pole system. Other researchers focus on minimizing the mass of the pole such that the energy input for the athlete-pole system can be maximized. This is discussed in detail in section 3.5.2. Although the studies of Burgess (1998) and Davis et al. (2004) describe the influence of pole pre-bend on pole vaulting performance, no research has been performed on how this should be implemented in the pole design to improve pole vaulting performance. The pre-bend is therefore not discussed in detail here but in section 3.7.

3.5.1 Pole Length and Pole Stiffness

For each attempt the athlete can choose the pole he wants to use. His choice is mainly based on the pole length and stiffness. Pole manufacturers can produce a pole with any combination of these properties, which make the choice more difficult for the athlete. Different studies conclude that there exist an optimum combination of pole length and pole stiffness that will maximize pole vaulting performance for a given athlete (Hubbard, 1980a; Ekevad & Lundberg, 1995, 1997; Ohshima et al., 2010). This underlines the importance of choosing the right pole. Several researchers have developed tools that can aid the athlete in choosing the right pole and hence improve their pole vaulting performance.

The first tool is developed by Ekevad and Lundberg (1995) and is a finite element model. The model developed can predict that the optimum length of a pole given the pole stiffness, initial velocity, athlete strength and motions of the athlete.⁶ Results indicate that a maximum vault height exists with respect to pole length.

The model can also be used to predict the optimal combination of pole stiffness and pole

⁶A sequence of motions the athlete had to carry through were prescribed.

length.⁷ This optimization has not been published for this model. Probably, because the computational time required is too high. This assumption is made because [Ekevad and Lundberg \(1997\)](#) performed this optimization using a simplified model of their earlier work. They simplified the detailed 'active' athlete sub-model developed earlier to a passive point mass. The results show that there exist a maximum vault height with respect to pole length and pole stiffness. The model could be used to estimate this optimal combination, although the simplification made for the athlete sub-model has a significant effect on the pole vault motion ([Hubbard, 1980a](#)). The result of the model most likely has a significant deviation from the the real optimum pole properties.

The model of [Ekevad and Lundberg \(1995\)](#) is further improved by [Ohshima et al. \(2010\)](#). [Ohshima et al. \(2010\)](#) refines the two-dimensional athlete sub-model to a three-dimensional sub-model. In addition he develops a genetic algorithm to solve the optimization problem of optimal pole stiffness and pole length. The genetic algorithm can also optimize for a pole with variable stiffness.

The application of such models by top-athletes to help choose the best pole is up till now limited. Top athletes usually determine the pole stiffness and pole length they want by trial and error.⁸ By years of experience most of the athlete have probably selected a pole close the optimum values for length and stiffness using this process. It seems that pole vaulting performance cannot be improved by only optimizing the pole length and pole stiffness.

3.5.2 Weight Minimization of the Pole

Other researchers focus on minimizing the mass of the pole ([Burgess, 1998](#); [Davis et al., 2004](#)). This is also the focus of most pole manufacturers.

The idea behind the weight minimization is to enable to athlete to achieve a higher run-up velocity. The experimental study of [Ropret et al. \(1998\)](#) studies the effect of arm loading on sprint kinematics. Results show a decrease in sprint velocity when the arm loading is increased. The work of [Frère et al. \(2009\)](#) determines the influence of pole carriage on run-up velocity. The results show a decrease in velocity of 0.5 [m/s] for the runs with pole compared to the runs without pole. This is a reduction of approximately five percent compared to free running. Frère contributes this to the forward displacement of the centre of gravity, the restriction of the arm swing and the motion coordination the athlete has to perform just before take-off. The two experiments show that reducing the mass of the pole will reduce the arm loading and decrease the anterior imbalance. As a result, the run-up velocity will increase. However, the arm swing restriction will remain.

As shown in section 3.4, the run-up velocity is one of the kinematic parameters that seems to have a large influence on vault performance. The correlation between run-up velocity and vault height has been measured by [Adamczewski and Perlt \(1997\)](#). Their study tests the hypothesis that the correlation is linear instead of exponential. The run-up velocity is measured using an electro-optical test set-up. The test set-up is limited as it cannot take

⁷As the athlete sub-model includes an active control of six body segments, the model can also be used to evaluate the optimum vaulting technique and motion coordination the athlete.

⁸Athletes have access to a large number of poles with different properties through, for example, sponsor contracts with pole manufacturers

into account any variations in conditions, athlete and vaulting style. However, the very large sample size of 725 vaults and the long period of time (1991-1996) averages these variations to some extent.

The results support the hypothesis that is tested. An increase of 1 [m/s] in run-up velocity resulted in an increase of approximately 0.5 [m] in vault height. The findings of [Adamczewski and Perlt \(1997\)](#) are confirmed by [Linthorne and Weetman \(2012\)](#). Although their study has a very small sample size, it has the advantage that the run-up velocity was measured for the same athlete under the same conditions and using the same vaulting style. Combined these experiments show the significant effect the run-up velocity has on vault height and the results support the philosophy of weight minimization of the pole.

However, the results of [Adamczewski and Perlt \(1997\)](#) also show that no increase in run-up velocity occurs for the period of 1991-1996. Also, the take-off speed measured in later years by [Zagorac et al. \(2008\)](#) and [Linthorne and Weetman \(2012\)](#) do not show an increase in run-up velocity compared to the run-up velocities measured by [Adamczewski and Perlt \(1997\)](#). Although, the experiments did not measure the pole mass, it is reasonable to assume that the pole manufacturers produced lighter poles over this time period ([Davis et al., 2004](#)). This indicates that the current limit in vault height improvement can be linked to the limit reached in run-up velocity. As current poles already weigh as little as 1.8 [kg]⁹, decreasing the pole mass further will yield a marginal or no return in run-up velocity. Hence the vault height will not increase with the required 15 [cm].

3.6 Pole Vault Models

The pole vault is a complex event to model. The pole is subjected to large deformations and there is a complex interaction between the athlete and the pole. Furthermore the problem is described by a combination of athlete properties, pole properties, initial conditions and a control set ([Hubbard, 1980a](#)). For accuracy, the model should include all these aspects. Commonly, the athlete and pole are modeled separately after which the interaction between them is defined. The models already developed can be split in analytical and finite element models. Both will be discussed below. The results shown here are also used for step two to develop a model that can explore, identify and assess different innovations for the pole vault (see chapter 4).

3.6.1 Analytical Models

The pioneering work for the analytical model is performed by [Walker and Kirmser \(1973\)](#). They were the first to model the pole using a non-linear large deflection theory. However, the athlete is modeled as a simple pendulum system suspended from the top end of the pole. This neglects a part of the interaction between the athlete and the pole as it does not include the moment the athlete applies to the top end of the pole.

The analysis of [Hubbard \(1980a\)](#) shows that the moment applied by the athlete to the top end of the pole has a significant influence on the pole forces. His findings are later

⁹[Davis et al. \(2004\)](#)

confirmed by experiments of [Morlier and Mesnard \(2007\)](#). Hubbard therefore modifies the non-linear large deflection theory formulated by [Walker and Kirmser \(1973\)](#) so that the pole is loaded by a compressive force as well as an applied moment at one side. He has solved this elastica problem with a numerical iterative method, which is published in a separate paper ([Hubbard, 1980b](#)). He further improved the athlete model such that it includes three torque generators for the wrists, hips and shoulders to simulate the athlete's muscle actions. Results demonstrate the high sensitivity of the vault height to initial conditions and motion coordination of the athlete. Hubbard's analytical results for the mechanical energies are in line with the experimental results of [Arampatzis et al. \(2004\)](#). However, the results for the pole forces are not in line with the pole forces measured by [Morlier and Cid \(1996\)](#). The difference can be explained by the difference in initial conditions, pole characteristics and motion coordination of the athlete used for each study.

The work of Walker demonstrates that large deflection theory is required to model the pole. In addition, the study of Hubbard proves that the moment applied by the athlete to the top end of the pole significantly influences the motion of the athlete and the pole. Both aspects should be accounted for to model the pole vault motion.

3.6.2 Finite Element Models

Finite element models have been developed by [McGinnis and Bergman \(1983\)](#), [Ekevad and Lundberg \(1995\)](#), [Ekevad and Lundberg \(1997\)](#) and [Ohshima et al. \(2010\)](#).

The pole sub-model is modeled the same by all. All four finite element models use beam elements that can account for the transverse shear and large deformations. Only the model developed by [Ohshima et al. \(2010\)](#) considers a non-uniform bending stiffness along the pole length, though this can be easily implemented in the other models as well.

The athlete sub-model differs in complexity among the different models. [Ekevad and Lundberg \(1997\)](#) simplify the athlete to a passive point mass at the top end of the pole. Although it reduces computation time, this simplification reduces the accuracy quite significantly. The forces and moment the athlete exerts on the pole have been proven to have quite a significant influence on the pole reaction forces ([Hubbard, 1980a](#); [Morlier & Mesnard, 2007](#)). [Ekevad and Lundberg \(1997\)](#) made this simplification to reduce the computational time such that it could be used for an optimization of pole bending stiffness.

In their previous work, [Ekevad and Lundberg \(1995\)](#) modeled the athlete in much more detail. They modeled the athlete using seven elements connected with pin joints. Each pin joint could be torque controlled. The control strategy implemented tries to follow a prescribed trajectory and style (body motions of the athlete). The research of [Ohshima et al. \(2010\)](#) refines this model even more. The two-dimensional athlete model is adapted to a three-dimensional body and a genetic algorithm is developed to solve the optimization problem of optimal pole characteristics (length and bending stiffness).

Detailed finite element models have been developed to predict the motion of the pole vault. However, the computational time of the finite element models developed is in the order of hours. Such a high computational time is undesired for a model based exploration of the possibilities to improve pole vaulting performance.

3.7 Potential Innovations to Increase Pole Vaulting Performance

Section 3.5 revealed that the current approach to improve pole vaulting performance through engineering innovations will most likely not result in improvements in pole vaulting performance. The athletes have reached their limit in run-up velocity while carrying a pole and use a pole close to the optimal properties. Other approaches have to be thought of.

Section 3.5 also showed that one aspect of pole design has not been explored. The pole pre-bend has not yet been examined. Current poles have a pre-bend to initiate bending during the impact of the pole with the planting box. This reduces the impact force. Section 3.7.1 examines why reducing the impact force improves pole vaulting performance. This section also presents an innovation on how the pole impact force can be further reduced.

Pole vaulting performance can also be improved by improving the motions of the athlete. It is interesting to note that already in 1980 the work of Hubbard (1980a) shows the significant influence of motion coordination on pole vault performance. He recommends to develop a tool that can predict the optimal motion coordination of the athlete. However, despite its potential no further work is published on this topic. Section 3.7.2 explores the optimization in more detail.

3.7.1 Innovation 1

During the impact of the pole with the take-off box energy is lost. In literature there is still a discussion about the causes of the energy loss. The discussion is limited to observations as no direct experiment or analysis has been performed. Ekevad and Lundberg (1997) and Frère et al. (2010) state in their work that they believe the impact energy loss is a result of the damping of the stress waves generated in the pole by the impact.

The pole forces have been measured in the experimental studies of Morlier and Cid (1996), Arampatzis et al. (2004), Schade et al. (2006) and Morlier and Mesnard (2007). It is interesting to see that the same response is measured by all four experiments and the damping of the stress waves is visible in the results. An example of a force response measured is given in figure 3.3. The force response measured shows a high frequency peak that quickly dampens out. The damping indicates that energy is lost here. As the damping coefficient of the human body is an order of magnitude higher than the pole and the planting box materials, it is likely that most of the energy damping is done by the athlete.

The experimental study of Dillman and Nelson (1968) indicates that the impact energy loss increases when run-up velocity increases. The results suggest that the magnitude of the impact force is related to the energy loss during impact. The energy loss increases for an increasing impact force.

The magnitude of the energy loss is difficult to determine as these have not been measured directly yet. However, with a simple elementary analysis based on the conservation of momentum, Johnson et al. (1975) suggests that the energy loss during the pole impact is in the order of 10 percent of the initial energy of the system. This amount of energy is

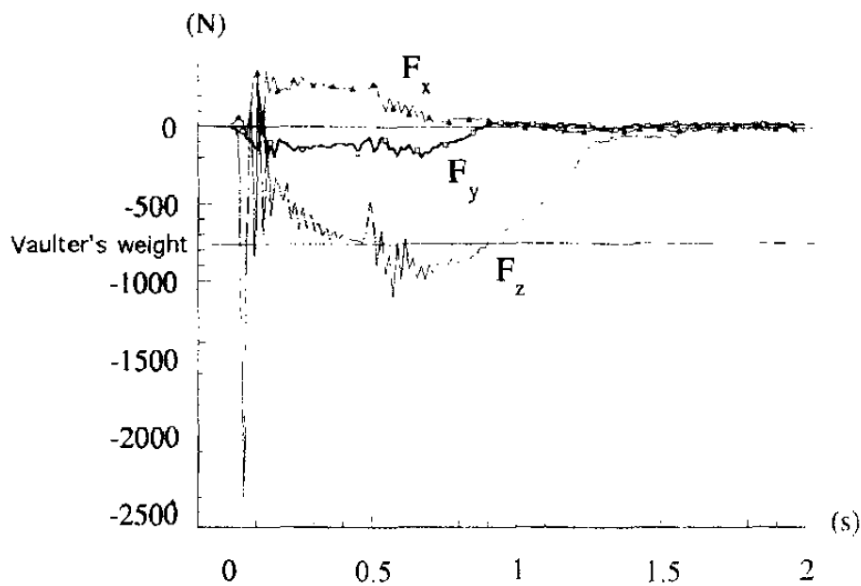


Figure 3.3: Three force components of the pole force during a vault measured using a force plate fixed under the planting box. The forces shown are opposite to those measured by the force plate. The x -axis is aligned with the direction of the run-way (positive axis moving away from the planting box), the z -axis is the vertical axis (positive pointing upwards) and y -axis complies with the right hand rule. The origin is defined at the back of the planting box. (Morlier & Cid, 1996)

equivalent to an extra height gain in the order of 50 [cm]. This is in my opinion a very high value, but it does seem to roughly indicate the order of magnitude of the impact energy loss. This indicates that still a large amount of energy can be conserved and converted into potential energy (equivalent to vault height).

The peak force and oscillations can be reduced in several ways. For example the pre-bend already used can be increased. This is however undesirable as the force the pole returns to the athlete during the pole straightening phase will be lower. In addition, the pole might no longer support the weight of the athlete and not straighten at all. The decrease in energy loss is then probably outweighed by the reduction in vertical velocity at pole release.

Another solution would be to design a pole that can change its stiffness after impact. The pole could then have a low axial stiffness when the pole impacts the planting box and hence reducing the energy loss here. After the impact the pole could increase its stiffness such that the athlete will be propelled upwards faster. A pole with time varying stiffness can be designed by for example inserting shape memory alloy wires, adding actuators or varying the circumferential stiffness¹⁰. After a first exploration it was thought doubtful whether a time varying stiffness pole was feasible. The solutions would either require a significant change in technique for the athlete, add extra weight or the change in stiffness that could be achieved was too small.

¹⁰The athlete should then twist the pole during the vault

The peak force and the oscillations can also be reduced, while maintaining the pole return force, by adding a spring to the pole (Johnson et al., 1975). The spring reduces the impact force and the energy loss during impact. Moreover, the spring can be designed such that the elongation of the spring happens simultaneous with pole straightening. This can even increase the pole return force.

The rules of the IAAF for 2016-2017 do not prohibit the use of a spring in the pole. The only rule for the pole is rule 183.11 and states the following.

Athletes may use their own pole. No athlete shall use any other athlete's pole except with the consent of the owner. The pole may be of any material or combination of materials and of any length or diameter, but the basic surface must be smooth. The pole may have layers of tape at the grip end (to protect the hand) and of tape and/or any other suitable material at the bottom end (to protect the pole). Any tape at the grip end must be uniform except for incidental overlapping and must not result in any sudden change in diameter, such as the creation of any "ring" on the pole.

In addition, the IAAF Rule Committee confirmed by e-mail contact that this was the only rule concerning pole design. The spring does not have to be a classical coiled spring but can also be for example an air spring or a piece of rubber. The innovation of adding a spring to the pole is believed to have the potential of improving the pole vaulting performance of the top Dutch decathletes at the Summer Olympics of 2020. The evaluation of this innovation is presented in chapter 7.

3.7.2 Innovation 2

Until today, athletes still use different techniques. For example some athletes focus on rotating a longer pole to a vertical position while others focus more on bending the pole further. Some athletes prefer a vault of one second while other athletes prefer a longer vault so they have more time to rotate their body. The difference in technique is further demonstrated in the experimental research of Morlier and Mesnard (2007). The study measured the moment exerted by the athlete on the pole. The measurement results show significant disparities for the applied moment to the the pole between athletes. This is shown in figure 3.4.

The results indicate that there exist an optimal set of motions for a given athlete. These set of motions will yield the maximum height the athlete can achieve. No study has been performed that optimizes the pole vault motion. As shown, studies have optimized pole length and pole stiffness, but none include the motion coordination of the athlete and the take-off conditions. The study of Hubbard (1980a) already demonstrated the significant influence of the motion coordination and take-off conditions on pole vaulting performance.¹¹ He also suggested to optimize the pole vault motion but no further work has been done for this despite its potential to improve pole vaulting performance.

The optimization of the pole vault motion should take all these three aspects into account: pole properties, motion coordination and take-off conditions. Hence the optimization problem is three-fold and should determine the optimal combination of these three

¹¹It is generally believed Sergey Bubka had a superior motion coordination compared to his competitors and that he could therefore break the world-record so many times.

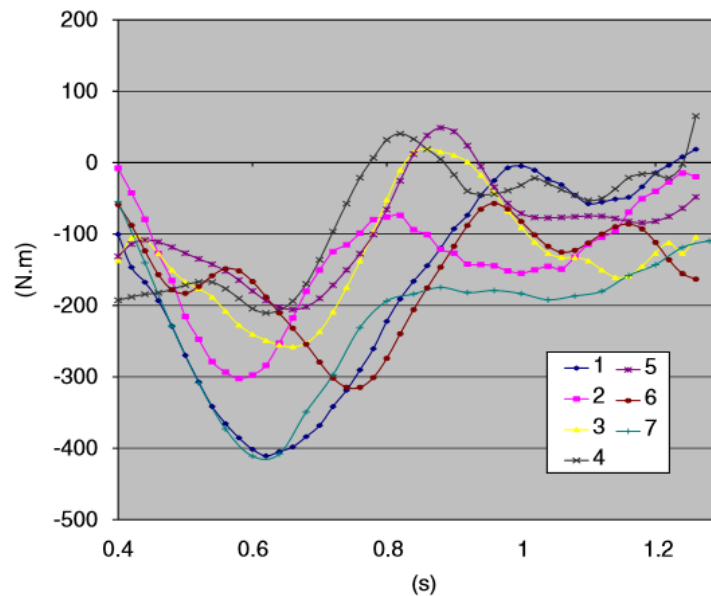


Figure 3.4: Transversal moment component of the moment applied to the top end of the pole by the athlete during a vault. The results are shown for seven different athletes. The time starts right after the take-off phase and ends when the athlete releases the pole. (Morlier & Mesnard, 2007).

sets. The optimal combination might of course change for an athlete with a different morphology.

The exploration of such an optimization is presented in chapter 8.

3.8 Summary

A definition is given for pole vaulting performance and it is demonstrated what variables are important for pole vaulting performance. The current pole vaulting performance is shown to be approximately 6.00 [m] with energy efficiency ratio's between 0.8 and 0.9. The literature study also presents the current approaches to improve pole vaulting performance. These consist out of reducing the mass of the pole and choosing the optimal combination of pole stiffness and length for a given athlete. It is demonstrated that a limit has been reached for both approaches. Furthermore, the advantages and disadvantages of different models that evaluate the pole vault motion are discussed. Finally two innovations are introduced that can improve pole vaulting performance. These two innovations are a pole with a spring and optimizing the motion coordination, pole properties and take-off conditions for a given athlete.

Pole Vault Model

In this chapter the mechanical model is developed that describes the motion of the athlete and the pole. First the principles of a mechanical model are discussed to create an understanding of the framework of the model. This section also defines the different inputs required for a mechanical model. For the model-based exploration the pole vault motion is simplified. The simplification choices made are discussed in the next section. This section is followed by the section that defines the outline of the athlete sub-model. The discretization of the athlete, the muscle model and the schematics of the athlete sub-model are discussed. The next section derives the equations of motion for the athlete sub-model defined in the section before. The solution to determine the pole forces required to solve the equations of motion is derived in the subsequent section. After this the equations of motion can be numerically integrated as explained in the section that follows. Finally it is presented how the maximum vault height during the fly-away can be determined.

4.1 Mechanical Model

The motion of physical objects can be described by classical mechanics. The motion of an object is caused by forces acting on it. Classical mechanics use Newton's law to relate the forces acting on an object to the motion of that object. A model that describes the motion of an object using classical mechanics is also called a mechanical model.

The motion of an object is how its position changes over time. It is tedious to determine the motion of every point on an object, therefore the objects are often idealized to point particles. When a body is (assumed to be) rigid the motion of every point of the object can be easily derived from the motion of the idealized point particle. The pole vault motion consists out of the separate motions of the pole and the athlete. The motion of the athlete again consists out of the motion of different body parts. The pole vault motion can be described by dividing the athlete-pole system into different objects or bodies. Each body can then be idealized as a point particle. The exact division will be determined in the rest of this chapter, but an example is shown in figure 4.1. For this example the

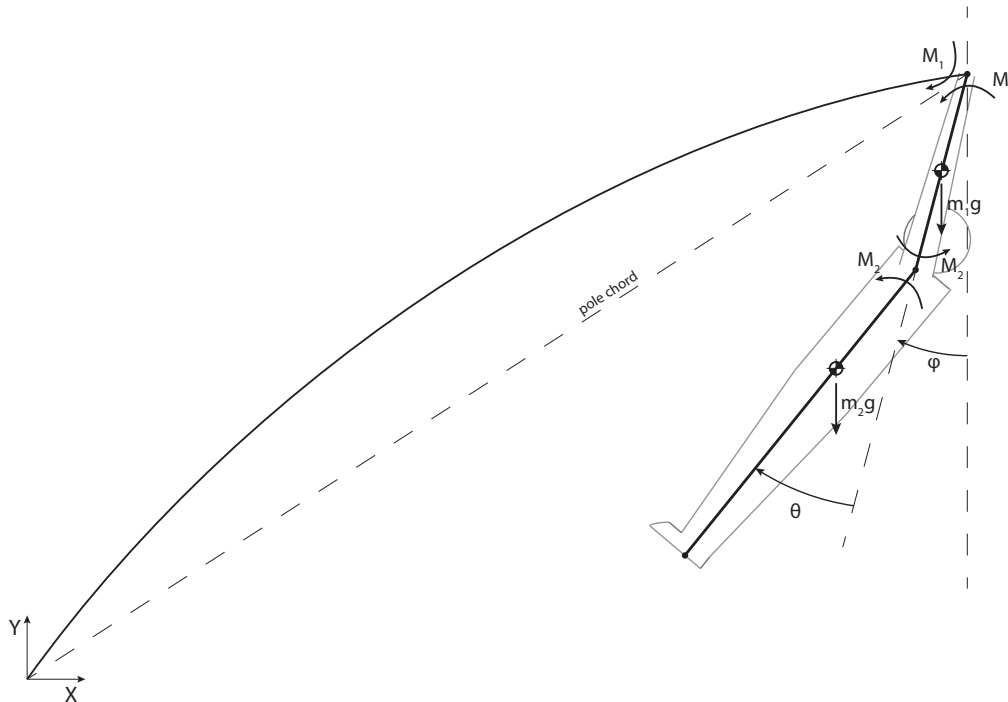


Figure 4.1: Schematic diagram of the pole vault

athlete-pole system is split into a body for the pole, a body for the arms of the athlete and a body for the torso, head and legs. The motion of each body can be described for one point. For the example the athlete bodies are idealized as point particles located at their center of mass. This is a convenient choice as will be explained later on. The rest of the body is assumed to be rigid such that the location of the hands or feet can be easily calculated from the idealized point particles. Note that for the pole vault the motion of the pole can be described by the motion of the arms body. As the arm body is rigid the location of the hands can be determined from the motion of the center of mass of the arms. The athlete holds the top end of the pole with his hands. So these locations coincide. The location of the bottom end of the pole does not change during the vault and remains placed against the back of the planting box. Hence the motion of the pole can be determined from the motion of the athlete. However, to determine the deformation of the pole a different model is required.

The motions of the athlete-pole system are caused by external forces acting on it. The external forces for the pole vault exist out of gravity forces for the body parts of the athlete. The pole is assumed to be massless so no gravity force is acting on the pole. The gravity forces act on the center of mass of each body part. Hence the choice of the location of the center of mass is convenient as the gravity forces will not cause an additional moment. The other external forces acting on the system consist out of the motion coordination of the athlete. By applying an action-reaction moment the athlete can actively control his body configuration during the vault. These actions can be idealized by torques acting on the joints of the athlete. In addition, the athlete applies a moment to the top end of

the pole to further bend it. This action can also be idealized by a control torque acting on the top end of the pole. For the example shown in figure 4.1 a control torque M_1 is placed at the top end of the pole and a control torque M_2 is placed at the shoulder joint. The control torque M_2 can rotate the rest of body relatively to the arms. All the external forces (gravity forces and control torques) defined here are inputs for the mechanical model that will be developed. The forces and motion of the different bodies also depend on the physical properties of each body, for example mass or arm length. These body properties are therefore also inputs for the mechanical model. The internal forces are acting on the pole-athlete system between each body part and equations should be determined that can compute these forces based on the inputs of the mechanical model. The motion described by a mechanical model can be considered a mixed problem. Either the motion or the external forces can be given as input. As the athlete controls his motion by applying joint moments it is chosen to define these as inputs.

The large deformation of the pole is determined using the elastica theory. The elastica solution rests on the following assumptions. The pole can be considered as an inextensible curve. As the pole is inextensible there is only a balance of moments. It is assumed that the bending moment depends linearly on the change in curvature. As the pole is assumed massless to solve the deformation using the elastica theory, no external gravity force is applied for the pole. As the weight of the pole is small compared to the weight of the athlete the effect of neglecting this force is small (2 [kg] compared to 70 [kg]).

4.2 Choices, Assumptions and Simplifications

The first choice made is to develop an analytical model. Results of the literature study show that both analytical models and finite element models have been developed to describe the pole vault motion (see chapter 3, section 3.6). For the exploratory research an analytical model is preferred above a finite element model. The lower complexity of an analytical model offers a better understanding of the dynamics of the pole vault. Also the smaller computational effort allows for faster analysis and the possibility to perform parametric studies or optimizations.

Another choice to be made is the level of complexity of the model. The mechanical model will be used to explore, identify and assess innovations that can improve pole vaulting performance. For this it is desirable that the principles of the mechanical model can be understood completely and that the mechanical model can be quickly solved. Therefore the approach was taken to model the pole vault motion as simple as possible which still accounts for the main features of the pole vault motion.

Next it is chosen to model the motion entirely two-dimensional. This choice simplifies the motion considerably. Although the pole bends out of plane and the athlete twists his body during the fly-away phase, these two aspects have a small influence on the dynamics of the vault. The experimental research of [Schade et al. \(2000\)](#) demonstrates that the difference between the two-dimensional and three-dimensional calculated mechanical energies is small. This proves that the main aspects of the pole vault can be described by a two-dimensional motion.

The pole vault can be split in a run-up phase and a jump phase. The third choice made is to omit the run-up phase in the model. The motion of the athlete and the pole is

straightforward in this phase. During this phase the athlete tries to end with the highest velocity possible. This can be accurately characterized with the final conditions of the athlete-pole system only.¹ These final conditions can then serve as initial conditions to describe the motion of the athlete and the pole during the jump phase.

In addition the fly-away phase is simplified using an energetic approach. The fly-away phase only consist out of the motion of the athlete.² There is no more interaction between the athlete and the pole. If the final conditions at pole release remain within a certain range³, only the maximum height the athlete reaches during this phase and the distance from the planting box has to be calculated.⁴ These properties can be calculated using the conservation of energy principle as will be shown in section 4.7.

It is chosen not to include an impact mechanism model. The physical processes happening during impact of the pole with the back of the planting box are completely different from the rest of the vault motion. Therefore, a completely new set of equations is required in order to describe the processes and motions during impact. The extra derivations and extra set of equations will make the model more complex for now. The impact is therefore not included. This is a qualitative decision. Further work is required to examine the effect of neglecting the pole impact on the motions of the athlete and pole. As no impact model is included the energy loss at impact is not determined. This means that the model will always overpredict the final vault height. Note that also other energy losses such as aerodynamic drag and visco-elasticity losses are not included. These energy losses are small and are therefore chosen to be neglected.

In order to keep the model as simple as possible, it is also chosen to neglect the pull-up action of the athlete. At the end of the pole straightening phase the athlete is in an inverted position but his arms still point downwards. The athlete then pulls himself up to get to a completely inverted position. This action will add to the complexity of the model as the motion is different from the previous rotational movement of the different body segments. First a new athlete model or equations of motion will be required to accurately describe this phase. Second, extra research is required to determine the bounds for the arm forces and work rate during this phase (Hubbard, 1980a). The results of the experimental study of Frère et al. (2012) demonstrate that the influence of the pull up force on pole vaulting performance is small. He measures the muscular activation during the pole straightening and fly away phase and shows that the muscular activities during these phases do not have a significant impact on vault height. The maximum height can still be predicted accurately while neglecting the pull-up force. Neglecting the pull-up force means that the motion described by the model ends when the athlete is in an inverted position with his arms pointing downwards and the rest of his body orientated

¹The final conditions are the location, orientation and velocities of the athlete-pole system at the end of the run-up phase just before take-off. The upward jump of the athlete at take-off is accounted for by the initial vertical velocity.

²The athlete has released the pole and will not use it anymore. We are therefore no longer interested in the motion of the pole. However, it is assumed that the athlete has pushed the pole away from the cross-bar such that the vault is legit (IAAF rules).

³For example the athlete is in an inverted position and there are no large rotational velocities or large rotational accelerations.

⁴According to the rules, the cross-bar can be placed at any point from that directly above the back end of the planting box to a point 80 [cm] in the direction of the landing cushion. The point at which the peak height is reached should be within this range.

straight upwards (such that the shoulders are below wrists).

The global origin is chosen to be at ground level above the deepest point of the pole planting box.⁵ The X -axis is defined as the horizontal axis in the direction of the running track (positive axis pointing to the right). The Y -axis is defined as the vertical axis (positive axis pointing upward). The motion of the athlete and pole will be from right to left.

4.3 Athlete Sub-Model Outline

Now that the general choices have been made for the mechanical model, choices have to be made for the sub-model of the athlete as well. First the choice on how the athlete is discretized is discussed. Second, a muscle model is chosen that can be used to control to body motion of the athlete during the vault. After this the schematics of the athlete are presented.

4.3.1 Athlete Body Discretization

In literature, the human body is commonly discretized in different segments (Hubbard, 1980a; Ekevad & Lundberg, 1995; Ohshima et al., 2010).⁶ The complexity of the model generally depends on the number of segments needed to describe the motion. For example, the simplest model would consist of one segment. As the motion of the athlete during the pole support phase is mostly rotational, this could be represented by a mass pendulum system. Or for example, the athlete can be discretized in four segments. A segment that represents the two arms, a segment that represent the head and the torso, a segment that represents the two upper legs and a segment that represent the two lower legs. The four segments can be connected with pin joints. The result is a four pendulum system. This discretization would be more detailed than the single pendulum, but the system would be more complex as more degrees of freedom are added.⁷

As mentioned before, the goal is to develop a model as simple as possible but that still accounts for the main features of a real vault. The goal is therefore to determine the minimum number of segments required to still capture the main features of the motions of the athlete. To determine this number a video analysis was carried out. The results can be visualized in four photographs shown in figure 4.2. The four photographs show the four body positions the athlete sequentially moves through.

The initial body position at take-off is shown in photograph (a) in figure 4.2. During take-off, both the arms and legs of the athlete are separated but can be considered to be almost straight. As discussed in chapter 3, the upper arm pulls on the pole and the lower arm pushes on the pole.

The next important body position is called the rock-back and is shown in photograph (b) in figure 4.2. Three separate rotations of the body occur between the two body positions.

⁵The deepest point is 20 *cm* below ground level (IAAF website).

⁶And the segments are commonly linked by pin-joints.

⁷As well as more control variables as the orientation of the extra segments have to be controlled.

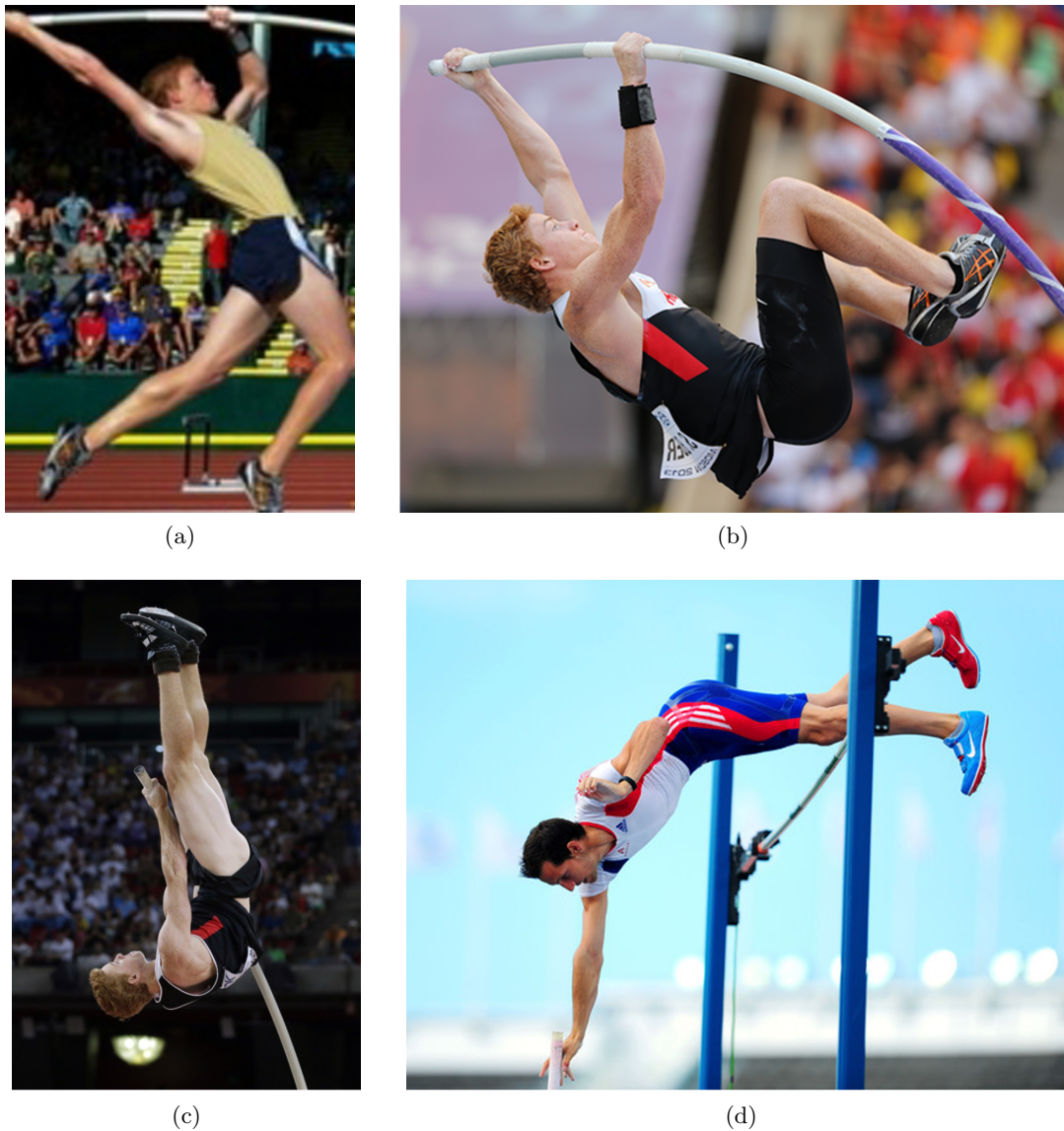


Figure 4.2: The four important body orientations during the pole support phase. (a) take-off position, (b) rock-back position, (c) inverted position, (d) fly-away position.

First the legs are brought together and rotated forward and completely upward (180 degrees). The rotation occurs around the hips. In the second rotation the legs are pulled up towards the chin by bending the knees (rotations around the knees). Third, the athlete rotates around his shoulder such that the torso becomes horizontal and parallel to the ground. Both arms of the athlete are still separated and pointing downwards. This position coincides with the time the pole reaches its maximum deflection.

The third position is shown in photograph (c) of figure 4.2 and occurs when the pole is almost straightened again. The athlete is in an inverted position. In between the two body positions, the athlete has further rotated his torso around his shoulder until he is in this upside down position. His torso is now placed close to his arms. The legs are

straightened again and brought upward. The torso and legs are aligned in an inverted position. The arms remain pointing downwards (thus the shoulder remains below the hands).

The last position, shown by photograph (d) in figure 4.2, is after the pull-up phase. As mentioned in section 4.2, the pull-up action is neglected to keep the model as simple as possible. The motion we have chosen to describe therefore ends when the athlete reaches the inverted position shown in photograph (c). Therefore, to determine the minimum number of segments required to model the body of the athlete only the first three photographs have to be analyzed.

The body orientation for these three positions can be exactly modeled using seven segments: two arms, head and torso, two upper legs, and two lower legs. However, a seven segment athlete sub-model is quite complex and for the interest of simplicity the number of segments has to be reduced as far as possible.

The minimum number of segments that still describes the main motion of the athlete is chosen to be two. This number is especially determined by the inverted position of the athlete as shown in photograph (c). To describe this body position at least two segments are required. A segment representing the arms and a segment representing the rest of the body (torso, head and legs).

Although the legs are separated at take-off and slightly bend, this position can still be approximated with a two segment model. The approximation of the rock-back position is less accurate. The legs are clearly bent at the knees and at a right angle with the torso. If it is desired to model this accurately the lower legs, upper legs and torso can be modelled separately. The model can relatively easy be adapted to include this refinement. However, the refinement is not included here to keep the model as simple as possible.

The approximation to model the two arms as a single segment seems quite poor as the first three photographs show that the arms are spread apart. However, this is quite a reasonable approximation as both the mass and moment of inertia of the arms is relatively small compared to those of the torso and legs.

In addition, to keep the model as simple as possible, it was chosen to keep the mass moment of inertia of both segments constant. From the photos in figure 4.2 this seems a correct assumption for the arm segments. These remain almost straight throughout the complete vault motion. However, this is not a correct representation for the rest of the body. The different body configurations (for example legs straight and legs bent) during the different phases have a significant difference in magnitude of the mass moment of inertia. This effect is thus for now neglected but can be included in the future by for example making the mass moment of inertia a function of time or body position. The change in mass moment of inertia during a vault of each segment will of course also diminish if the athlete discretization is further refined.

Note that all these decisions for the discretization of the athlete are qualitative. Further work is required to determine the effect of the choices made in this section on the accuracy of the mechanical model.

4.3.2 Muscle Model

As discussed in the results of the literature study, the work of Hubbard (1980a) and Arampatzis et al. (2004) show that the muscular work done by the athlete has a significant influence on the pole vault motion. To describe the main features of the pole vault motion the muscular work done cannot be neglected.

The athlete delivers work to the system in two ways. First the athlete applies a moment at the top end of the pole. The applied moment bends the pole converting muscular work into strain energy. Second the athlete performs work to rotate his body in the desired positions by applying action-reaction moments in his joints.

To keep the model as simple as possible it was chosen to use two instantaneous torque generators to model the muscular work. Torque generators are one of the simplest muscle models as the internal dynamics of the muscles are completely neglected (Hubbard, 1980a). Although it has been proven by Zomlefer et al. (1975) and Ghosh and Boykin (1975) that the accuracy is quite poor, Hubbard (1980a) shows that the values generated by the torque generators can be transformed to approximately true torque values delivered by the muscles of the athlete if necessary. This transformation is left out this MSc thesis for now but can be relatively easy included in the future.

The first torque generator is located at the top end of the arm segment (representing the wrists) and represents the moment applied by the athlete to the top end of the pole. A pure applied moment is assumed at the top end of the pole. However, in reality the athlete applies equal and opposite shear forces some distance apart. The distance is equal to the handgrip of the athlete. Since the handgrip width (0.5 [m]) of the athlete is an order of magnitude smaller than the pole length (5.0 [m]), the pure moment is considered a good approximation (Hubbard, 1980a).

The second torque generator is applied at the pin joint between the two segments (representing the shoulder joint) to control the rotation of the two segment athlete.⁸

The bounds for muscle torques of the athlete have been studied by McGinnis and Bergman (1986). The maximum values of the muscle torques of course depend on the type of muscles. Results for the shoulder and wrists indicate a maximum value of 500-600 [Nm]. These values shall be used as the torque bounds for the torque generators. The control torques are an external force and are therefore inputs of the mechanical model. Hence a torque profile has to be defined to solve the mechanical model.

4.3.3 Schematics of the Athlete

The two segment athlete model can now be described by the schematics shown in figure 4.3. The two segments are connected by a pin joint. The compressive pole force R is split into a normal R_n and a tangential component R_t . This is illustrated in figure 4.3. These pole forces act equal in magnitude but in opposite direction on the athlete at the top end of the arms segment (representing the location of the wrists). The forces can be calculated using the iterative numerical solution presented in the section 4.5. Control torques act at

⁸If more segments are added, more torque generators can be added to control the rotation of each body segment of the athlete.

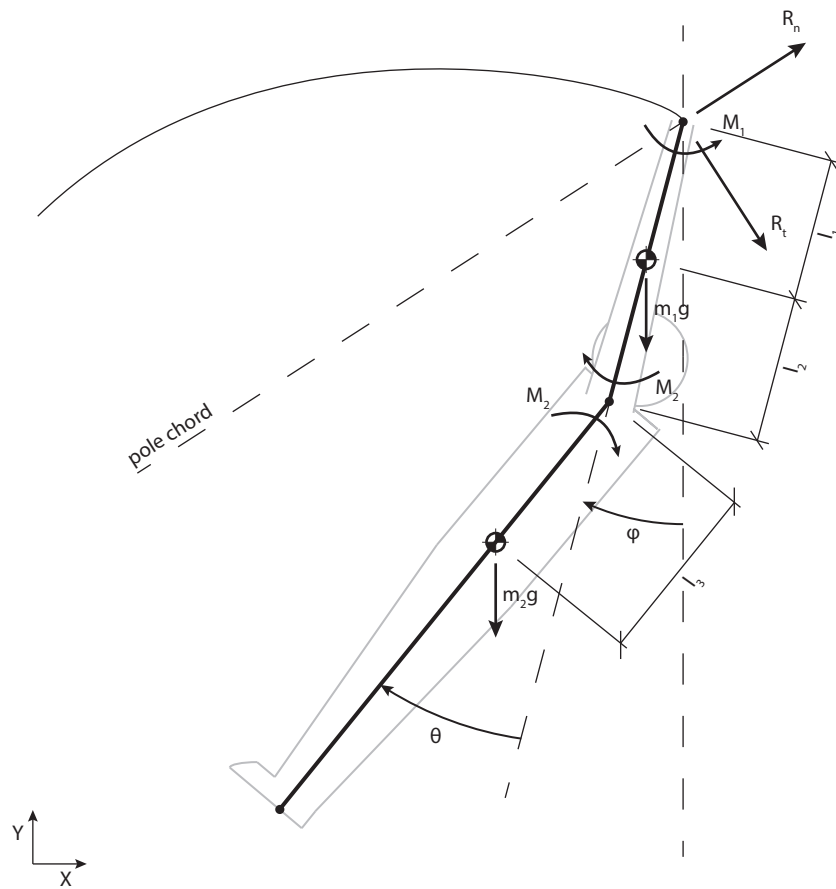


Figure 4.3: Schematic diagram of the athlete

the pin-joint between the two segments and at the top end of the arms segment. The two segments are idealized by point particles located at the center of mass of each segments. These are also shown in figure 4.3. The length of each segment is shown as well. Finally not defined in the figure, is that each segment has a mass and an inertia. Hence, each segment also has a gravity force acting on the location of the center of gravity.

The system of the massless pole and the two segment athlete results in the following four degrees of freedom:

- X -coordinate of the center of mass of the segment representing the arms: X_{cm1}
- Y -coordinate of the center of mass of the segment representing the arms: Y_{cm1}
- The angle ϕ that determines the orientation of the first segment representing the arms relative to the vertical
- The angle θ that determines the orientation of the second segment representing the rest of the body relative to the first segment

The location of the center of mass of the second segment can be calculated from the state variables defined above.

$$X_{cm2} = X_{cm1} - l_2 \sin \phi - l_3 \sin(\phi + \theta) \quad (4.1)$$

$$Y_{cm2} = Y_{cm1} - l_2 \cos \phi - l_3 \cos(\phi + \theta) \quad (4.2)$$

The motion of both the athlete and pole can be described the athlete sub-model only. As the athlete holds the top end of the pole, the location of the wrists is also the location of the top end of the pole. The location of the top end of the pole can thus also be calculated with the state variables defined above.

$$X_{top} = X_{cm1} + l_2 \sin \phi + l_3 \sin(\phi + \theta) \quad (4.3)$$

$$Y_{top} = Y_{cm1} + l_2 \cos \phi + l_3 \cos(\phi + \theta) \quad (4.4)$$

Since the bottom end of the pole remains placed against the back end of the planting box during the vault the motion of the pole chord can be described by the top end of the pole only.

The next section will derive the equations of motion for the two segment athlete sub-model presented in figure 4.3.

4.4 Equations of Motion

The equations of motion are derived using a combination of the Newton-Euler method and Lagrange equations. Formulating the Newton-Euler equations is cumbersome as the position and orientation of every segment has to be defined as well as the constraints imposed on these coordinates. Besides, the solutions of the Newton-Euler method can have a large error when the equations of motions are numerically integrated (which often is the case due to the complexity of the differential equations).⁹

The Lagrange method solves this problem by imposing the constraints directly on coordinate level. This can be done by using a minimum set of independent generalized coordinates for which the constraints are naturally fulfilled. However, the symbolic computation of the partial derivatives requires significant computational time. (Schwab & van der Linde, 1997).

The drawbacks of both methods can be eliminated by using the independent generalized coordinates of the Lagrange method and the virtual power principle (using the d'Alembert principle) of the Newton-Euler method. The equations of motion for the athlete model

⁹For example joints might come apart and configurations might differ depending on the step size taken. (Schwab & van der Linde, 1997)

are derived using this combined method, also called TMT-method. The derivation is based on the work of Schwab and van der Linde (1997).

Each of the two segments shown in figure 4.2 has three degrees of freedom¹⁰. The position coordinates $X - Y$ of the center of gravity of each segment and the orientation angles ϕ and θ . The degrees of freedom are placed in a vector x_i .

Note that in the following equations the matrices and vectors are expressed in bold unless the matrix or vector can be recognized from the indices. A bold capital letter indicates a matrix and a bold smaller case letter a vector. Scalars remain indicated in italics.

$$x_i = \begin{bmatrix} X_{cm1} \\ Y_{cm1} \\ \phi \\ X_{cm2} \\ Y_{cm2} \\ \phi + \theta \end{bmatrix} \quad (4.5)$$

As this is a mechanical model, the motion for each degree of freedom can be described by the second law of Newton.

$$M_{ii}\ddot{x}_i = \Sigma f_i \quad (4.6)$$

The vector \ddot{x}_i is the second time derivative and thus contains the accelerations of the six degrees of freedom. Here the mass matrix M_{ii} is a diagonal matrix either containing the mass m or mass moment of inertia I of each segment, dependent on the degree of freedom (translational or rotational). The mass matrix is shown below.

$$M_{ii} = \begin{bmatrix} m_1 & & & & & \\ & m_1 & & & & \\ & & I_1 & & & \\ & & & m_2 & & \\ & & & & m_2 & \\ & & & & & I_2 \end{bmatrix} \quad (4.7)$$

The force vector f_i contains the summation of all the forces and constraint conditions on each degree of freedom. The exact formulation of this vector will be established in the independent generalized coordinates later on.

The previous paragraph mentions generalized coordinates. Not all six variables defined in \mathbf{x}_i are required to determine the complete motion of the athlete. Two of the variables are redundant (or dependent on the other variables). The generalized coordinates are the minimum degrees of freedom required to describe the complete motion of the system. As

¹⁰Three degrees of freedom as the motion is 2-dimensional

already shown in section 4.3.3, the $X - Y$ coordinates of segment two can be expressed in terms of x_{cm1} , y_{cm1} , ϕ and θ as follows.

$$g_i = \begin{bmatrix} x_{cm1} \\ y_{cm1} \\ \phi_1 \\ x_{cm2} \\ y_{cm2} \\ \phi_2 \end{bmatrix} = \begin{bmatrix} x_{cm1} \\ y_{cm1} \\ \phi \\ x_{cm1} - l_2 \sin(\phi) - l_3 \sin(\phi + \theta) \\ y_{cm1} - l_2 \cos(\phi) - l_3 \cos(\phi + \theta) \\ \phi + \theta \end{bmatrix} \quad (4.8)$$

Thus the six degrees of freedom can be described by four independent degrees of freedom. These four are the independent generalized coordinates. This seems obvious and was already defined in section 4.3.3. However, the notation using six degrees of freedom increases the understanding on how the equations of motion are derived. The four independent degrees of freedom are placed in the vector q_j .

$$q_j = \begin{bmatrix} x_{cm1} \\ y_{cm1} \\ \phi \\ \theta \end{bmatrix} \quad (4.9)$$

The velocities \dot{x}_i can also be described by these four variables using a kinematic transformation matrix T_{ik} . The kinematic transformation is formulated as follows.

$$T_{ik} = \frac{\partial g_i}{\partial q_k} = \begin{bmatrix} 1 & 0 & 0 & 0 \\ 0 & 1 & 0 & 0 \\ 0 & 0 & 1 & 0 \\ 1 & 0 & -l_2 \cos(\phi) - l_3 \cos(\phi + \theta) & -l_3 \cos(\phi + \theta) \\ 0 & 1 & l_2 \sin(\phi) + l_3 \sin(\phi + \theta) & l_3 \sin(\phi + \theta) \\ 0 & 0 & 1 & 1 \end{bmatrix} \quad (4.10)$$

The velocities \dot{x}_i can now be described by the four independent variables using this transformation matrix T_{ik} .

$$\dot{x}_i = T_{ik} \dot{q}_k \quad (4.11)$$

The transformation of the accelerations \ddot{x}_i can be derived in a similar way.

$$\ddot{x}_i = \frac{\partial g_i}{\partial q_l} \ddot{q}_l + \frac{\partial^2 g_i}{\partial q_m \partial q_p} \dot{q}_m \dot{q}_p \quad (4.12)$$

The second term is also known as the convective acceleration h_i . The complete expression is shown in appendix A.

$$h_i = \frac{\partial^2 g_i}{\partial q_m \partial q_p} \dot{q}_m \dot{q}_p \quad (4.13)$$

Observe that the Jacobian $\frac{\partial g_i}{\partial q_l}$ (or transformation matrix T_{il}) is equal to the transformation matrix T_{ik} that converts \dot{q}_k to \dot{x}_i . Actually the subscript k, l, m and p are all equal in magnitude to j .

The expression for the accelerations can be rewritten to the following if these expressions are substituted.

$$\ddot{x}_i = T_{ij}\ddot{q}_j + h_i \quad (4.14)$$

These expression of the coordinates, velocities and accelerations in the generalized independent variables will be substituted in the virtual power equation.

Newton's second law, as stated in equation 4.6, can be rewritten in the d'Alembert form as follows.

$$\Sigma f_i - M_{ii}\ddot{x}_i = 0 \quad (4.15)$$

The d'Alembert form essentially changes the dynamic situation to a static situation. The system is now in equilibrium by the action of the real forces Σf_i and the fictitious force $-M_{ii}\ddot{x}_i$. This fictitious force is also called inertial force or d'Alembert force. Together, the d'Alembert form of the second law of Newton and the virtual velocities $\delta\dot{x}_i$ yield the virtual power equation.

$$\delta\dot{x}_i (\Sigma f_i - M_{ii}\ddot{x}_i) = 0 \quad (4.16)$$

The virtual velocity $\delta\dot{x}_i$ can be transformed to the independent coordinates in a similar way as was done for the velocity \dot{x}_i .

$$\delta\dot{x}_i = T_{ij}\delta\dot{q}_j \quad (4.17)$$

Substitute this expression in the virtual power equation 4.16.

$$T_{ij}\delta\dot{q}_j (\Sigma f_i - M_{ii}\ddot{x}_i) = 0 \quad (4.18)$$

Next substitute the transformed expression of the accelerations of equation 4.14.

$$T_{ij}\delta\dot{q}_k (\Sigma f_i - M_{ii}(T_{ij}\ddot{q}_j + h_i)) = 0 \quad (4.19)$$

Since the generalized coordinates are independent, so are the virtual velocities. So each k equation must be zero. This means:

$$T_{ij}^T (\Sigma f_i - M_{ii}(T_{ij}\ddot{q}_j + h_i)) = 0 \quad (4.20)$$

This equation can be solved for the generalized independent accelerations \ddot{q}_k .

$$T_{il}M_{ij}T_{jk}\ddot{q}_k = T_{il}(\Sigma f_i - M_{ij}h_j) \quad (4.21)$$

The combined force vector Σf_i can be split into a part containing the external forces acting on the athlete-pole system and a part containing internal forces of the athlete-pole system. The internal forces are the pole forces acting on the athlete and the gravity forces. The internal forces are placed in the vector f_i and can be defined as follows:

$$f_i = \begin{bmatrix} R_n \cos \eta + R_t \sin \lambda \\ R_n \sin \eta + R_t \cos \lambda - m_1 g \\ l_1 R_n \cos(\phi + \lambda) + l_2 R_t \sin(\phi + \lambda) \\ 0 \\ -m_2 g \\ 0 \end{bmatrix} \quad (4.22)$$

where the angle λ is the slope between the pole chord and the horizontal (as shown in figure 4.4). The derivation of the equations for the pole forces R_n and R_t is given in the next section.

The external forces are the control torques defined in section 4.3.2. These are inputs and do not need to be transformed. The control torques can be added directly to the right hand side of the equations. Using the sign convention as shown in figure 4.3 the external forces (control inputs) are defined as follows.

$$y = \begin{bmatrix} 0 \\ 0 \\ -M_1 \\ M_2 \end{bmatrix} \quad (4.23)$$

Substituting these expressions for the combined force vector results in the following system of equations of motion.

$$T_{il}M_{ij}T_{jk}\ddot{q}_k = y_l + T_{il}(\Sigma f_i - M_{ij}h_j) \quad (4.24)$$

The equations of motion consist of a system of four equations. By using the TMT-method the equations of motion are expressed such that these can be easily solved numerically. Only the transformation matrix T_{ij} has to be computed symbolically, hence the computational time is reduced compared to the Lagrange method. All the values for the force vector and mass matrix can be defined for each body. In this way an overview is maintained. Finally, the equations of motion can be numerically integrated without the problems encountered in the Newton-Euler method as the constraints are defined in the generalized independent coordinates via the transformation matrix T_{ij} .

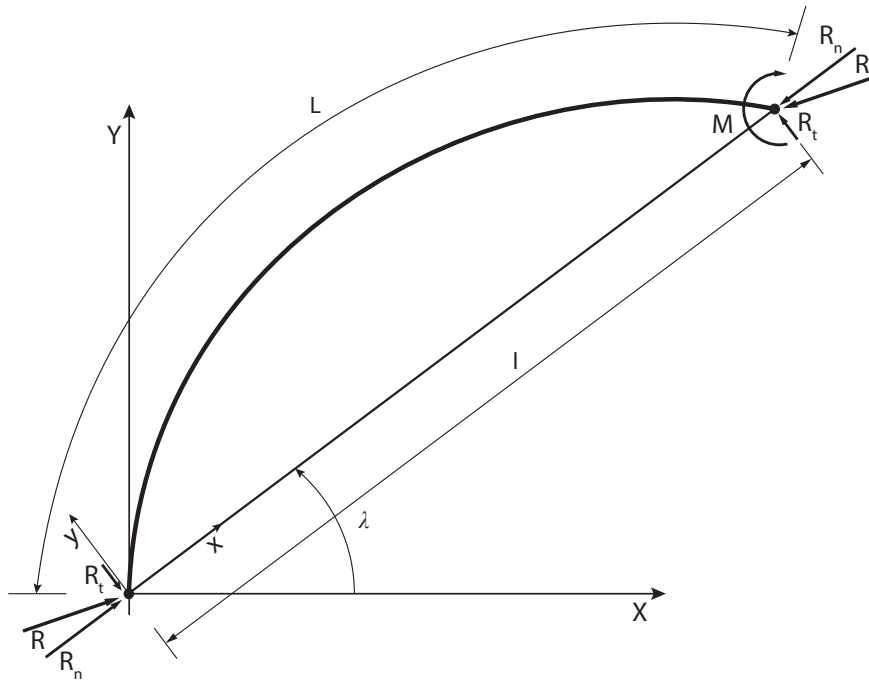


Figure 4.4: Schematic diagram of the pole

4.5 Pole Sub-Model

The pole sub-model calculates the pole forces R_n and R_t required for the equations of motion for the athlete. The pole sub-model also calculates the deformed shape of the pole. The internal forces and moments of the pole can then in turn be determined from the deformed shape.

The pole is subjected to a compressive force R and an applied moment M at the top end of the pole. The compressive force is an internal force of the athlete-pole system, while the applied moment is external to the system and defined as a control input in section 4.1. A schematic diagram of the massless pole is given in figure 4.4. In the figure the global coordinate system $X - Y$ is shown. In addition a local coordinate system $x - y$ is defined for the pole. The origin is defined at the bottom end of the pole. The x -axis is aligned with the pole chord axis (shortest distance between the two ends of the pole). The positive axis points in the direction of the top end of the pole. The y -axis is perpendicular to the x -axis and positive pointing upwards.

Because the pole is placed free against the back end of the planting box, no moment can be transferred at this point. The applied moment at the top end generates a tangential force R_t at the bottom end of the pole.

$$R_t = -M/l \quad (4.25)$$

In order to maintain force equilibrium, there is an equal but opposite tangential force at the top end of the pole. The tangential force helps the rotation of the pole to a vertical position. The tangential force is a component of the total compressive force R . The other component is the normal force R_n , which is aligned with the pole chord. The link between the tangential force and the applied moment also causes that the total compressive force R and normal force R_n are a function of the applied moment.

The applied moment M was defined as a control input in section 4.1. Furthermore the location of the top end of the pole is determined in the athlete sub-model with equations 4.3 and 4.4. The pole length and pole stiffness are defined to be system properties and are also inputs of the model. A solution has to be found that can determine the forces R_n and R_t from these inputs. In addition, the solution should take into account the large deformations of the pole. Measurements during a vault demonstrate that the pole chord length l can almost be half the total pole length ($l = 0.6L$).

No elastica solution exists for a slender pole loaded by a compressive force and an applied moment at one end with large deformations. However, elastica solutions exist for the simpler case when the slender pole is subjected to a compressive force R only (Love, 1944; Southwell et al., 1941). The shape of a slender pole loaded by a compressive force can be calculated analytically when the compressive force R and the slope γ of the pole at the origin relative to the compressive force direction R are known (see figure 4.5). The compressive force R and the slope γ are yet unknown. Hubbard (1980b) uses this simpler case to solve the shape of a pole loaded by a compressive force and a moment applied at one end. Consider a slender pole subjected to a compressive force only that is cut at some point. This internal point is loaded by an internal normal reaction force N , internal tangential force T and internal moment M as is illustrated in figure 4.5. The load case for the left segment of the cut is similar to that of the pole in figure 4.4, only the compressive force is now split into the components N and T . If the compressive force R and the slope γ are given as input the internal moment M' , the chord length l' and the arclength s can be calculated for this cutting point. The compressive force R and the slope γ can be varied until M' , l' and s are equal to the applied moment M , chord length l and total pole length L given as input. The detailed derivation of this will be given below.

First the derivation is presented for the elastica solution for a slender pole loaded by a compressive force only. Second, the numerical iterative solution is given that can be used to determine the pole forces R_t , R_n and the shape for a slender pole loaded by a compressive force and an applied moment at one end.

4.5.1 Elastica Solution for a Slender Pole under Compression

The goal of the analytical solution is to determine the shape of a slender pole for a given compressive load R and a slope γ . The derivation of this analytical solution is based on the works of Love (1944) and Southwell et al. (1941).

For the derivation a second local coordinate system $x'-y'$ is defined for the pole loaded by a compressive force only. The x' -axis is aligned with the direction of the compressive force R . The positive axis points to the right. The y' -axis is perpendicular to the x' -axis and positive pointing upwards. The origin is defined in the middle of the chord length for the pole loaded by a compressive force only. The global and local coordinate system are

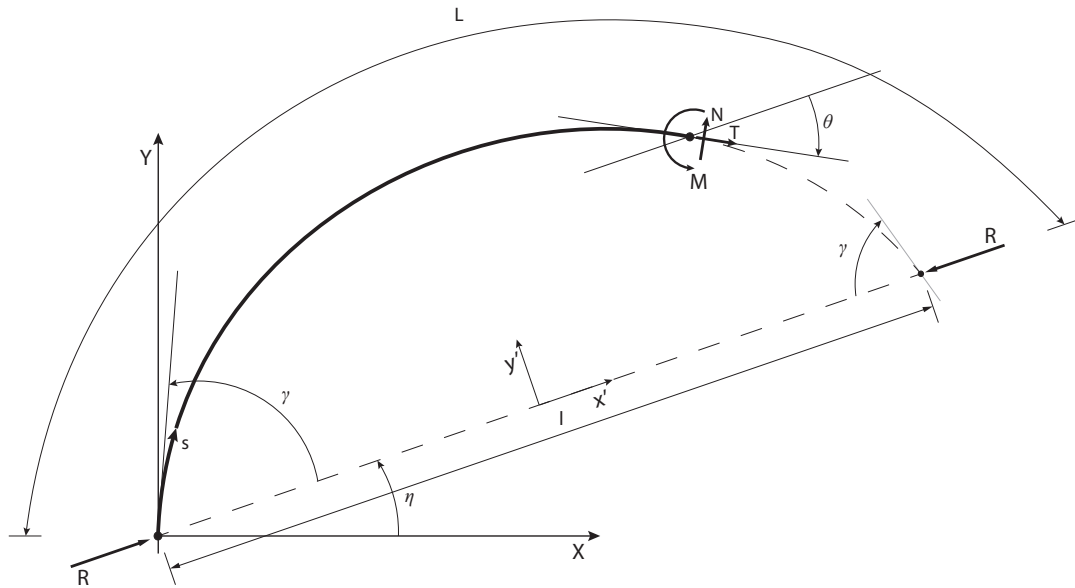


Figure 4.5: Schematic of a slender subjected to a compressive load

shown in figure 4.5. The angle between the pole chord of the pole loaded by a compressive force only and the global X axis is defined as η .

Love (1944) starts the derivation from the internal equilibrium equations. The equilibrium equations can be set up for the cutting point shown in figure 4.5.

$$\begin{aligned}
 T &= -R \cos \theta \\
 N &= -R \sin \theta \\
 \frac{dM}{ds} + N &= 0
 \end{aligned}
 \tag{4.26}$$

where θ is the angle between the local x' -axis and the line tangent to the central line of the pole at the cross-section. The distance measured along the central line of the pole is defined as the arclength s (Southwell et al., 1941).

Southwell et al. (1941) and Love (1944) recognized that the elastica problem can be solved with elliptic functions. The equilibrium equations formulated above, can be rewritten to include expressions of elliptic integrals.

Elliptic Integrals

The form of the elliptic integrals have to be known in order to rewrite the equilibrium equations into this form. There are several types of elliptic integrals. For the derivation of the elastica solution the elliptic integral of the first kind and the elliptic integral of the

second kind are required. Hence, only the definitions of these elliptic integrals are given here. The elliptic integral of the first kind is defined as follows.

$$K(k, \varphi) = \int_0^\varphi \frac{1}{\sqrt{1 - k^2 \sin^2 \phi}} d\phi \quad (4.27)$$

and the elliptic integral of the second kind is defined as

$$E(k, \varphi) = \int_0^\varphi \sqrt{1 - k^2 \sin^2 \phi} d\phi \quad (4.28)$$

The variable k is called the elliptic modulus and is defined as

$$k = \sin \frac{1}{2} \gamma \quad (4.29)$$

where the variable γ is the angle of the line tangent to the pole at the global origin and the local x' -axis as shown in figure 4.5.

As can be seen in the elliptic integrals, the distance along the arc of the ellipse is defined by the variable ϕ . It is a transformed variable of γ and θ . The transformation is defined as follows

$$\sin \phi = \frac{\sin \frac{1}{2} \theta}{\sin \frac{1}{2} \gamma} \quad (4.30)$$

Substituting the elliptic modulus k , the equation can be rewritten.

$$k \sin \phi = \sin \frac{1}{2} \theta \quad (4.31)$$

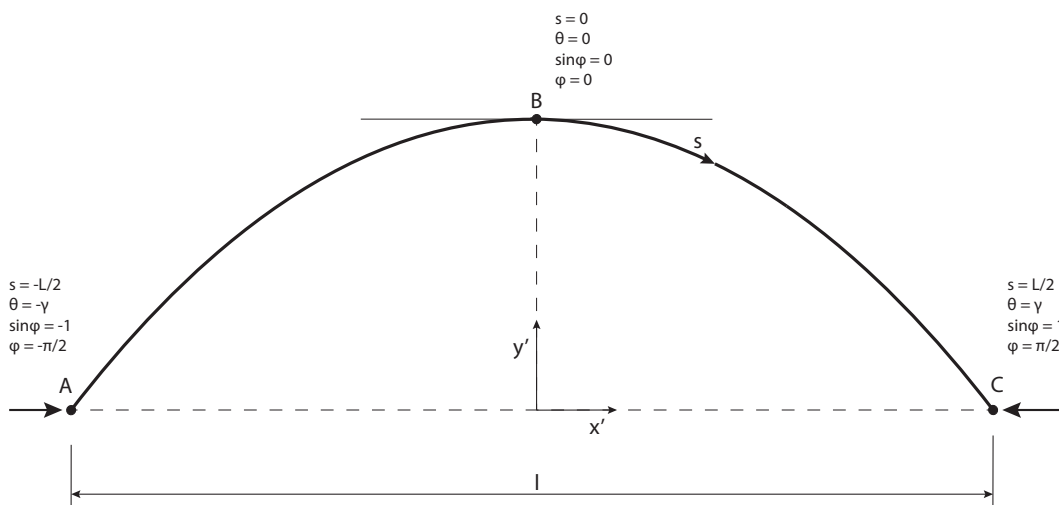


Figure 4.6: Definition of ϕ

In essence ϕ is similar to the variable θ defined above only the reference frame is defined differently as is shown in figure 4.6. No matter the angle γ of the pole at the global origin, at this point the variable ϕ is always $-\pi/2$. Similar at the other end point $\phi = \pi/2$. At point B, where the maximum deflection is achieved, $\phi = 0$. The transformation is done to normalize the elliptic integral. The upper limit of the elliptic integral is defined by φ . The end point C has the same angle γ relative to the horizontal when $\varphi = \pi/2$. The ellipse is then symmetrical. The elliptic integrals for the upper limit of $\varphi = \pi/2$ are also called the complete elliptic integrals of the first and second kind. However, φ can also be larger or smaller than $\pi/2$ or $-\pi/2$.

The expressions found for the elliptic integrals and the variables introduced in this section will be used in the derivation below to obtain expressions for the shape of the deformed pole.

Derivation of Arc Length

The derivation of Southwell et al. (1941) rewrites the equilibrium equations established in equation 4.26 as expressions of the elliptic integrals above. The shape of the pole is defined by the term ds in the equilibrium equation. However, we do not yet know what the function of ds looks like. The goal is to find an expression for ds as a function of the variables k and ϕ (see section above). However, this takes several steps and cannot be done at once. The first step is to derive an expression for ds as a function of the variables θ and s .

The elastica solution assumes that the bending moment is linear over the change in curvature. Love (1944) defines this as follows.¹¹

$$M = -B \left(\frac{d\theta}{ds} \right) \quad (4.32)$$

where B is the bending stiffness (EI) of the pole.¹² The expression found for M can be substituted in the moment equilibrium shown in equation 4.26 (Love, 1944).

$$\frac{d(-B \left(\frac{d\theta}{ds} \right))}{ds} + N = 0 \quad (4.33)$$

Next a new expression can be found for the normal force N , by solving this equation for N .

$$N = B \left(\frac{d^2\theta}{ds^2} \right) \quad (4.34)$$

¹¹Note that for small deflections the curvature is expressed as d^2y/dx^2 , while for larger deflections the curvature is expressed as $d\theta/ds$.

¹²The bending stiffness is for now assumed constant but a variable stiffness along the pole length can be implemented by making B a function of s .

The normal force is now expressed as a function of the variables θ and s and the system property B . Substitute this expression of N in the normal force equilibrium equation shown in equation 4.26.

$$B \left(\frac{d^2\theta}{ds^2} \right) + R \sin \theta = 0 \quad (4.35)$$

This is the equation for s we wanted to accomplish. The arclength s is a function of the variables θ and s and the inputs B and R . However, along the way, we ended up with the second derivative of θ with respect to s . To obtain an expression for ds , this equation can be integrated with respect to θ .

$$\frac{1}{2}B \left(\frac{d\theta}{ds} \right)^2 - R \cos \theta = C \quad (4.36)$$

where C is a constant of integration. As shown in figure 4.5, γ is the value of θ at the global origin ($s = 0$). When this condition is substituted in equation 4.36 the term $d\theta/ds$ vanishes. The equation can then be solved for the integration constant C .

$$C = -R \cos \gamma \quad (4.37)$$

So equation 4.36 can be rewritten as

$$\frac{1}{2}B \left(\frac{d\theta}{ds} \right)^2 - R \cos \theta = -R \cos \gamma \quad (4.38)$$

or even

$$\left(\frac{d\theta}{ds} \right)^2 = \frac{2R}{B} (\cos \theta - \cos \gamma) \quad (4.39)$$

The next step is a trick to rewrite the equation such that in the following steps the elliptic integral variables k and ϕ can be easily substituted. Therefore equation 4.39 is rewritten using the double angle formula.¹³

$$\left(\frac{d\theta}{ds} \right)^2 = \frac{4R}{B} \left(\sin^2 \frac{1}{2}\gamma - \sin^2 \frac{1}{2}\theta \right) \quad (4.40)$$

Now the variables k and ϕ can be substituted. Substitute the expressions found in equation 4.29 and equation 4.31 into equation 4.40.

$$\left(\frac{d\theta}{ds} \right)^2 = \frac{4R}{B} (k^2 - k^2 \sin^2 \phi) \quad (4.41)$$

¹³The double angle formula is given in appendix B.

Unfortunately we are still left with the $d\theta$ term on the left hand side. This term can also be expressed in the variables ϕ and k . However, to do this it is first convenient to rewrite equation 4.41 a little. Therefore we solve for $\frac{d\theta}{ds}$:

$$\frac{d\theta}{ds} = \sqrt{\frac{R}{B}} 2k \sqrt{1 - \sin^2 \phi} \quad (4.42)$$

and use the Pythagorean identity to rewrite this equation to¹⁴

$$\frac{d\theta}{ds} = \sqrt{\frac{R}{B}} 2k \cos \phi \quad (4.43)$$

The term $d\theta$ can now be expressed in the variable ϕ by differentiating the relation found for ϕ and θ in equation 4.31.

$$k \cos \phi d\phi = \frac{1}{2} \cos \frac{1}{2} \theta d\theta \quad (4.44)$$

Solve for $d\theta$.

$$d\theta = \frac{2k \cos \phi}{\cos \frac{1}{2} \theta} d\phi \quad (4.45)$$

This is still not completely what we wanted. The variable $d\theta$ is still also a function of θ . However, as it turns out, the variable θ can be easily substituted for an expression of k and ϕ in the last step of the derivation. Therefore, it is left in place for now. Substitute equation 4.45 into equation 4.43.

$$\frac{2k \cos \phi}{\cos \frac{1}{2} \theta} \frac{d\phi}{ds} = \sqrt{\frac{R}{B}} 2k \cos \phi \quad (4.46)$$

This expression can be simplified to

$$\frac{d\phi}{ds} = \sqrt{\frac{R}{B}} \cos \frac{1}{2} \theta \quad (4.47)$$

and solved for ds . The cosine term can now be rewritten to a sine function using the Pythagorean identity. This transformation is desired as the sine term of θ can then be substituted with the elliptic integral variables k and ϕ .

$$ds = \frac{d\phi}{\sqrt{\frac{R}{B}} \cos \frac{1}{2} \theta} = \sqrt{\frac{B}{R}} \frac{d\phi}{\sqrt{1 - \sin^2 \frac{1}{2} \theta}} \quad (4.48)$$

¹⁴The Pythagorean identity is also given in appendix B.

Now substitute the expression found in equation 4.31 for $\sin^2 \theta$.

$$ds = \sqrt{\frac{B}{R}} \frac{d\phi}{\sqrt{1 - k^2 \sin^2 \phi}} \quad (4.49)$$

This is the desired result as mentioned at the beginning of this subsection. The next step is to integrate this equation to obtain an equation for the arclength s .

$$s = \sqrt{\frac{B}{R}} \int_0^\varphi \frac{1}{\sqrt{1 - k^2 \sin^2 \phi}} d\phi \quad (4.50)$$

The integral on the right hand side is the elliptic integral of the first kind K as defined in equation 4.27. Using this expression the arclength can be defined as follows.

$$s = \sqrt{\frac{B}{R}} K(k, \varphi) \quad (4.51)$$

The half arc length can be calculated by substituting $\varphi = \pi/2$ in the previous equation.¹⁵ As the shape is symmetrical (only for the case when the pole is loaded by a compressive force only) the total arc length can be computed by multiplying the half arc length by two. So the total arc length can be described as follows.

$$L = \sqrt{\frac{B}{R}} 2K(k, \pi/2) \quad (4.52)$$

Derivation Curve Shape

To determine the shape of the curve, let x' and y' be the coordinates of a point referred to in the local coordinate system as shown in figure 4.5. Love (1944) derives the the position coordinates x' and y' from the following definitions for dx and dy .

$$\begin{aligned} \frac{dx}{ds} &= \cos \theta \\ \frac{dy}{ds} &= \sin \theta \end{aligned} \quad (4.53)$$

Again we want to obtain an expression of x in the form of the elliptic integrals with the variables k and ϕ . Therefore, ds is rewritten in terms of ϕ and k .

To determine x' substitute the expression found in equation 4.48 for ds (in terms of θ) into equation 4.53 and solve for dx' .

$$dx' = \cos \theta ds = \sqrt{\frac{B}{R}} \cos \theta \frac{1}{\cos \frac{1}{2}\theta} d\phi \quad (4.54)$$

¹⁵It is only half the arc length as the lower limit of the integral is 0, which corresponds to the middle of the pole (see figure 4.6).

Next the cosine terms are rewritten to sine terms using the double angle formula and Pythagorean identities. The reason for this is that then the sine term of θ can be substituted with a sine function of k and ϕ found in equation 4.31.

$$dx' = \sqrt{\frac{B}{R}} \frac{1 - 2 \sin^2 \frac{1}{2}\theta}{\sqrt{1 - \sin^2 \frac{1}{2}\theta}} d\phi \quad (4.55)$$

Now substitute the expression found in equation 4.31.

$$dx = \sqrt{\frac{B}{R}} \frac{1 - 2k^2 \sin^2 \phi}{\sqrt{1 - k^2 \sin^2 \phi}} d\phi \quad (4.56)$$

The expression for dx can be rewritten in the following way to obtain elliptic integral expressions. This is purely a mathematical procedure.

$$\begin{aligned} dx' &= \sqrt{\frac{B}{R}} \frac{2 - 2k^2 \sin^2 \phi - 1}{\sqrt{1 - k^2 \sin^2 \phi}} d\phi \\ &= \sqrt{\frac{B}{R}} \frac{2(1 - k^2 \sin^2 \phi) - 1}{\sqrt{1 - k^2 \sin^2 \phi}} d\phi \\ &= \sqrt{\frac{B}{R}} \frac{2\sqrt{1 - k^2 \sin^2 \phi} \sqrt{1 - k^2 \sin^2 \phi} - 1}{\sqrt{1 - k^2 \sin^2 \phi}} d\phi \\ &= \sqrt{\frac{B}{R}} 2\sqrt{1 - k^2 \sin^2 \phi} d\phi - \sqrt{\frac{B}{R}} \frac{1}{\sqrt{1 - k^2 \sin^2 \phi}} d\phi \end{aligned} \quad (4.57)$$

Integrate the final expression found for dx' .

$$x = \sqrt{\frac{B}{R}} \left(2 \int_{\pi/2}^{\varphi} \sqrt{1 - k^2 \sin^2 \phi} d\phi - \int_{\pi/2}^{\varphi} \frac{1}{\sqrt{1 - k^2 \sin^2 \phi}} d\phi \right) \quad (4.58)$$

The second term between brackets is again equal to the elliptic integral of the first kind K as defined in equation 4.27. The first term is equal to elliptic integral of the second kind E as defined in equation 4.28. The equation can be rewritten as follows.

$$x = \sqrt{\frac{B}{R}} (2E(k, \varphi) - K(k, \varphi)) \quad (4.59)$$

The expression for y' can be found with a similar method. Substitute the expression found in equation 4.48 for ds into equation 4.53 and solve for dy' .

$$dy' = \sqrt{\frac{B}{R}} \sin \theta \frac{1}{\cos \frac{1}{2}\theta} d\phi \quad (4.60)$$

Rewrite using the double angle formula. The reason for this is to simplify the equation.

$$dy' = \sqrt{\frac{B}{R}} 2 \cos \frac{1}{2}\theta \sin \frac{1}{2}\theta \frac{1}{\cos \frac{1}{2}\theta} d\phi = \sqrt{\frac{B}{R}} 2 \sin \frac{1}{2}\theta d\phi \quad (4.61)$$

Again the sine term of θ can be substituted with the sine term of k and ϕ found in equation 4.31.

$$dy' = \sqrt{\frac{B}{R}} 2k \sin \phi d\phi \quad (4.62)$$

Now the expression found for dy' can be integrated.

$$y' = -\sqrt{\frac{B}{R}} 2k \cos \phi \quad (4.63)$$

The expression found for x' and y' in equation 4.59 and 4.63 are the analytical solution for slender pole loaded by a compressive force only. Now, given a slope γ and a compressive load R , the shape of the pole can be determined by varying ϕ and computing the x' and y' positions for each ϕ (using equation 4.59 and 4.63).¹⁶ Various kind of large deflections can be described by these equations and are shown in appendix C.

4.5.2 Numerical Iterative Solution for Combined Load

As discussed in the beginning of this section, Hubbard (1980b) uses the elastica solution of the simpler case derived above to formulate a numerical iterative solution for a slender pole subjected to a compressive load and an applied moment at one end. This is the load case of the pole vaulting pole shown in figure 4.4.

His solution starts by imagining a fictitious pole. The fictitious pole is chosen such that the orientation of the pole chord is parallel to the direction of the total compressive force R . As a result, the moment at the top end of the pole vanishes and the pole is loaded by a compressive force only. The fictitious pole is thus identical to the analytical solution described in the previous section. An example of such an imagined fictitious rod is shown in figure 4.7 by the dashed line.

The real pole can be seen as a part of the fictitious rod. If the fictitious pole is cut at some point, this internal point is loaded by an internal normal reaction force N , internal tangential force T and internal moment M' . This load case is similar as for the real pole. The pole forces and deflection of the real pole will be similar when the cutting point is at an arclength equal to that of the total length of the pole $s = L$, the bending stiffness B of the fictitious pole is equal to that of the real pole, the internal moment M' is equal to the moment applied by the athlete M and the pole chord length l' for this cutting point is equal to that of the real pole chord length l . These four variables (B , L , M and l) are the inputs for the numerical iterative solution.

¹⁶Note that the total pole length varies for different combinations of R and γ . This is not a constant.

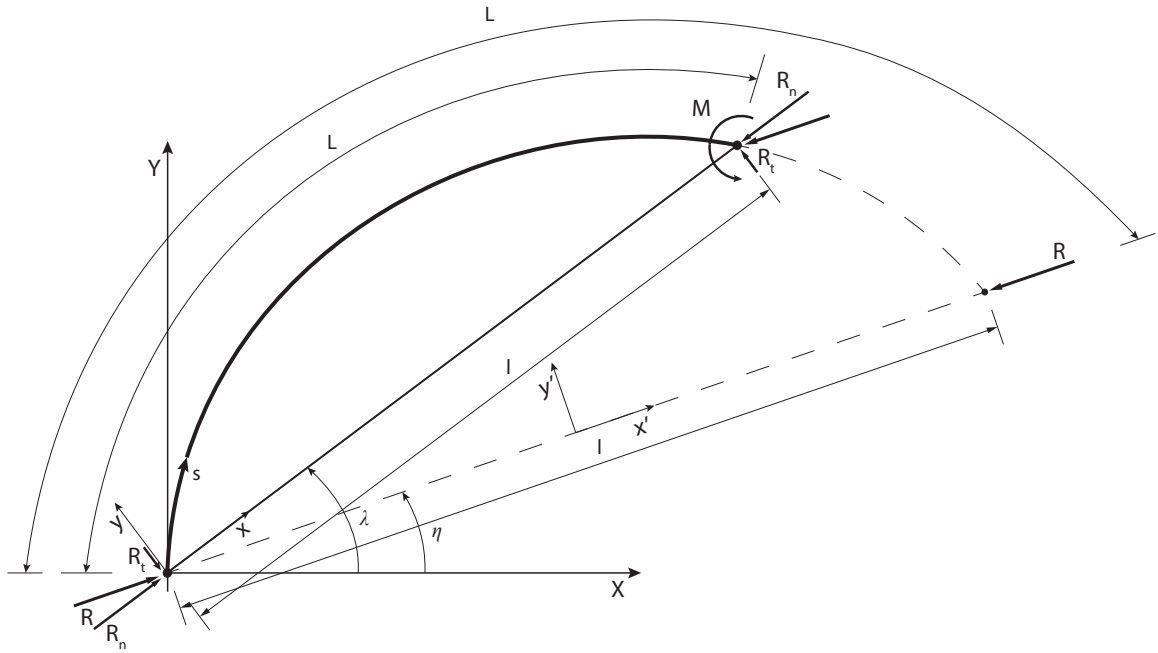


Figure 4.7: Schematic diagram of the pole and fictitious pole

The shape of the pole subjected to a compressive force only can be determined for a given slope γ and compressive load R . However, these two variables are still unknown. The numerical iterative solutions starts with an initial value for the compressive force R and the slope γ . Next, the location of the cutting point at $s = L$ has to be determined. This can be done with the $x' - y'$ position coordinates equations 4.59 and 4.63 derived for the simpler case.¹⁷ The variable φ for an arclength $s = L$ can be calculated using the ratio of the real pole length divided by the fictitious pole length L' .

$$\varphi = \pi \frac{L}{L'} - \frac{\pi}{2} \quad (4.64)$$

where total length L' of the fictitious pole can be calculated using equation 4.52. This value for φ can be substituted in equations 4.59 and 4.63 to determine the location of the top end of the pole based on the initial values chosen for R and γ .

The internal moment M' and chord length l' can be calculated for the top end of the pole as follows.

$$M' = Ry' \quad (4.65)$$

$$l' = \sqrt{x'^2 + y'^2} \quad (4.66)$$

¹⁷The coordinates are calculated in the local coordinate system $x' - y'$ of the fictitious pole

The internal moment M' and compressed length l' are based on the initial choice of the compressive force R and slope γ and will almost surely not be equal to the defined inputs for M and l . Using the pre-programmed non-linear system solver 'fsolve' in MATLAB 2013, the system of two equations as defined in equations 4.65 and 4.66 can be solved. The initial choice for the compressive force R and the slope γ is updated using the thrust-region dogleg algorithm. The values are updated until the values for M' and l' are arbitrarily close to the input M and l . This numerical iterative procedure makes sure that the left hand segment of arclength $s = L$ is exactly equal to the real pole for its shape, reaction forces and applied moment.

The complete shape of the real pole only has to be calculated at the end of the numerical iterative solution, this does not have to be done for each guess (as only the location of the top end of the beam is required to compute M' and l'). The shape of the real pole can be computed using the analytical solution for the simpler case. The only difference is that the real pole is a segment of the fictitious pole. As a result the upper boundary for ϕ is limited to the value it has at $s = L$ (see equation 4.64). So the shape of the real pole can be determined by the following equations.

$$\begin{aligned} x' &= \sqrt{\frac{B}{R}} (2E(k, \varphi) - K(k, \varphi)) & -\frac{\pi}{2} \leq \varphi \leq \pi \frac{L}{L'} - \frac{\pi}{2} \\ y' &= -\sqrt{\frac{B}{R}} 2k \cos \varphi & -\frac{\pi}{2} \leq \varphi \leq \pi \frac{L}{L'} - \frac{\pi}{2} \end{aligned} \quad (4.67)$$

Where the final values for R and γ , as determined by the numerical iterative solution, are used.

The normal and tangential components of the compressive force can be determined from the total compressive force. At the beginning of this section the tangential force was defined as

$$R_t = \frac{-M}{l} \quad (4.68)$$

The normal component of the reaction force can then be determined using the Pythagorean theorem.

$$R_n = \sqrt{R^2 - R_t^2} \quad (4.69)$$

The normal and tangential components of the compressive force need to be substituted in the internal force vector f_i of the equations of motion for the two segment athlete shown in equation 4.22.

4.6 Runge-Kutta

Now that the normal and tangential components of the compressive force have been determined in the previous section, the equations of motion derived in section 4.4 shown

in equation 4.24 can be integrated with respect to time. The non-linear system is too complex to solve analytically, but can be easily solved using numerical integration schemes.

It was chosen to use the Runge-Kutta fourth order numerical integration scheme as it is straightforward to use and accurate enough for most problems (Boyce et al., 1969). The Runge-Kutta formula approximates the solution with a weighted average of values of $f(t, y)$ at different points between the time intervals t_i and $t_i + h$ (where h is the step size). For a first order problem the weighted average is given by

$$y_{n+1} = y_n + h \left(\frac{k_{n1} + 2k_{n2} + 2k_{n3} + k_{n4}}{6} \right) \quad (4.70)$$

where

$$\begin{aligned} k_{n1} &= f(t_n, y_n) \\ k_{n2} &= f\left(t_n + \frac{1}{2}h, y_n + \frac{1}{2}hk_{n1}\right) \\ k_{n3} &= f\left(t_n + \frac{1}{2}h, y_n + \frac{1}{2}hk_{n2}\right) \\ k_{n4} &= f(t_n + h, y_n + hk_{n3}) \end{aligned} \quad (4.71)$$

The term in between brackets can be seen as the average slope. The term k_{n1} approximates the slope at the left end of the time interval, both k_{n2} and k_{n3} approximate the slope at the midpoint of the interval and k_{n4} approximates the slope at the right end of the time interval.

There are always two fundamental sources of error when using a numerical iteration scheme to approximate a solution. First, there is a round-off error as the computer can only store a finite number of digits. Secondly, if the round-off error is neglected, there is a difference between the exact solution and the approximated solution. This is called the local truncation error. For the fourth order Runge-Kutta method this error is equal to h^5 . Note that this error accumulates each time step as it is based on the previous value which already has an error.

The fourth order Runge-Kutta method described above can be used to solve first order differential equations only. The system of four second order differential equations derived in section section 4.4 has to be rewritten to a system of eight first order differential equations. For this, four new variables are defined v_x , v_y , ω_1 and ω_2 . These variables are related to the first order time derivatives of the current four state variables as follows.

$$\begin{bmatrix} v_x \\ v_y \\ \omega_1 \\ \omega_2 \end{bmatrix} = \begin{bmatrix} \dot{X} \\ \dot{Y} \\ \dot{\phi} \\ \dot{\theta} \end{bmatrix} \quad (4.72)$$

These four equations are added to the existing system of four equations given in equation 4.24. Now the second time derivative of the four state variables can be substituted with the first time derivative of the four new variables introduced above. The second time derivative of the X position is for example replaced with the first order time derivative

of the velocity v_x . And the second time derivative of the angle ϕ is for example replaced with the first order time derivative of the angular velocity w_1 . The result is a system of eight first order differential equations. This can be solved using the fourth order Runge-Kutta method as described in this section. To solve the system of differential equations initial conditions for X , Y , ϕ , θ , v_x , v_y , ω_1 and ω_2 have to be given as input. The initial conditions represent the conditions at take-off and form the third set of inputs beside the system properties and the control inputs.

4.7 Fly-Away Phase

Finally, the motion during the fly-away phase has to be determined. As discussed in section 4.2 the fly-away phase is simplified using an energetic approach. For this phase we are only interested in the peak height of the athlete and at what x location the athlete reaches this peak height.¹⁸

The maximum height is reached when all the vertical kinetic energy at pole release is converted into potential energy. The change in height Δh can then be calculated as follows.

$$\Delta h = \frac{mv_y^2}{2mg} = \frac{v_y^2}{2g} \quad (4.73)$$

This change in height Δh is added to the height the athlete has at pole release. To determine the maximum height the height has to be corrected for the depth of the planting box. The origin of the global coordinate system is defined to be at ground level above the deepest point of the planting box. The deepest point of the planting box is 20 [cm] below ground level. The maximum height can thus be determined as follows.

$$h_{max} = Y_{cm1}(t_{end}) + \Delta h - 0.2 \quad (4.74)$$

The change in horizontal position ΔX can also be easily calculated by multiplying the time to maximum height after pole release Δt with the horizontal velocity v_x .

$$\Delta X = v_x \Delta t \quad (4.75)$$

The time to maximum height after pole release can be determined using the following equation.

$$\Delta t = \frac{v_y}{g} \quad (4.76)$$

The change in horizontal position ΔX should be subtracted from the horizontal position at pole release. The horizontal position at the time when the athlete reaches maximum height should be within 80 [cm] of the planting box at the side of the landing mat.

¹⁸It is assumed that if the athlete releases the pole under feasible conditions (no high rotational velocities, athlete is in an vertical inverted position) he can always follow his normal technique to negotiate the cross-bar.

4.8 Summary

In this chapter a mechanical model is developed. There are three sets of inputs for the system. The system properties of the athlete and the pole, the initial conditions for the equations of motion and the values for the control inputs. The pole vault motion is simplified to a two dimensional motion. A two segment athlete is defined. One segment representing his arms and one segment the rest of his body. Control torques are placed at his wrists and shoulder. The equations of motion are derived for the two segment athlete for the state variables x_{cm1} , y_{cm1} , ϕ and θ using the TMT-method. The complete body position of the athlete can be derived from these four variables as well as the top end of the pole. The pole forces and deformation of the pole can be determined by the pole sub-model using an iterative numerical method. Inputs for the pole sub-model are the applied moment of the athlete to the top end of the pole and the location of the top end of the pole. The equations of motion of the athlete are integrated with respect to time using a fourth order Runge-Kutta method. Initial conditions have to be supplied for the state variables. The initial conditions are defined for time of take-off. Finally the maximum height and location are determined using an energetic approach. The model developed in this chapter has been implemented in MATLAB 2013. Some problems encountered implementing the model in MATLAB are discussed in appendix D.

Pole Stiffness and Internal Forces

The pole sub-model can also be used to examine the along the chord and bending stiffness of the pole. Due to the large deformations, the pole has a non-linear along the chord stiffness and bending stiffness. In addition, the stiffness is a function of the moment the athlete applies to the top end of the pole. By plotting the along the chord and bending stiffness for a range of values of the chord length l the understanding on how the pole will deform can be increased. The internal forces and moments can also be determined for the pole during a vault using the pole sub-model. An envelope can be generated for the maximum force for each point along the pole length. This envelope can be used to determine the load requirements of the pole.

5.1 Along the Chord Stiffness

The iterative numerical solution developed in chapter 4 and section 4.5 can be used to determine the along the chord stiffness. The iterative numerical solution calculates the normal force component R_n for a given pole and a range of values for M and l . The normalized results are shown as a function of the percent shortening δ/L in figure 5.1. The percent shortening is defined as

$$\frac{\delta}{L} = L - l \quad (5.1)$$

Note that the normal force component R_n is equal to the Euler buckling load of a simply supported column for zero moment and a very small chord compression. In addition, it can be seen in the figure that the normal force component is a function of the applied moment. A given pole with a bending stiffness of $B = 2022 \text{ [Nm}^2\text{]}$ and a length of $L = 4.57 \text{ [m]}$, an applied moment of 200 [Nm] and a chord shortening percentage of 0.05 gives a twenty percent difference either above or below the normal force component for zero moment. This demonstrates that the athlete can actively control the motion of the top end of the pole.

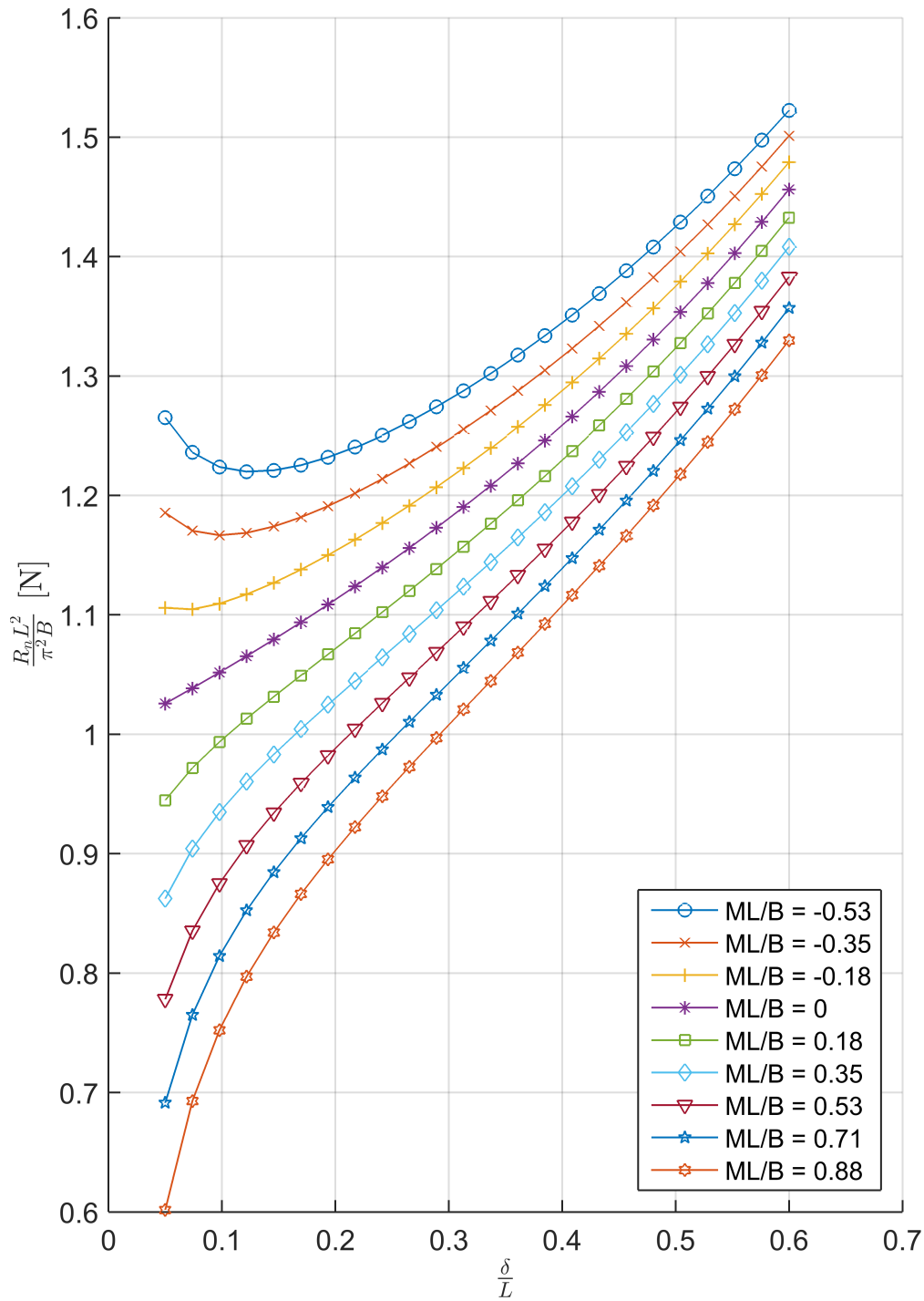


Figure 5.1: The normal force component R_n versus the chord shortening percentage δ/L a range of values of the input variables M and l .

The along the chord stiffness is equivalent to the slope of the curves. From the figure it can be seen that the along the chord stiffness is non-linear. Especially for the region when the pole is almost straight. There appears a singularity at $\delta/L = 0$ and a non-zero moment. In this regime the chord shortening due to bending is much smaller than the axial strain shortening (neglected in the pole sub-model). Hence, in reality the pole will shorten in this regime due to the axial strain and the singularity does not exist (Hubbard, 1980a).

A small angle solution can be formulated for this regime to ensure the continuity of the model. A derivation for this is given in appendix E. However, further work is required to implement this in the iterative numerical model developed in the previous chapter. For now, the mechanical model starts when the pole is already slightly bend to avoid this singularity.

5.2 Bending Stiffness

To examine the bending stiffness the pole sub-model has to be slightly adapted. The inputs and outputs are now reversed. Instead of an applied moment M and compressed chord length l , the normal force R_n and the slope θ at the top end of the pole (see figure 4.5) are now the inputs. The detailed derivations of the modifications are shown in appendix F.

The normalized results are shown in figure 5.2 for a range of values for R_n (normalized

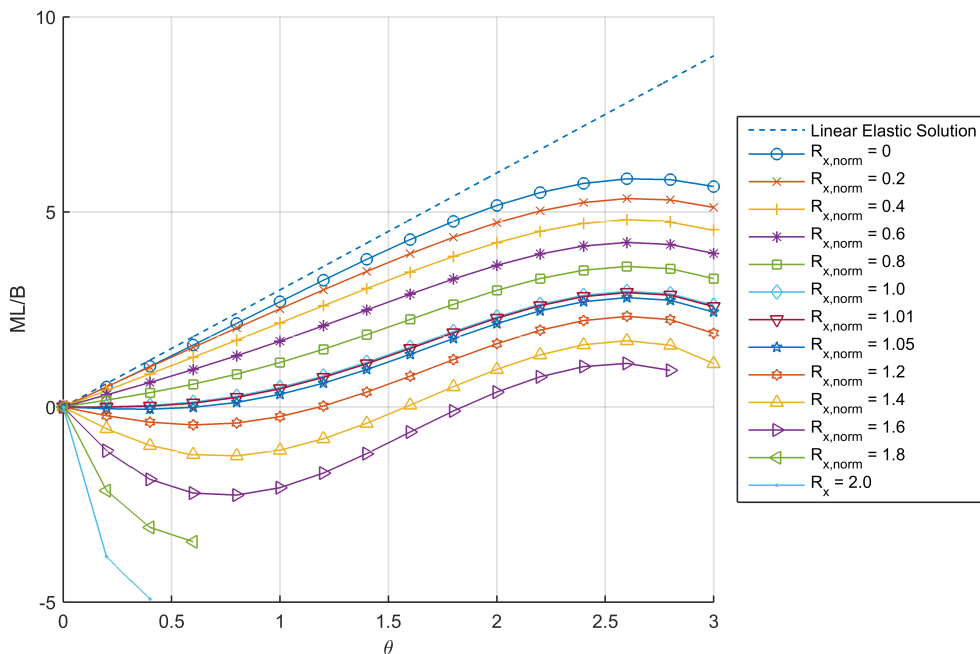


Figure 5.2: The normalized applied moment versus the angle between the pole tangent at the top end and pole chord for various values of the normal force component N

to the Euler buckling load). The bending stiffness of the pole is equal to the slope of the curves plotted. For a compressive force equal to the Euler buckling load and very small values of θ the structure seems to have almost no bending stiffness. The bending stiffness increases when the compressive force is reduced. For a normal force R_n higher than the Euler buckling load the structure has a negative bending stiffness. This is as expected. There seems to be a minimum for the applied moment at approximately $\theta = 0.8$ and a maximum at $\theta = 2.6$. Here the bending stiffness is equal to zero. Furthermore the bending stiffness seems to be constant for a normal force R_n below the buckling load and small values of θ .

A critical remark has to be placed at the results shown in figure 5.2. The values for small angle values for θ and no compressive force R are compared to the linear elastic theorem solution for a simply supported structure loaded with a moment applied to one end.¹ This solution is indicated with the dashed line in figure 5.2. There is a difference between the linear elastic solution and the bending stiffness predicted by the pole sub-model. No explanation for this difference has been found.

Figure 5.2 also shows that the pole still bends for a R_n lower than the Euler buckling load if the athlete applies a positive moment. This demonstrates that reducing the impact force will not prevent the pole from bending if the buckling load is not reached. Reducing the impact force by adding a spring to the pole still remains a potential innovation that can improve pole vaulting performance.

5.3 Envelope of Maximum Internal Forces and Moments

The pole sub-model can also determine the internal forces and moments along the pole length during a vault using equation 4.26. The definition of the internal forces and moments are illustrated in figure 4.5. For each point along the pole length the maximum force during a vault can be determined. This envelope is shown in figure 5.3 and figure 5.4 for an illustrative example. The system properties used are defined in table 6.1, the initial conditions in table 6.2 and the control torques in figure 6.3. The input values listed in the tables will be discussed in more detail in chapter 6.

The maximum internal normal force N is almost symmetrical over the pole length. It becomes zero slightly further than halfway because the pole is asymmetrically loaded. The maximum values are reached during the maximum curvature of the pole. The maximum tangential force is a combination of different pole shapes. The maximum internal tangential forces for both ends of the pole are reached when the pole is almost straight. The compressive force is than almost aligned with the internal tangential force. However, the compressive force increases as the curvature of the pole increases. For large deflections the internal tangential force of the middle part of the pole is still aligned with the compressive force. Hence for this part, the maximum internal tangential force occurs at large curvatures of the pole. The asymmetry in N and T can also be seen for the internal moment M' . The maximum internal moment at the top end of the pole is equal to the maximum moment applied by the athlete to the top end of the pole. The internal moment at the bottom end of the pole is always zero during the vault as it cannot transfer a

¹ $\theta = \frac{-ML}{3EI}$

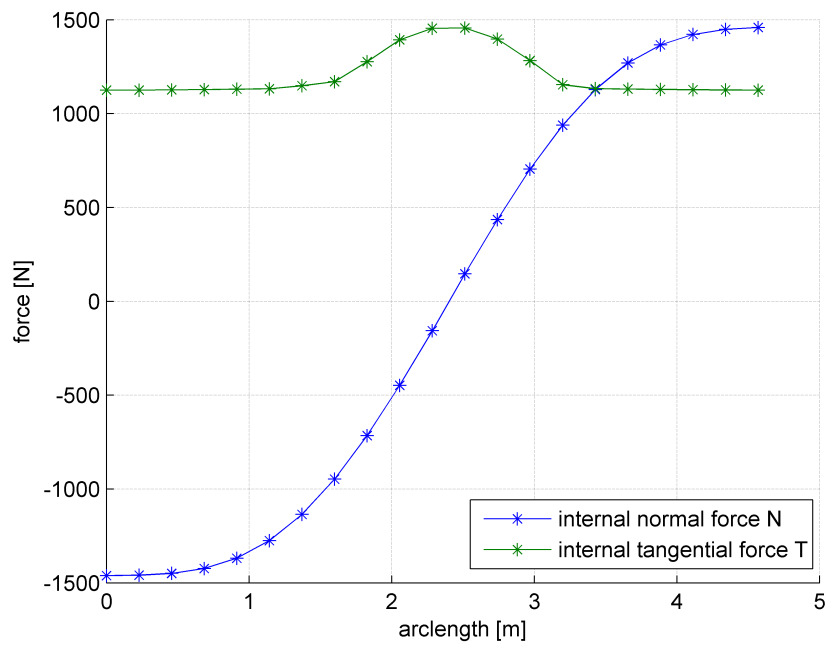


Figure 5.3: Maximum internal normal and tangential force during a vault along the pole length.

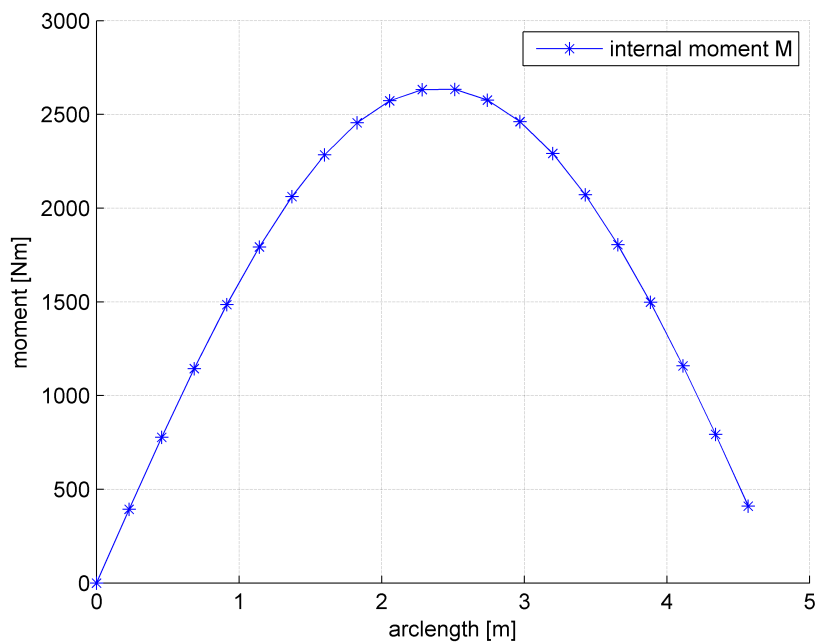


Figure 5.4: Maximum internal moment during a vault along the pole length.

moment. The maximum internal moment is reached slightly further than halfway at the time of maximum curvature.

The results shown for the internal forces and moment can be used to estimate the load requirements for the pole design. The maximum force the pole has to withstand before failure can be determined for each point along the pole length. Hence, the requirement for maximum force can be given as a function of pole length. This can be used to generate an uniform and maximum stress level all along the pole when the pole is subjected to maximum load. In this way the mass of the pole can be minimized (Burgess, 1998).

5.4 Summary

In this chapter the use of the pole sub-model is demonstrated. The pole sub-model can be used to examine the stiffness response of a given pole as a function of the compressed chord length and applied moment or compressive force. Results for a normalized pole proof the non-linearity for the along the chord and bending stiffness. The results show that the athlete can actively control the motion of the top end of the pole. It was also demonstrated that the pole sub-model can be used to determine the maximum internal forces and moments during a vault as a function of the pole length. These maximum forces and moments can be used to generate load requirements for the pole design.

Chapter 6

Validation

In this chapter an illustrative example is presented for the mechanical model developed in chapter 4. The inputs and results are presented for a particular athlete-pole system. The results are compared with experimental data in literature to determine the accuracy of the model. Finally, the robustness and sensitivity of the model are examined with an for two input variables.

6.1 Illustrative Example

As a first validation of the model, the results of the mechanical model for a particular athlete-pole system are compared with data of experiments already performed on the pole vault motion. The inputs for the mechanical model consist out of system properties (both for the athlete and the pole), initial conditions defined at take-off and a time profile for the control torques. The three sets include a lot of parameters and a lot of these are not relevant for the purpose of the experiments already performed. No experiment exist that measured all the inputs used for the mechanical model. It is therefore recommended to carry out an own experiment that can measure the required input and output parameters. This is essential for an accurate validation of the mechanical model. Further work is required to design such an experimental set-up and carry out the experiment.

Hence a direct comparison cannot be made. However, most of the data measured was for vaults of top athletes. The physical properties of the athlete and properties of the pole were approximately similar for several experiments. Also the values for the initial conditions were all in a certain range. So an average value for these can be determined by combining several experiments. Due to the high complexity to measure, no data exist for the control torques. Although, if these would have been measured, the simplification of the athlete to two segments results in such a different motion of the athlete that these values could likely not have been used anyway.

For a first validation it was chosen to compare the results of particular athlete-pole system, based on the combined data of several experiments for the initial conditions, physical

properties of the athlete and the pole properties. The control torques are then varied until a realistic vault is achieved. A realistic vault is defined to possess the following characteristics. At the end of the pole support phase only potential and kinetic energy are left. The kinetic energy consists mainly out of upwards vertical kinetic energy and a small portion of forward kinetic energy to cross the bar. At the end of the vault the pole is in a vertical position and almost completely straightened such that it lifts the vaulter as high as possible. Furthermore, the athlete and the pole follow a feasible trajectory. This includes for example that the athlete does not touch the ground or ends up on the wrong side of the bar. Finally, the translational and rotational velocities do not exceed the maximum values measured by experimental studies, such that for example the athlete does not perform a somersault.

The difference in system properties, initial conditions and control torques will cause a difference between the results. However, as the model is already a simplification of reality it is believed that this difference is reasonable. This first validation will mostly serve as an indication for the quality of the mechanical model.

6.2 Inputs

This section will show the inputs values used for the mechanical model. First, the values used for the physical properties of the athlete, properties of the pole and initial conditions are presented. Then the process of how the control torques are determined is explained.

6.2.1 System Properties, Initial Conditions

The illustrative example represents a vault of an top vaulter. The pole properties and initial conditions of a vault of an top vaulter have been measured in the experimental research of McGinnis and Bergman (1983); Ekevad and Lundberg (1995); Morlier et al. (2008); Linthorne (2000); Adamczewski and Perlt (1997); Angulo-Kinzler et al. (1994); Arampatzis et al. (2004). The pole properties and initial conditions are based on this experimental data and are listed in the tables 6.1 and 6.2. The properties of the athlete are taken for an average sized male and the inertias are calculated using a tin-man model as described by Moore et al. (2009) and discussed in more detail in appendix G.

Table 6.1: Athlete and Pole Properties

Symbol	Value	Unit	Symbol	Value	Unit
m_1	20	kg	l_2	0.35	m
m_2	50	kg	l_3	0.4	m
I_1	2.96	kgm ²	L	4.57	m
I_2	5.67	kgm ²	B	2522	Nm ²
l_1	0.4	m			

Table 6.2: Initial Conditions

Symbol	Value	Unit	Symbol	Value	Unit
x_{cm}	3.57	m	ϕ	0.4	rad
y_{cm}	1.72	m	θ	0	rad
\dot{x}_{cm}	-8.7	m/s	$\dot{\phi}$	0.2	rad/s
\dot{y}_{cm}	1.2	m/s	$\dot{\theta}$	0	rad/s

6.2.2 Motion Coordination of the Athlete

The motion coordination of the athlete is represented in the mechanical model by control torques. For the illustrative example, the control torques were determined through a process of trial and error. For the prescribed input values for the physical properties of the athlete, properties of the pole and the initial conditions shown in the previous subsection, the control torques were varied until a realistic vault was obtained.

However, as no data is available for the control torques it was difficult to estimate the profile that would result in a realistic vault. The first tries already showed the high sensitivity of the mechanical model to the control torques. Tiny variations already led to significantly different results. None of them remotely realistic. A different approach was required to determine the control torques.

Although no experimental data exist for the control torques, the motion coordination of the athlete was measured in some experiments. For example, the orientation of different body parts were measured during a vault. The body motion of most athletes is approximately similar for several experiments (Angulo-Kinzler et al., 1994; Morlier & Cid, 1996). The arms speed up to align with the chord of the pole and then remain aligned with the chord of the pole for the rest of the vault (always directed upwards). The motion of the torso is first similar to the motion of the arms, but when the arms remain aligned with the pole chord the torso continues to rotate to an upside down position. The rotational velocity is approximately constant. The legs rotate faster from the start and go past the vertical axis before they are brought back.

The orientation of the two segment athlete is defined in the mechanical model by the variables ϕ and θ (see figure 4.3). The values for these variables during a vault can be estimated from the motion coordination described above. The approximation is shown in figure 6.1. The behavior of the two segment athlete is similar to the motion coordination described above. The angle for the arms slightly increases until it aligns with the pole chord. During the rest of the vault it remains aligned with the pole chord and the angle returns to zero as the pole rotates to a vertical position. The orientation of the second segment is a combination of the behavior of the legs and torso. The second segment has an approximately constant angular velocity, but overshoots the vertical axis before it is brought back.

For the mechanical model developed in the previous chapter, the motion of the athlete is the result of the three sets of inputs (system properties, initial conditions and control torques). We do not prescribe the motion the athlete or pole has to follow as we do not

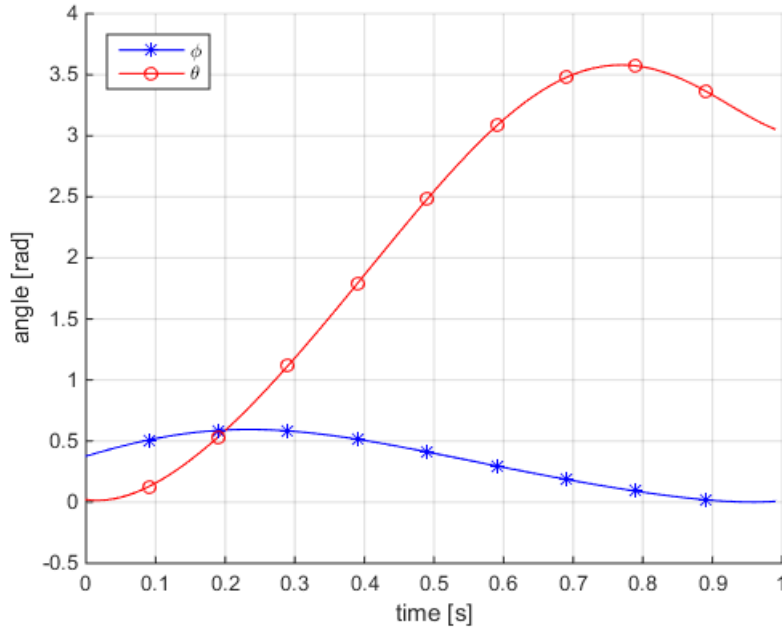


Figure 6.1: The orientation angle ϕ of the first segment of the athlete and the orientation angle θ of the second segment of the athlete during a vault. The time is defined from take-off until pole release.

know the optimum motion. However, to get an initial estimation for the control torques we can prescribe a motion for the athlete based on the estimation of ϕ and θ shown in figure 6.1.

The system of four second order differential equations of motion derived in chapter 4 has to be modified in order to do this. Let us reexamine the system of equations of motion.

$$T_{il}M_{ij}T_{jk}\ddot{q}_k = y_l + T_{il}(\Sigma f_i - M_{ij}h_j) \quad (6.1)$$

where the state vector \mathbf{q} was defined as follows.

$$q_k = \begin{bmatrix} X_{cm1} \\ Y_{cm1} \\ \phi \\ \theta \end{bmatrix} \quad (6.2)$$

and the control torques were defined in the control input vector \mathbf{y} .

$$r_l = \begin{bmatrix} 0 \\ 0 \\ -M_1 \\ M_2 \end{bmatrix} \quad (6.3)$$

From figure 6.1 the first and second time derivative of ϕ and θ can be determined as well. The state variables ϕ , $\dot{\phi}$, θ , and $\dot{\theta}$ are now input variables. The control torques M_1 and M_2 become the unknowns.

The system of four second order differential equations of motions (equation 6.1) now contains unknowns on the left hand side and right hand side and can no longer be solved with only the Runge-Kutta numerical integration scheme. However, the system can still be solved as we have four equations and four unknowns (X_{cm1} , Y_{cm1} , M_1 and M_2). To solve the system of equations with these unknowns the system is split into two parts, each part containing two equations. Before we divide the system into two parts, the equation is rewritten as follows. This is done such that the separation of the system of equations into two parts is easier.

$$\begin{bmatrix} \bar{M}_{11} & \bar{M}_{12} & \bar{M}_{13} & \bar{M}_{14} \\ \bar{M}_{21} & \bar{M}_{22} & \bar{M}_{33} & \bar{M}_{44} \\ \bar{M}_{31} & \bar{M}_{32} & \bar{M}_{33} & \bar{M}_{34} \\ \bar{M}_{41} & \bar{M}_{42} & \bar{M}_{43} & \bar{M}_{44} \end{bmatrix} \begin{bmatrix} \ddot{x}_{cm1} \\ \ddot{y}_{cm1} \\ \ddot{\phi} \\ \ddot{\theta} \end{bmatrix} = \begin{bmatrix} 0 \\ 0 \\ M_1 \\ M_2 \end{bmatrix} + \begin{bmatrix} g_1 \\ g_2 \\ g_3 \\ g_4 \end{bmatrix} \quad (6.4)$$

The matrix $\bar{\mathbf{M}}$ is used to define the resulting matrix of $T_{il}M_{ij}T_{jk}$. The vector \mathbf{g} defines the resulting vector of $T_{il}(\Sigma f_i - M_{ij}h_j)$. Both $\bar{\mathbf{M}}$ and \mathbf{g} only contain input values.

The system can now be broken down into the following two parts.

$$\begin{bmatrix} \bar{M}_{11} & \bar{M}_{12} \\ \bar{M}_{21} & \bar{M}_{22} \end{bmatrix} \begin{bmatrix} \ddot{x}_{cm1} \\ \ddot{y}_{cm1} \end{bmatrix} + \begin{bmatrix} \bar{M}_{13} & \bar{M}_{14} \\ \bar{M}_{23} & \bar{M}_{24} \end{bmatrix} \begin{bmatrix} \ddot{\phi} \\ \ddot{\theta} \end{bmatrix} = \begin{bmatrix} 0 \\ 0 \end{bmatrix} + \begin{bmatrix} g_1 \\ g_2 \end{bmatrix} \quad (6.5)$$

$$\begin{bmatrix} \bar{M}_{31} & \bar{M}_{32} \\ \bar{M}_{41} & \bar{M}_{42} \end{bmatrix} \begin{bmatrix} \ddot{x}_{cm1} \\ \ddot{y}_{cm1} \end{bmatrix} + \begin{bmatrix} \bar{M}_{33} & \bar{M}_{34} \\ \bar{M}_{43} & \bar{M}_{44} \end{bmatrix} \begin{bmatrix} \ddot{\phi} \\ \ddot{\theta} \end{bmatrix} = \begin{bmatrix} M_1 \\ M_2 \end{bmatrix} + \begin{bmatrix} g_3 \\ g_4 \end{bmatrix} \quad (6.6)$$

The only unknowns in the two equations of 6.5 are \ddot{x}_{cm1} and \ddot{y}_{cm1} . The rest of terms all contain input values. This system of two second order differential equations of motion can be rewritten to a system of four first order differential equations of motions by again introducing the variables $v_x = \dot{X}_{cm1}$ and $v_y = \dot{Y}_{cm1}$. This system can be solved using the same Runge-Kutta numerical integration scheme presented in chapter 4.

Once equation 6.5 is solved, the values for \ddot{x}_{cm1} and \ddot{y}_{cm1} can be substituted in equation 6.6. The only unknowns left are the control torques M_1 and M_2 . The two equations of 6.6 can then be easily solved for these.

The results for the control torques are shown in figure 6.2 for a system with the properties shown in table 6.1, initial conditions shown in table 6.2 and the orientation angles ϕ and θ as a function of time as shown in figure 6.1.

The control torques derived in this way only make sure that the segments of the athlete have the prescribed orientation as defined in figure 6.1. However, this set of control torques does not necessarily result in a realistic vault in combination with the prescribed system properties and initial conditions shown in table 6.1 and table 6.2 (as the motion of the pole and trajectory of the center of gravity are not prescribed). And this was the case. However, the control torques derived in this way served as a good initial estimation for the control torques.

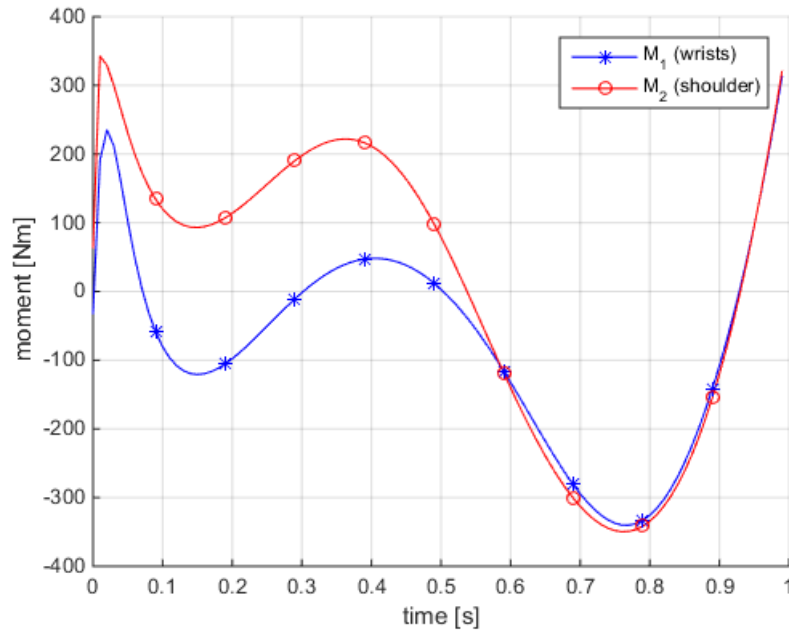


Figure 6.2: The control torques M_1 (wrists) and M_2 (shoulder) during a vault for an illustrative example (system properties of table 6.1 and initial conditions of table 6.2) and prescribed motion of a two segment athlete (figure 6.1). The time is defined from take-off until pole release.

With a process of trial and error the control torques are varied until a realistic vault is achieved (satisfying the definition of a realistic vault given in section 6.1). The final set of the control torques M_1 and M_2 that result in a realistic vault is shown in figure 6.3.

The control torques shown in figure 6.3 are derived by a process of trial and error and most likely result in a sub-optimal vault. There most likely exist an optimal control torque set if the system properties and initial conditions are prescribed. It is recommended to formulate an optimization procedure for the control torques. This would help in analyzing the effect of different system properties and initial conditions on pole vaulting performance.

6.3 Comparison with Literature

The results of the mechanical model for the illustrative example using the inputs defined in the previous section can be compared with results in literature of experiments already performed. The system properties used are shown in table 6.1, the initial conditions in table 6.2 and the torque controls in figure 6.3. The time step used for the numerical integration is 0.02[s].

The parameters that will be compared are the motion of the athlete and pole, the trajectory of the center of mass, the maximum height, the forces during the vault and the energy transformations during the vault.

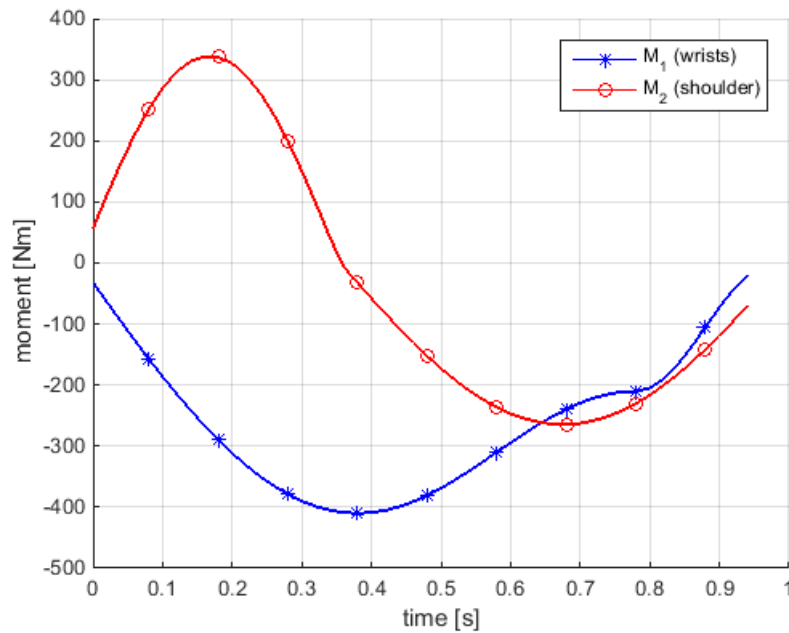


Figure 6.3: The final control torques M_1 (wrists) and M_2 (shoulder) during a vault for an illustrative example (system properties of table 6.1 and initial conditions of table 6.2) that resulted in a realistic vault for the mechanical model of a massless pole and two segment athlete. The time is defined from take-off until pole release.

6.3.1 Motion of the Athlete and Pole, Trajectory and Peak Height

Figure 6.4 shows the motion of the two segment athlete and the massless pole during the pole support phase as calculated by the mechanical model using the inputs shown in the previous section. The deformation of the pole and body position of the two segment athlete are shown for every time interval of 0.2 [s] starting from zero until the end. The last position is shown as well. Also the velocity vector of the total center of mass of the athlete is shown for these time intervals. The trajectory of the total center of mass of the two segment athlete is shown for every time increment of 0.02 [s]. The grey area indicates the area in which the cross-bar can be placed. The maximum height the athlete reaches in this area is defined as the maximum height of the vault.

The total motion of the pole vault predicted by the mechanical model shows good correspondence with videos of real vaults. During the first part of the vault the motion is mainly horizontal. The athlete decelerates while the bend of the pole increases. During the second part of the vault the motion is mainly vertical. The pole straightens and the athlete accelerates again. Also the separate motion of the two segment athlete and the massless pole are comparable with real vaults.

The motion of the two segment athlete is reasonably similar to the motion described in 6.2.2. The arms speed up and align with the pole chord. At the end of the pole support phase the arms remain pointed in an upward position. The torso and legs rotate faster and at the end of the pole supports phase are more or less in an inverted position. However, there are some difference. The torso and legs go past the vertical and do not completely

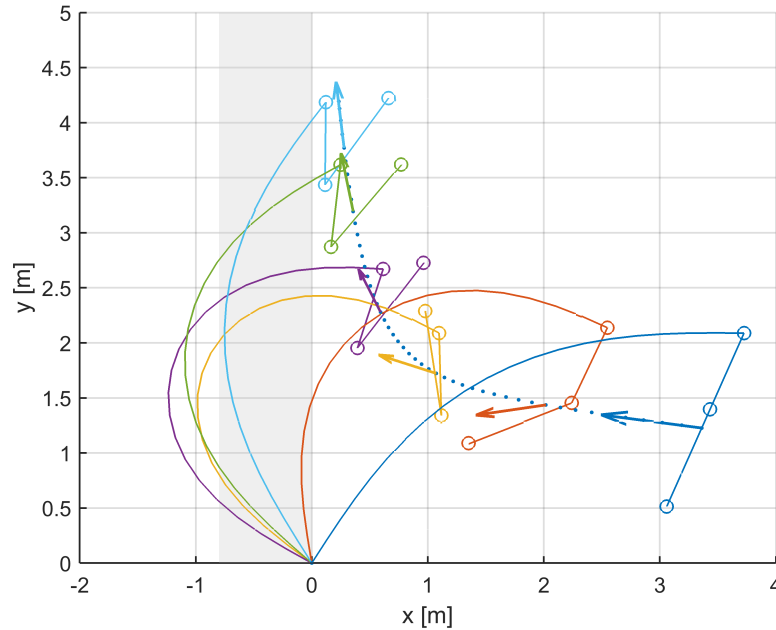


Figure 6.4: Diagram showing the deformation of the pole, body orientation of the two segment athlete and the velocity vector of the total center of mass of the athlete for every time interval of 0.2 [s] starting from take-off until pole release. The final position is shown as well. The trajectory of the total center of mass of the athlete is shown for every time increment of 0.02 [s]. The grey area indicates the area in which the cross bar can be placed. The results are for the system properties of table 6.1, initial conditions of table 6.2 and torque control profile shown in figure 6.3.

return at the end of the vault. Also the arms show an oscillation before they align with the pole chord. Further work is required in tuning the control torque profiles to eliminate these differences. These small difference are left in place for now as the trajectory of the center of gravity and velocity vectors are close to that of a realistic vault.

The motion of the pole is also quite realistic. During the first part the pole deflects significantly until it reaches its maximum bend at approximately halfway the vault. During the second part of the vault the pole straightens again and ends in a vertical position. The minimum compressed chord length during the vault is $l_{chord} = 0.52L$ at $t = 0.4[s]$. The experimental research study of [Angulo-Kinzler et al. \(1994\)](#) measured chord shortenings in the order $0.62L$. The model will always overpredict as the energy losses during the impact of the pole with the planting box are neglected. Hence the larger deflection predicted by the mechanical model can be expected. Further evaluation of the pole deflection demonstrated that conventional poles will fail for the maximum deflection shown in figure 6.4. This is discussed in appendix H.

The maximum height reached by the athlete in the illustrative example is 6.10 [m] at a distance of 28 [cm] behind the planting box. This result seems realistic as it is in line with the vault heights of top athletes. The result seems a bit high for a first attempt using a trial and error process. However, the mechanical model will always overpredict

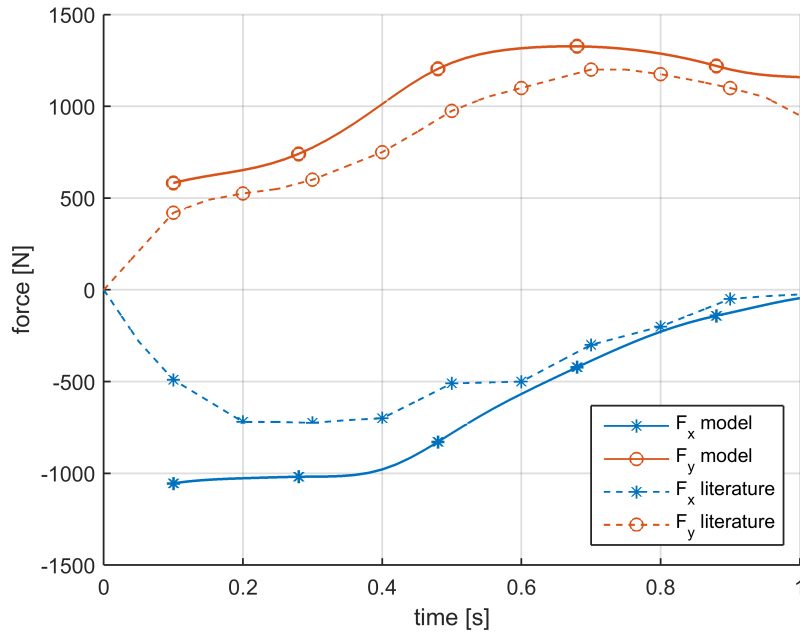


Figure 6.5: The horizontal ground reaction force component F_x and the vertical ground reaction force component F_y . The continuous lines are the forces predicted by the mechanical model. The dashed lines are the average forces measured during the experiments of [Arampatzis et al. \(2004\)](#), [Morlier and Mesnard \(2007\)](#) and [Schade et al. \(2006\)](#). The forces are the ground reaction forces and thus have the opposite direction of the forces acting on the bottom end of the spring. The forces predicted by the mechanical model start after 0.1 [s] as the mechanical model does not take into account the impact process of the pole with the planting box.

the pole vaulting height as the energy loss during impact is neglected. In addition, the steep vertical trajectory, as shown in figure 6.4, is often not attempted in practice by the athlete as he usually takes a higher safety margin to cross the bar and land further back on the cushion ([Hubbard, 1980a](#)).

6.3.2 Pole Forces

In their experimental research of the pole vault, [Arampatzis et al. \(2004\)](#), [Morlier and Mesnard \(2007\)](#) and [Schade et al. \(2006\)](#) measured the ground reaction force of the pole. The approximation of their data of the horizontal ground reaction force component F_x and vertical ground reaction force component F_y are shown by the dashed lines in figure 6.5.¹

The same forces measured by the experiments can be easily predicted with the mechanical model (see figure 4.4).

$$F_x = -R_n \cos \lambda - R_t \sin \lambda; \quad (6.7)$$

¹ x and y in the global coordinate system.

$$F_y = -R_n \sin \lambda + R_t \cos \lambda; \quad (6.8)$$

The results for the inputs and system properties of the illustrative example as discussed in the previous section are shown by the continuous lines in figure 6.5. The forces of the mechanical model start at $t = 0.1$ [s]. The reason for this is that the impact is not taken into account in the mechanical model. The model starts when the massless pole is already placed in the box.²

The pole forces predicted by the mechanical model are comparable to the pole ground reaction forces measured by Arampatzis et al. (2004), Morlier and Mesnard (2007) and Schade et al. (2006). Both the magnitudes and the profiles are approximately the same.

During the first phase of the vault the horizontal force component is higher than the vertical force component. This corresponds with the pole deformation as seen in figure 6.4. In the first phase, the motion of the athlete and hence the compression of the pole is mainly horizontal (till approximately $t = 0.4$ [s]). In the next phase the motion is mainly vertical and the vertical force component is higher than the horizontal force component. In this phase the horizontal force component also rapidly reduces.

The pole forces do not return to zero as the mechanical model stops just before the pole is completely straight again. This is to stay away from the singularity in the pole sub-model for small values of δ/L . When the small angle solution is implemented the pole can straighten completely and the pole forces should return to zero.

6.3.3 Energy Transformations

In the experimental study of Arampatzis et al. (2004) the energy transformations of the pole vault are determined. He measured the potential energy of the athlete, the kinetic energy of the athlete, the total mechanical energy of the athlete and the pole strain energy. All these energies can also be predicted by the mechanical model.

The potential energy E_{pot} of the two segment athlete can be calculated for the two segment athlete as follows (see figure 4.3).

$$E_{pot} = m_1 g Y_{cm1} + m_2 g (Y_{cm1} - l_2 \cos \phi - l_3 \cos(\phi + \theta)) \quad (6.9)$$

The kinetic energy E_{kin} of the two segment athlete can be calculated with the following equation.

$$E_{kin} = \frac{1}{2} (m_1 + m_2) (v_x^2 + v_y^2); \quad (6.10)$$

The pole strain energy E_{pole} can be calculated by (see figure 4.4)

$$E_{pole} = \int R_n dl \quad (6.11)$$

²The velocity of the pole is then equal to zero.

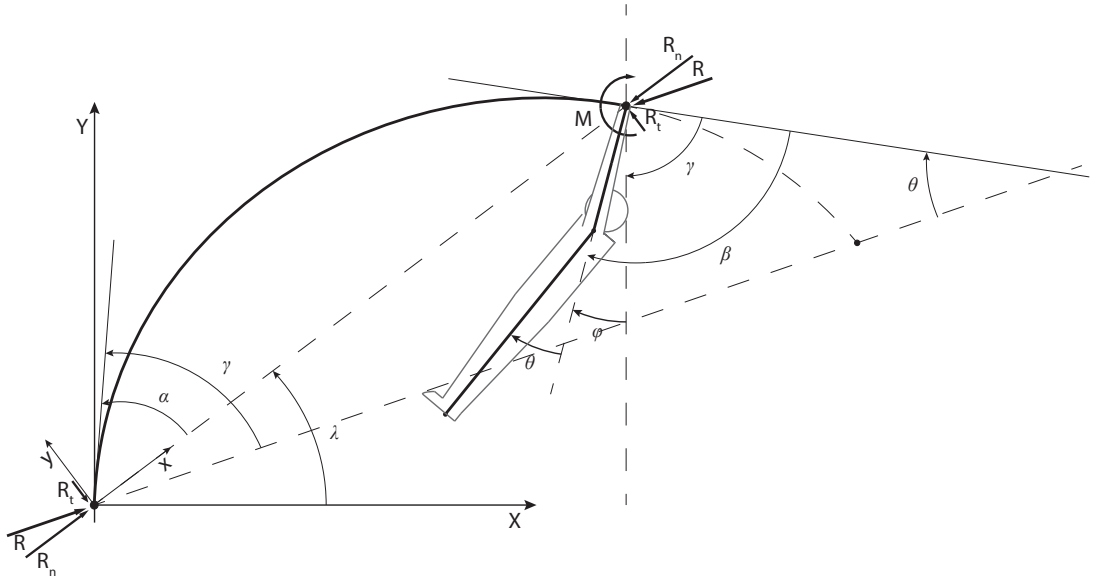


Figure 6.6: Schematic diagram of pole with angle definitions.

The total mechanical energy of the athlete consists out of his potential energy, kinetic energy, rotational energy and the work done by the wrists and shoulder joint.

$$E_{tot,ath} = E_{pot} + E_{kin} + E_{rot} + W_1 + W_2 \quad (6.12)$$

where the rotational kinetic energy of the two segment athlete can be calculated using the following equation.

$$E_{rot} = \frac{1}{2}I_1\dot{\phi}^2 + \frac{1}{2}I_2\dot{\theta}^2 \quad (6.13)$$

And the work done by the wrists by

$$W_1 = \int M_1 d\beta \quad (6.14)$$

and finally the work done by the shoulder by

$$W_2 = \int M_2 d\theta \quad (6.15)$$

The angles β and θ are illustrated in figure 6.6.

The energies predicted by the mechanical model for the system and input properties discussed in the previous section are compared to the energies determined by [Arampatzis et al. \(2004\)](#) in figure 6.7. The magnitude and profile between the different mechanical energies are approximately in line. The main difference is that the duration of the vault

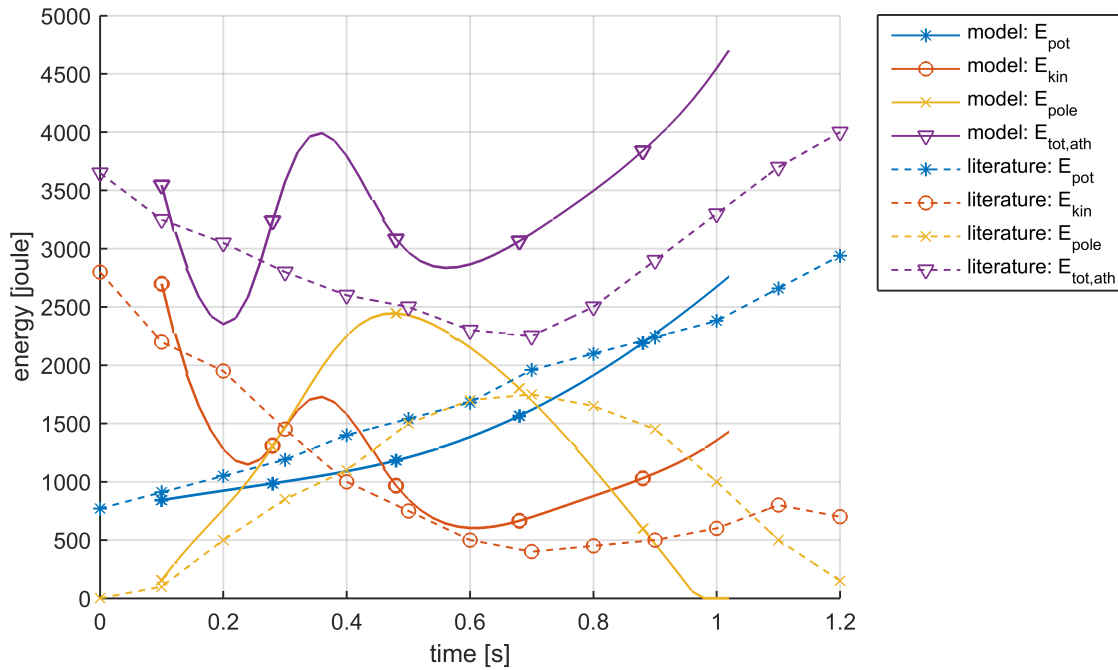


Figure 6.7: The mechanical energy transformation of the pole vault during the pole support phase. The continuous lines are the mechanical energies predicted by the mechanical model. The dashed lines are the energies predicted by [Arampatzis et al. \(2004\)](#). The potential energy E_{pot} and kinetic energy E_{kin} are both of the athlete only and are also a fraction of the total mechanical energy of the athlete. E_{pole} is the pole strain energy. The total mechanical energy of the athlete $E_{tot,ath}$ consists out of the potential energy, translational kinetic energy, rotational kinetic energy and work done by the athlete.

simulated by the mechanical model is 1 second, whereas the duration of the vault of the experiment of [Arampatzis et al. \(2004\)](#) is 1.2 seconds.

The difference in magnitude of the potential energy at the start and end of the vault is within ten percent. There is a small difference in the profile. The potential energy given by the experimental data is approximately linear while the potential energy calculated by the model is more like a power function. The difference might be explained by the extra safety concern of the athlete. As explained above, the ideal steep vertical trajectory as shown in the illustrative example is usually not attempted by athletes in practice. The steep trajectory offers little room to maneuver over the cross-bar. Usually the athlete takes some margin to cross the bar and safely land on the mat. Thus in reality the trajectory of the athlete is less convex and more linear.

The kinetic energy shows the biggest difference. Both in magnitude and profile. The kinetic energy of the illustrative example shows some oscillations. This is a characteristic of a (double) pendulum system. It can be reduced by further tuning of the control torques. Looking past the oscillations the profile of both vaults are almost similar. The difference in magnitude at the beginning is approximately ten percent. The difference at the end of the vault is approximately forty percent. The big difference at the end of the vault

might partially be explained by the fact that the impact energy loss (approximately ten percent) is not taken into account in the mechanical model.

The difference in strain energy suggests a difference in pole length and stiffness between the two vaults. The strain energy for the illustrative example increases and decreases more rapidly. The shorter time period for bending and straightening can imply that the pole of the illustrative example is stiffer. Also the strain energy reaches a higher maximum value. The difference in maximum strain energy can be caused by difference in work done by the athlete. This might also partially explain the large difference in kinetic energy at the end of the vault.

The oscillations are of course also present in the total mechanical energy of the athlete as it is a summation that includes the kinetic energy. The total mechanical energy of the athlete consist out of his potential energy, rotational energy, kinetic energy and the work he has done. The athlete of the illustrative example ends with much higher mechanical energy. This might again be partially explained by the fact that the impact energy loss is neglected for the illustrative example. Also the strain energy suggested that more muscular work is added to the athlete of the illustrative example. These two reasons can explain the large difference in total mechanical energy.

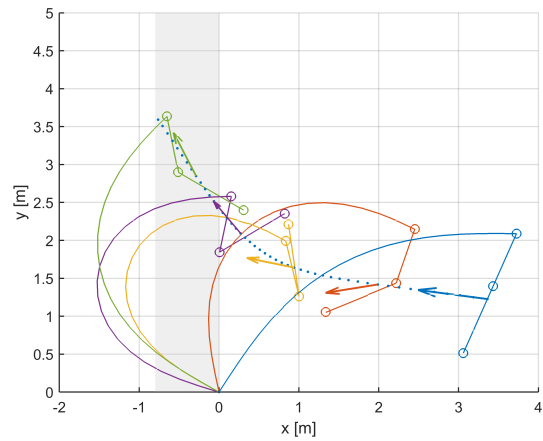
Overall, also the energies predicted by the model are comparable to the data available literature.

6.4 Sensitivity of the Model

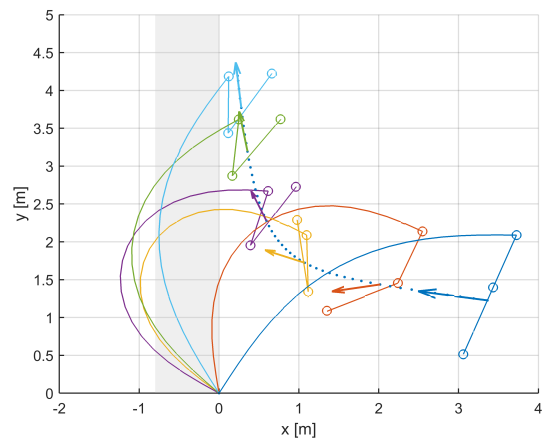
The final conditions of the athlete (when the pole is straightened again) are highly sensitive to almost all parameters. Small perturbations in initial conditions, control torques and even pole properties result in large differences in the final conditions of the athlete. The sensitivity of the mechanical model will be illustrated by examining the pole stiffness and initial horizontal velocity. These two properties were chosen to show that the vault motion is highly sensitive to parameters of either the system properties or initial conditions. Section 6.2.2 already showed the high sensitivity of the pole vault motion to variations in the control torques. This will demonstrate that the vault motion and vault height is sensitive to all three input sets: the system properties, initial conditions and control torques.

For the illustrative example the pole bending stiffness was $B = 2522 \text{ [Nm}^2\text{]}$ and the initial horizontal velocity 8.7 [m/s] . To illustrate the sensitivity of the pole vault motion to these parameters, the trajectory will be plotted for a value lower and a value higher than these. For example the bending stiffness will be reduced or increased with ten percent. The rest of the properties and inputs remain the same as shown in table 6.1, table 6.2 and figure 6.3. The new trajectory will be compared to the trajectory of the illustrative example shown in figure 6.4. The results are shown in figure 6.8 and figure 6.9.

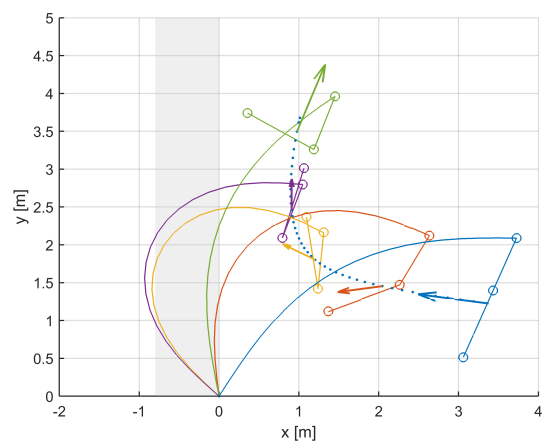
Figure 6.8 shows that the athlete rotates the pole too far when the bending stiffness of the pole is reduced to $B = 2222 \text{ [Nm}^2\text{]}$. He will land further back on the cushion. The maximum height decreases significantly as the athlete crosses the grey area when only a small amount of the horizontal energy has been converted to potential energy. The athlete will reach his maximum height a large distance behind the cross bar. The



(a)



(b)



(c)

Figure 6.8: Sensitivity of the trajectory of the athlete to variations in pole stiffness. (a) $B = 2222$ [Nm^2], (b) $B = 2522$ [Nm^2], (c) $B = 2822$ [Nm^2].

maximum height reached in the area where the cross-bar can be placed is approximately 3.6 [m]. When the pole stiffness is increased to $B = 2822$ [Nm²] the pole propels the athlete backward and the athlete will never cross the bar. The result is no score.

Also for both cases only changing the pole stiffness already causes a completely different motion of the athlete. For the vault with the lower bending stiffness of the pole the torso and legs perform a complete somersault (which is not realistic). For the vault of the stiffer pole the athlete even rotates faster. The increase in pole bending stiffness also reduces the time of the vault with approximately forty percent.

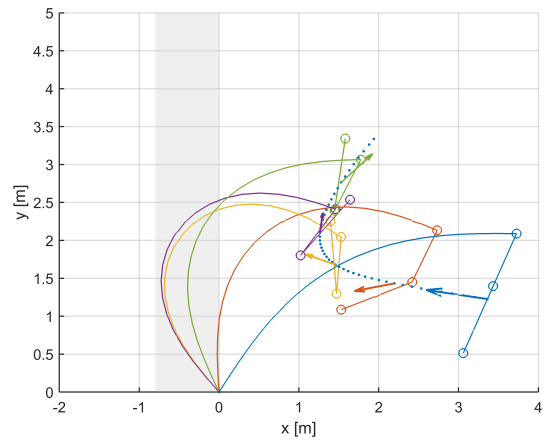
Similar sensitivity responses can be seen for the initial horizontal velocity in figure 6.9. When the initial horizontal velocity of the athlete is reduced with 1 [m/s], there is not enough energy to rotate the pole to vertical. The pole again propels the athlete backwards and the athlete sets no score. When the initial horizontal velocity is increased with 1 [m/s], too much energy is put into pole rotation causing the pole to rotate past vertical. The maximum height decreases with approximately fifty percent as the athlete cannot convert his horizontal motion into vertical motion in time. Again the athlete will reach his maximum height at a large distance behind the cross bar. The initial velocity seems to have less influence on the motion of the athlete compared to the bending stiffness.

These two examples illustrate that the vaulting performance is highly sensitive to the initial conditions of the vault and the pole properties. Although only the results of two parameters are shown, similar sensitivities were found for pole length, vertical take-off velocity, take-off location of the center of gravity and orientation of the body of the athlete. The high sensitivities decrease the robustness of the model. A tiny perturbation in one of the parameters will most likely result in a non-realistic vault. This makes using the model hard. When one parameter is changed, other parameters have to be changed as well to once again obtain a realistic vault. This makes it also hard to compare the vaults as several parameters have been changed at the same time.

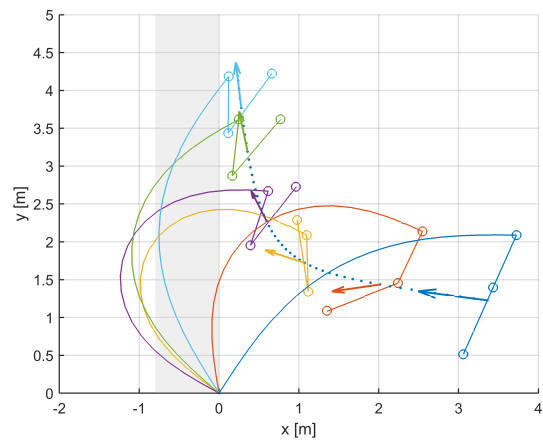
In practice, changes in pole properties and initial conditions are compensated by the athlete during the pole support phase. He adapts his motion coordination accordingly. For the model developed this would mean changing the control torques. Further work is required to establish a procedure that can determine the control torques of the athlete for a realistic vault given the pole properties and initial conditions, preferably including an optimization procedure to maximize pole vaulting height. In this way the effect of varying system properties or initial conditions can be compared.

6.5 Summary

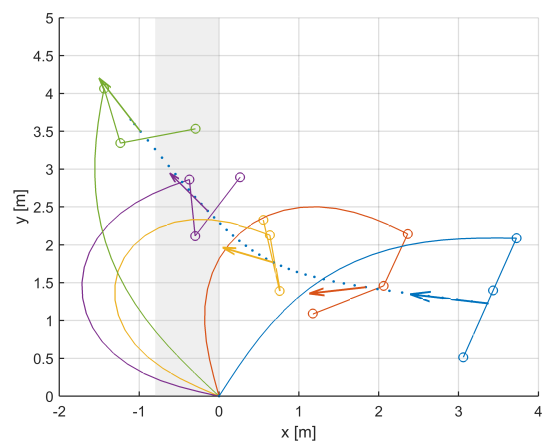
In this chapter the quality of the mechanical model is examined. First the inputs are defined, including a detailed explanation of the strategy how the control torques are determined. Next the results are compared to results available in literature. The results for the trajectory, motion of the athlete, pole forces and energies are comparable for both magnitude and profile. Finally, the sensitivity of the pole vault motion was presented by varying the pole stiffness and initial horizontal velocity. The model has a high sensitivity to several parameters. This reduces the robustness of the model.



(a)



(b)



(c)

Figure 6.9: Sensitivity of the trajectory of the athlete to variations in initial horizontal velocity. (a) $v_x = 7.7$ [m/s], (b) $v_x = 8.7$ [m/s], (c) $v_x = 9.7$ [m/s].

Innovation 1: A Pole with a Spring

In this chapter the innovation of implementing a spring to the bottom end of the pole is examined. The impact force can be reduced by inserting a spring in the pole. For a maximum increase in pole vaulting performance the spring should elongate again during the pole straightening phase such that the return force is increased. This chapter will evaluate whether this is feasible and what the influence is on the pole vaulting performance and motion. In the first section the choices made on how the spring is modeled and how the mechanical model can be used to predict the motion of a pole with a spring are described. In the next section the effect on pole vaulting performance is evaluated. The motion of the athlete, the motion of the pole, the maximum height, the pole forces and the energy transformation are discussed to determine the potential of adding a spring to the pole to increase pole vaulting performance. The implementation of the spring in the pole is discussed in the last section.

7.1 Deformation of the Pole with Spring

The spring is inserted at the bottom end of the pole. This is the most favorable location as the mass that then directly impacts the planting box is the lowest. The rest of the pole will decelerate slower as it has a longer path to decelerate by compressing the spring. The stress-waves will only be generated by the small mass that then impacts the planting box. The energy loss due to impact will be the lowest in this way.

In order to keep the model as simple as possible it is assumed that the spring is always aligned with the pole chord axis.¹ In addition it was chosen to examine a linear spring only. As discussed before, the pole can also be considered as a spring (a highly non-linear spring). The system can thus be regarded as two springs in series. A schematic diagram is given in figure 7.1.

¹In reality this deformation cannot happen and the spring will be aligned with the tangent of the lower end of the pole.

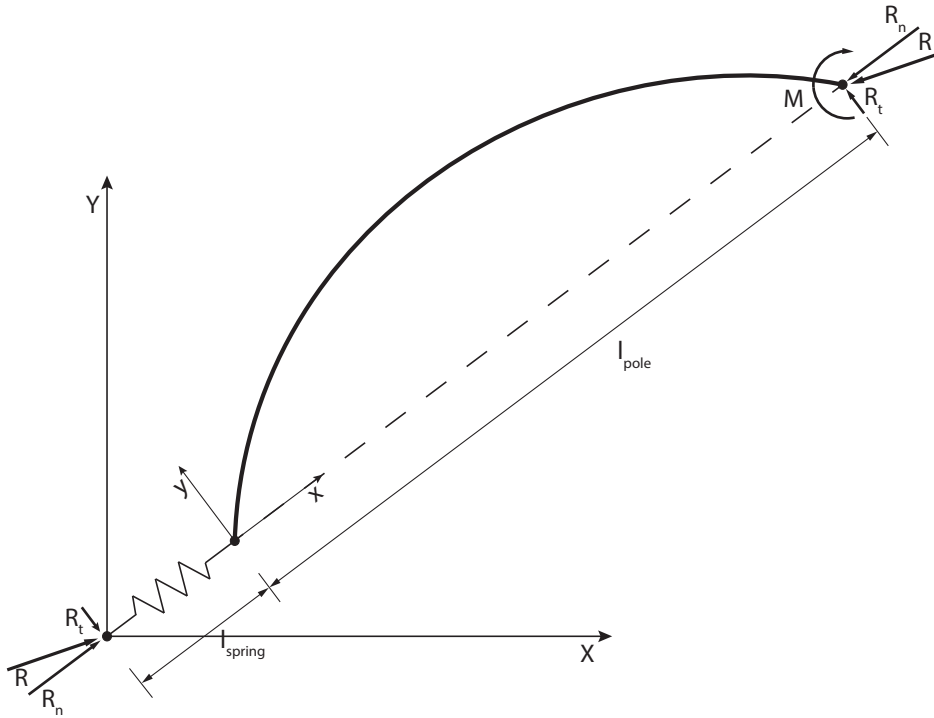


Figure 7.1: Schematic diagram of pole with a spring at its bottom end.

The motion and deformation of the pole with spring is different from the regular pole. When a compressive force and moment are applied, both the spring and the pole will shorten. As the stiffness of both parts is different, the percent shortening will be different for each. Three equations are required to determine the deformation for the pole with spring. An equation that determines the chord length of the pole l_{pole} , an equation that determines the compressed length for the spring l_{spring} and a compatibility equation that determines the axial force that act on each part.

The compressed length of the linear elastic spring can be easily calculated with the following equation.

$$l_{spring} = l_{0,spring} - \frac{F}{K} \quad (7.1)$$

Where $l_{0,spring}$ is the uncompressed spring length, K is the spring stiffness and F is the axial force acting on the spring.

The compatibility condition can be derived from the fact that the spring and pole are aligned and in series. Because of this, the axial force F acting on the spring is equal to the axial force acting on the pole. The axial force acting on the pole was defined in chapter 4 as the normal force component R_n of the compressive force R . Hence $F = R_n$.

The normal force component R_n can be calculated using equation 4.69 given in chapter 4.

$$R_n = \sqrt{R^2 - (-M/l_{pole})^2} \quad (7.2)$$

Substituting this expression of R_n into the equation 7.1 for F , the compressed spring length can be defined as follows.

$$l_{spring} = l_{0,spring} - \frac{\sqrt{R^2 - (-M/l_{pole})^2}}{K} \quad (7.3)$$

This definition clearly shows that the compressed length of the spring l_{spring} is also a function of the compressed chord length of the pole l_{pole} .

The deformation of the pole (without the spring part) can be calculated using the iterative numerical method developed in chapter 4. The inputs for the iterative numerical method are the applied moment M and the compressed chord length l . The numerical iterative solution updates the initial values of the compressive force R and the slope γ until the following two equations are satisfied.

$$M = Ry' \quad (7.4)$$

$$l = \sqrt{x'^2 + y'^2} \quad (7.5)$$

where x' and y' are determined in the fictitious pole coordinate system. As mentioned above the definition for the total compressed chord length l (smallest distance between the bottom end of the pole and the top end of the pole) is different for a pole with a spring. It consists out of the compressed length of the spring and the compressed length of the pole part.

$$l = \sqrt{x'^2 + y'^2} + l_{spring} \quad (7.6)$$

Substituting the expression derived for the compressed spring length given in equation 7.3. yields the following result.

$$l = \sqrt{x'^2 + y'^2} + l_{0,spring} - \frac{\sqrt{R^2 - (-M/l_{pole})^2}}{K} \quad (7.7)$$

This equation is only a function of γ , R , M and l . The same four variables used for the iterative numerical solution of the regular pole. The same iterative numerical solution to determine the pole deformation can now also be used to determine the deformation for the pole with a spring, only the new expression derived for the compressed chord length l for the pole with a spring has to be substituted. The input variables remain M and l . The variables R and γ will be updated until the following system of two equations is solved.

$$M = Ry' \quad (7.8)$$

$$l = \sqrt{x'^2 + y'^2} + l_{0, spring} - \frac{\sqrt{R^2 - (-M/l_{pole})^2}}{K} \quad (7.9)$$

7.2 Inputs of the Mechanical Model

The same system properties as for the illustrative example for the regular pole (as shown in chapter 4) were used for a first evaluation of the motion of the pole and athlete for a pole with spring. The system properties are given in table 6.1 and the initial conditions in table 6.2. The control torques are shown in figure 6.3. As a first value the spring stiffness and uncompressed length were chosen to be 2100 [Nm²] and 1 [m]. The length of the spring is included in the total length of the pole (so not added). The motion predicted by the mechanical model is shown in figure 7.2. The spring is visualized by the lower segment of the pole.

The motion of the athlete and pole changed compared to a vault with a regular pole. A

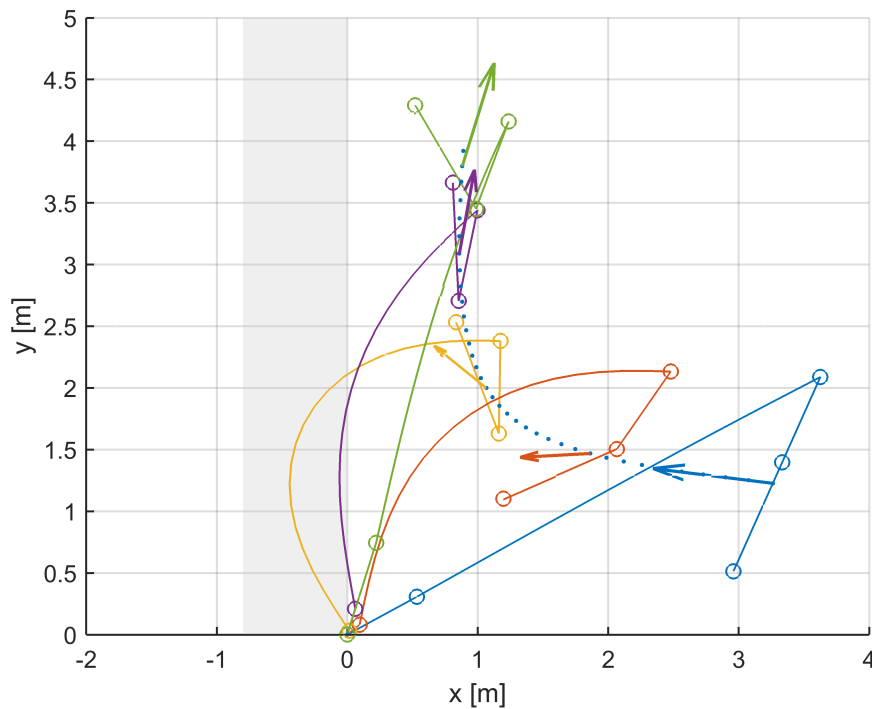


Figure 7.2: Diagram showing the deformation of the pole with a spring, body orientation of the two segment athlete and the velocity vector of the total center of mass of the athlete for every time interval of 0.2 [s] starting from take-off until pole release. The final position is shown as well. The trajectory of the total center of mass of the athlete is shown for every time increment of 0.02 [s]. The spring is visualized at the bottom end of the pole. The grey area indicates the area in which the cross bar can be placed. The results are for the system properties of table 6.1, initial conditions of table 6.2 and torque control profile shown in figure 6.3.

Table 7.1: Athlete and Pole Properties

Symbol	Value	Unit	Symbol	Value	Unit
m_1	20	kg	K_{sp}	2100	N/m ²
m_2	50	kg	$l_{0,sp}$	1	m
I_1	2.96	kgm ²	L	4.57	m
I_2	5.67	kgm ²	B	2522	Nm ²
l_1	0.4	m	l_3	0.4	m
l_2	0.35	m			

Table 7.2: Initial Conditions

Symbol	Value	Unit	Symbol	Value	Unit
x_{cm}	3.47	m	ϕ	0.4	rad
y_{cm}	1.72	m	θ	0	rad
\dot{x}_{cm}	-10.2	m/s	$\dot{\phi}$	0.2	rad/s
\dot{y}_{cm}	1.2	m/s	$\dot{\theta}$	0	rad/s

large part of the kinetic energy is now absorbed by the spring. There is too little energy left to rotate the pole to vertical and the athlete is propelled backwards. The athlete sets no score. Also, the duration of the vault is much shorter.

Thus the inputs used to determine the motion of the pole vault for a regular pole cannot be used directly for that of the pole with a spring. Some input parameters have to be varied in order to also obtain a realistic vault for the pole with a spring. It was chosen to only increase the horizontal velocity and keep the rest of the input values constant. Increasing the initial horizontal velocity helps to further rotate the pole to vertical. By trial and error the initial horizontal velocity was set to 10.2 [m/s]. This value resulted in a realistic vault according to the definition given in chapter 4.

The pole properties and initial conditions are shown in table 7.1 and table 7.2. Still, the same control torques are used as for the illustrative example presented in chapter 4 and shown in figure 6.3. These input values are used for the results discussed in the rest of the chapter.

7.3 Influence on Pole Vaulting Performance

In this section the influence a pole with a spring at the bottom end has on pole vaulting performance is evaluated. The motion of the athlete, the motion of the pole, the maximum height, the pole forces and the energy transformation are examined and discussed to determine the influence on pole vaulting performance .

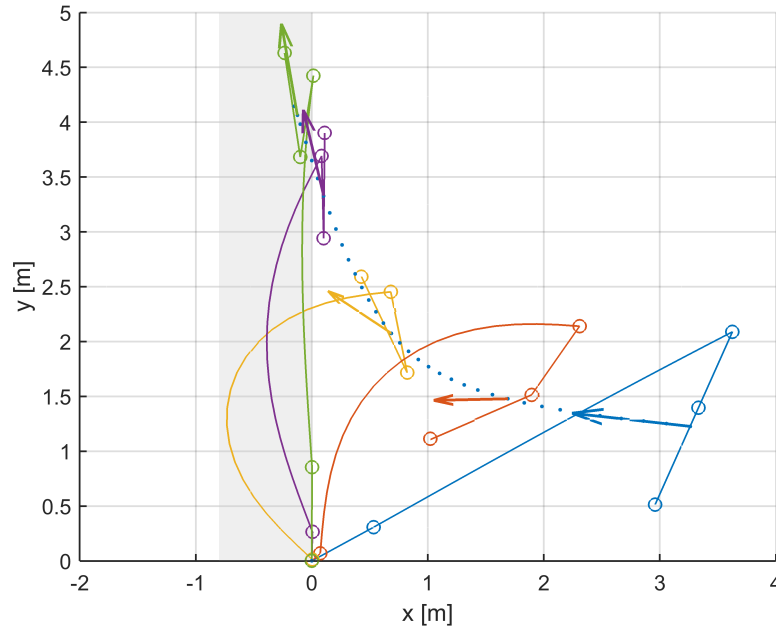


Figure 7.3: Diagram showing the deformation of the pole with a spring, body orientation of the two segment athlete and the velocity vector of the total center of mass of the athlete for every time interval of 0.2 [s] starting from take-off until pole release. The final position is shown as well. The trajectory of the total center of mass of the athlete is shown for every time increment of 0.02 [s]. The grey area indicates the area in which the cross bar can be placed. The results are for the system properties of table 7.1, initial conditions of table 7.2 and torque control profile shown in figure 6.3.

7.3.1 Motion of the Athlete and Pole, Trajectory and Peak Height

The motion of the athlete and pole is shown in figure 7.3 for the system properties shown in table 7.1, initial conditions in table 7.2 and the control torques shown in figure 6.3. The deformation of the pole and spring, as well as motion of the athlete are shown for every time step of 0.2 s and the final time $t_{end} = 0.7$ [s].

As can be seen in figure 7.3, the spring behaves as desired. The spring completely compresses until the pole is rotated to vertical. At this moment the spring starts to elongate again propelling the athlete upwards. This corresponds with the behaviour we specified for the spring in chapter 3 and the behavior that will maximize pole vaulting performance.

The trajectory of the vault seems similar to that of the vault for a regular pole shown in figure 6.4. The addition of the spring to the pole does not seem to have a large effect on the motions of the athlete and the deformation of the pole. This seems to indicate that the athlete can use a similar technique and can follow similar motions as when he jumps with a regular pole. The time of the vault is however reduced from 1 [s] to 0.7 [s]. This means he has to perform his actions faster. The time of 0.7 s might be too short for the athlete to rotate his body in an inverted position. If so the time of the vault can be increased again by for example reducing the bending stiffness of the pole.

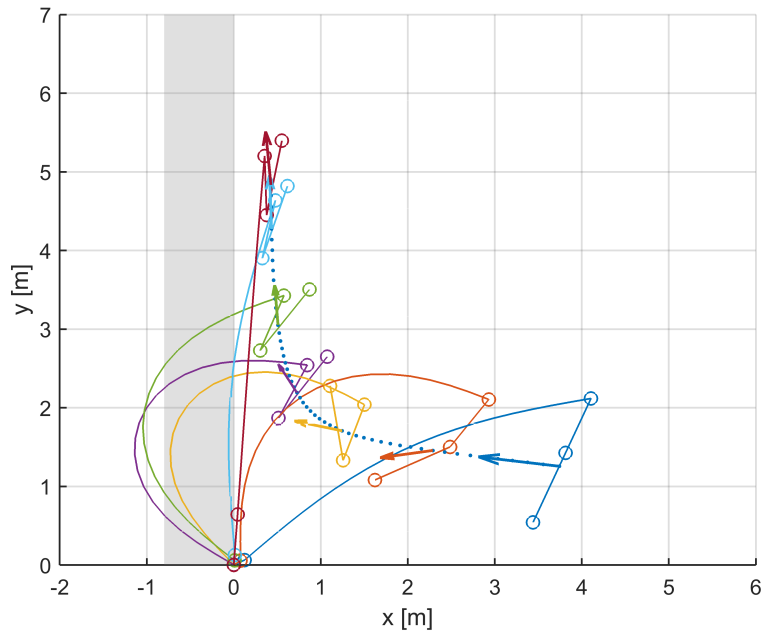


Figure 7.4: Diagram showing the deformation of the pole where a spring is added to the length ($L = 5.47$ [m]), body orientation of the two segment athlete and the velocity vector of the total center of mass of the athlete for every time interval of 0.2 [s] starting from take-off until pole release. The final position is shown as well. The trajectory of the total center of mass of the athlete is shown for every time increment of 0.02 [s]. The grey area indicates the area in which the cross bar can be placed. The results are for the system properties of table 6.1, initial conditions of table 6.2 and torque control profile shown in figure 6.3.

The deformation of the pole is much smaller. The maximum deflection (distance perpendicular to the pole chord) is much smaller compared to that of the regular pole shown in figure 6.4. This is because the spring does not bend and therefore the part of the pole that can bend is much shorter. This increases the bending stiffness.

Both, the duration of the vault and the deformation of the pole, can be increased if the spring is added to the pole length instead of inserted. By increasing the length, the pole bending stiffness will remain the same as for the vault with the regular pole. The trajectory of a vault where the spring is added to the pole length is presented in figure 7.4. The inputs used are shown in appendix I. A lot of parameters had to be varied in order to obtain a realistic vault, among others the take-off location, take-off velocity and control torques. Hence it is difficult to directly compare with the vault where the spring is inserted in the pole length shown in figure 7.3. However, adding the spring to the length of the pole increases the duration of the vault and increases the deflection of the pole as expected.

The maximum height reached by the athlete is 7.63 [m] at a distance of 74 [cm] behind the planting box. This is a significant increase compared to the 6.10 [m] of the vault with regular pole discussed in chapter 4. This increase is not only because of the spring. The initial velocity was increased to 10.2 [m/s] in order to obtain a feasible vault. This added

an extra 992 [J] to the system, which is equivalent to a height increase of 1.4[m]. However, the major increase in pole vaulting performance for a pole with a spring would be the reduction of the impact energy loss when the pole hits the back of the planting box. This energy loss is not included in the model so this effect cannot be determined. Adding a spring will however result in an approximately similar motion for the athlete and pole and similar maximum height when the impact energy loss is neglected. The increase in pole vaulting performance due to an increased return force seem small, in the order of 10 [cm]. This is too small to accurately determine with this mechanical model.

A critical remark has to be placed at this value. In order to obtain the right period for the spring to elongate during the pole straightening phase, the compression of the spring is almost 1 [m]. This is approximately 20 percent of the total length of the pole. The choice of modeling the spring aligned with the chord axis is now a significant simplification and not a correct representation of the real deformed shape. The real deformed shape of the pole will be different, and hence also the maximum height. A more accurate approach is to model the spring aligned with the tangent at the bottom end of the pole. The mechanical model developed is capable of this, but further work is required to implement this.

7.3.2 Pole Forces

The return force for the pole with the spring is higher than the regular pole. As can be seen in figure 7.5, the maximum vertical force reaches 2000 N compared to a maximum

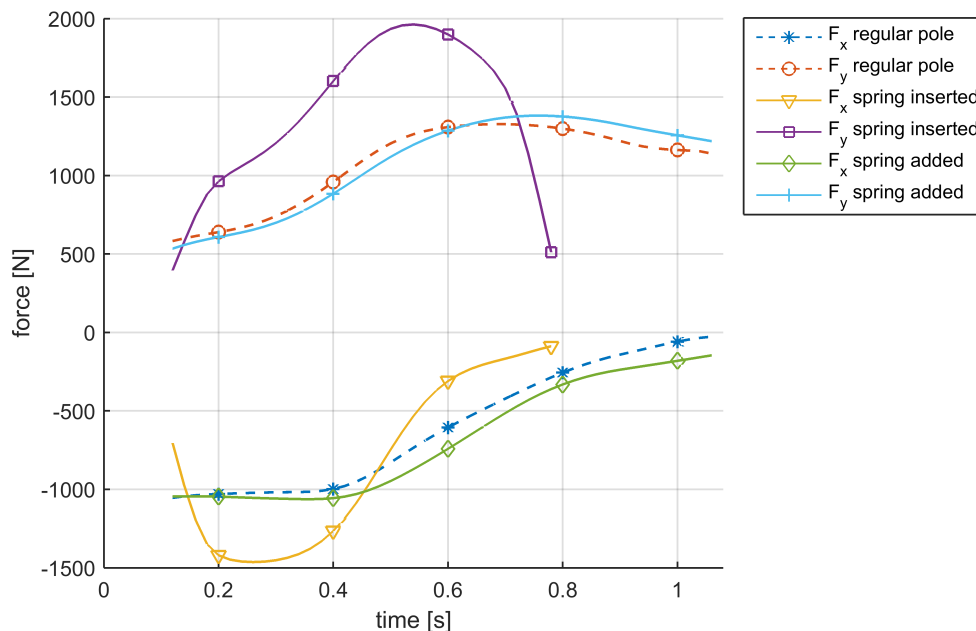


Figure 7.5: The horizontal F_x and vertical F_y ground reaction force component of the pole with a spring inserted and with a spring added to the pole length. The values for the pole with spring are compared to the results of the regular pole presented in chapter 6.

force of approximately 1250 N for the regular pole. As no impact mechanism is included the reduction in impact force cannot be compared directly. The increase in return force is because the pole with spring has a higher bending stiffness. The increase in maximum force also means that the pole should be designed for this.

The increase in pole force is because of the increased bending stiffness of the pole. When the spring is added to the pole the pole forces are similar to that of the regular pole. This is also shown in figure 7.5.

7.3.3 Energy Transformations

The energy transformations for the pole with spring are compared to that of the regular pole in figure 7.6. There are some differences. The pole with spring stores 22 percent more strain energy than the regular pole while the chord shortening is three percent less. The total strain energy stored in the pole with the spring at the time of maximum deflection is 22 percent higher compared to that of the regular pole. Almost one third of the total strain energy is stored in the spring.

It is interesting to see that the pole with the spring has a higher strain energy, but reaches this value for a smaller chord shortening. The minimum pole chord is $0.55L$, while for the regular pole the minimum pole chord is $0.52L$. However, the maximum deflection for the regular pole is significantly higher. At the time of maximum pole bend, the deflection is 1.66[m] (measured perpendicular to the pole chord axis). For the pole with the spring the

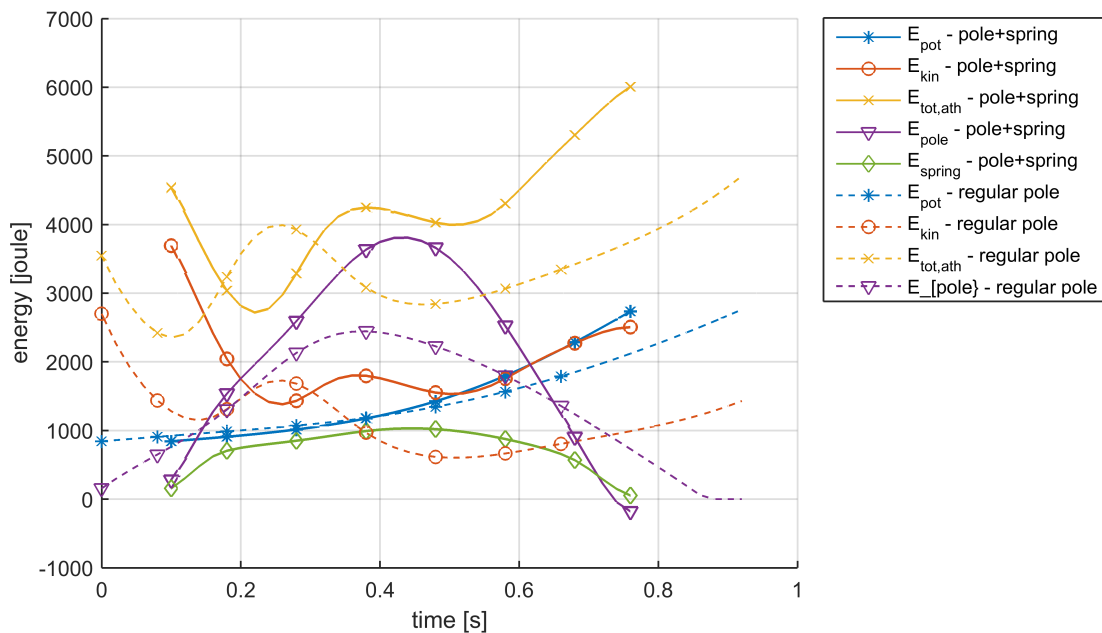


Figure 7.6: The different mechanical energies of the athlete and the pole. The values estimated by the model are compared to the energy transformations for the regular pole presented in chapter 6.

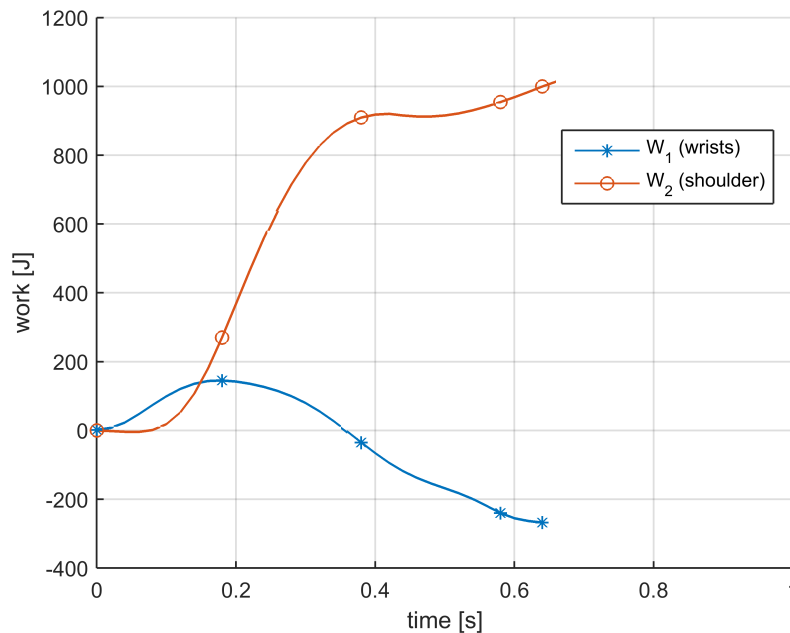


Figure 7.7: Work done by the wrists M_1 and hips M_2 during the vault for a pole with a spring inserted.

maximum deflection is 1.10[m]. This is as expected as the bending stiffness of the pole is higher.

Due to the higher initial kinetic energy, the athlete does not decelerate to the same velocity as for the illustrative example of the regular pole. The minimum kinetic energy value of the pole with the spring is more than double that of the regular pole (1400[J] versus 600[J]). This also speeds up the vault.

Although the same control torques are used as for the example of the regular pole, the work the athlete can do during the vault is higher for the pole with spring than for the regular pole. The work done by the athlete for the vault with a spring inserted to the pole is presented in figure 7.7. For the regular pole the work done by the hips was 650 [J] while for the pole with spring this is a 1000 [J]. Although the negative work done by the wrists is increased with a 100 [J] there is still a net energy gain.

Adding all the energy inputs, the theoretical maximum height the athlete could achieve for the example of the pole with spring inserted is 8.8 [m]. The energy efficiency ratio is thus 0.87. For the regular pole the energy efficiency ratio is 0.96.² This shows that the motion coordination for the vault using a pole with a spring is less optimal.

²Note that the values are higher than measured by experiments as all the energy losses are neglected. Hence the energy ratio will always be overpredicted.

7.4 Implementation

The compression of the spring is now quite significant. It is compressed for almost one meter. As discussed above, the influence on the motion of the athlete and pole seem relatively small. The vaulter can use the same technique and the pole deforms approximately the same. Also the trajectory seems similar. Nonetheless, to design a spring with a displacement of one meter that can be implemented in the pole is challenging.

Other solutions can be thought of. The compression of the spring could be reduced. The spring can then reach a completely compressed state during the vault. If the normal force component R_n is high enough, the spring will remain compressed. When the force is lower than the force required to completely compress the spring, the spring will start to elongate again. In this way the elongation can still happen during the pole straightening phase. The mechanical model can be used to determine the forces and help to determine the properties of the spring. It should be kept in mind that the energy stored in the spring should have a reasonable value in order to have a significant effect. If for example the spring can only store 100 [J] the impact on the return force will be small.³ The extra mass added to the pole by adding the spring might then outweigh the increase in performance due to the spring.

Also a non-linear spring can be used. A non-linear spring will have a different behavior over the time of the vault and can be used to obtain the required period. Either a spring that softens over compression or hardens over compression can be thought of. A spring that has a high stiffness during the first part of the compression might be more favorable as this would also already help to bend the pole.

7.5 Summary

In this chapter it is shown how the mechanical model developed in chapter 4 can be used to evaluate a pole with a spring. Two examples are evaluated for a pole where the spring is inserted in the pole and where the spring is added to the pole. The results showed that the motion, forces and energy transformation are similar to that of a vault with a regular pole, demonstrating the feasibility of this innovation. The improvement in pole vaulting performance is difficult to assess as the energy loss during impact is not included in the model. The increase in pole vaulting performance due to an increase in pole return force is too small to determine with this mechanical model. Further work has to be done to determine the optimum spring properties and determine how the spring can be implemented in the pole.

³A 100 [J] is very small compared to the initial energy of the athlete of approximately 4800 [J]

Innovation 2: Optimization of the Pole Vault Motion

In this chapter the second innovation will be evaluated. Results of the literature study indicated the potential of optimizing the pole vault motion. Tiny variations in take-off conditions, pole properties and motion coordination have a significant influence on pole vaulting performance. Currently, athletes use different motions and poles suggesting at least some athlete have a sub-optimal combination of motion, take-off and pole. Predicting the optimal combination can thus improve pole vaulting performance for these athlete.

First the contribution of the motion coordination of athlete to the pole vaulting performance are examined, both magnitude and sensitivity. Next an optimization formulation is presented and discussed how it can be implemented in the mechanical model.

8.1 Motion Coordination of the Athlete

The motion coordination of the athlete can be examined in more detail by examining the work done. The work done by the athlete for the example discussed in chapter 6 is again presented here in figure 8.1.

The energy added to the athlete-pole system is defined by the value of the work at the end of the pole support phase. For the example given this is approximately 650 [J] for the shoulder and -120 [J] for the wrists. Approximately 520 [J] is added to the system by muscular work, which is equivalent to a height increase of approximately 75 [cm]. This is approximately 15 percent of the height increase of the center of gravity of the athlete. The work done thus forms a significant contribution to the vaulting performance.

However, looking at figure 8.1 even more energy could have been added to the system. The work of the should rapidly increases during the first 0.3 [s] of the vault until a maximum is reached of approximately 750 [J]. This corresponds with the rotation of the body of athlete to an inverted vertical position. During the rest of the vault the athlete resist

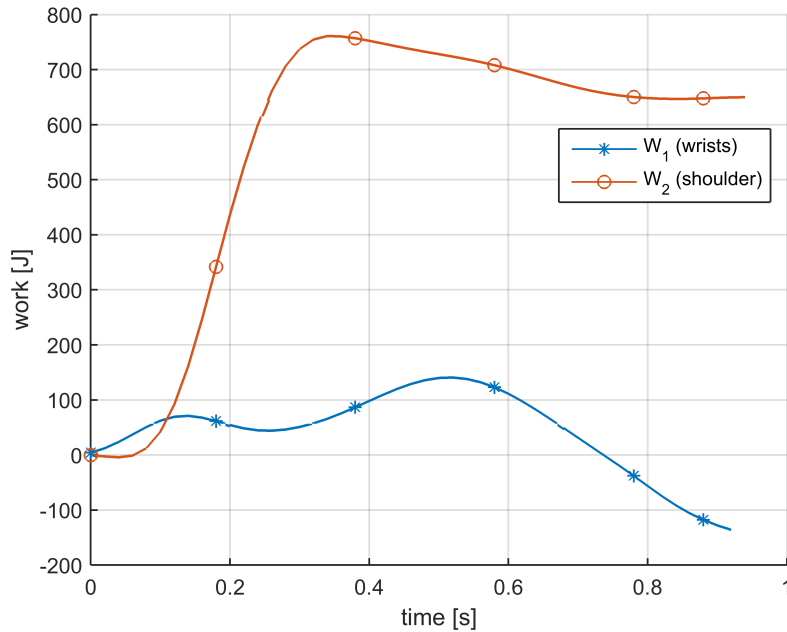


Figure 8.1: Work done by wrist M_1 and hips M_2 during the vault of the illustrative example.

further rotation of the body to remain in the upside down vertical position and hence performs negative work (work that resists the motion). The final value is approximately 100 [J] lower. This equivalent to a height of 15 [cm], the increase in height required to win an extra 50 points during the decathlon. This already indicates the importance of improving the motion coordination such that work done will remain at its maximum value.

Even better would be if the work could increase as in the first 0.3 [s], even more energy could be added to the system. It could not increase infinite as this would either include multiple somersaults of the athlete or super human strength.

Note that the work of the wrists will always be negative as the angle ϕ decreases relative to the initial condition as the arms align with the chord and rotate to vertical.

The athlete can either choose to increase the potential energy or kinetic energy of the different body parts he can control. The motion coordination can be seen as a strategy for this choice. The athlete can rotate certain body parts very fast while only slowly increase the potential energy or vice versa. The optimization of the motion coordination will result in the optimal strategy.

8.2 Sensitivity

The torque control is not only important because it is an energy input source. It is even more important as it largely determines how the energy input is converted into potential energy (determined by the motion of the athlete and pole). In that way it has a huge

influence on the energy conversion efficiency of the pole vault and hence pole vaulting performance as well.

There are three sets that determine the motion of the athlete and the pole during the pole support phase. As shown in the sensitivity section of chapter 6, the pole properties and initial conditions are the first two sets that determine the motion. The third set are the profiles of the control torques. Tiny time perturbations in the control torques result in significant changes in the motion of the pole and the athlete. An example is given in figures 8.2 and 8.4. The profile of the control torques are given in figures 8.3 and 8.5. The peak height of M_1 is reduced with 10 [Nm] for the first phase of the vault. This torque control profile is used for the trajectory presented figure 8.2. The system properties and initial conditions remain the same as defined in chapter 6. The maximum height of M_2 is increased with 10 [Nm] for the first phase for the trajectory shown in figure 8.4.

The reduction of 10 [Nm] for the minimum value of M_1 during the first phase of the vault already changes the direction of the trajectory significantly. At pole release the athlete is propelled backwards and hence will set a score. If the maximum value of M_2 is increased with 10 [Nm] during the first phase of the vault, the athlete will rotate his torso, head and legs too far. These cannot be brought back to vertical. Hence the athlete will not release the pole in an optimal body position.

The high sensitivities indicate that tiny perturbations can lead to significant deviations in vault height. Either significantly improving or decreasing vaulting performance. Athlete currently apply different strategies for their motion coordination. Further work has to be done to determine whether each athlete uses the optimal strategy given his initial conditions and pole properties, but this is most likely not the case. Based on the energy efficiency ratios determined by Ekevad and Lundberg (1995) there is still room for improvement. It is believed that the optimization model proposed can help the athlete to improve his performance significantly.

8.3 Optimization

The optimization problem can be simplified to two sets. It seems reasonable to assume that the optimal initial conditions for the athlete are close the following two limits. Approach as fast as possible and stretch his arms as far upwards as he can. If he approaches as fast as possible (highest resultant velocity) the kinetic energy put into the system is maximized. In theory if more kinetic energy is put into the system, more kinetic energy can be converted into potential energy.¹ By stretching his arms as far upwards the angle between the pole chord and the horizontal is maximized. Which means that the athlete has to put in less energy to rotate the pole to vertical. Using these two limits the initial conditions can be prescribed. That only leaves the control torques and the pole properties to be optimized.

The objective function for the optimization problem can be defined as follows.

$$f = \max(y_{cm,athlete}) \quad (8.1)$$

¹The effect of the take-off angle (and hence the ratio between the horizontal and vertical velocity) might still be an interesting parameter to investigate.

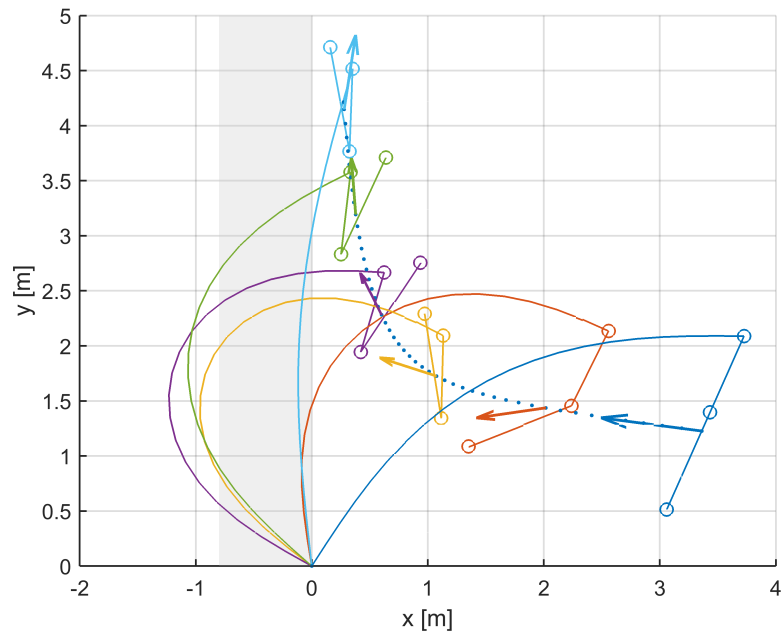


Figure 8.2: Trajectory of the pole vault for the control torques shown in figure 8.3.

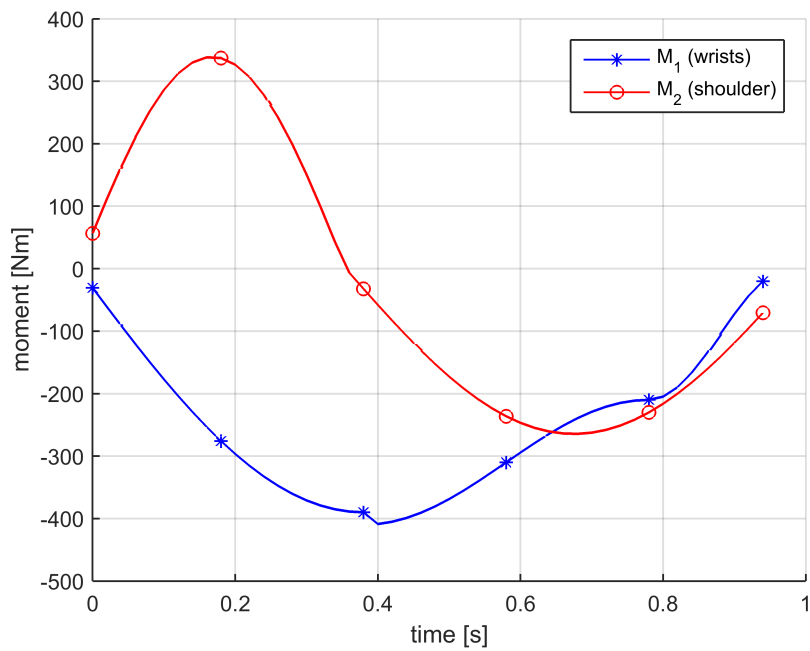


Figure 8.3: The control torques M_1 (wrists) and M_2 (shoulder) for the vault shown in figure 8.2.

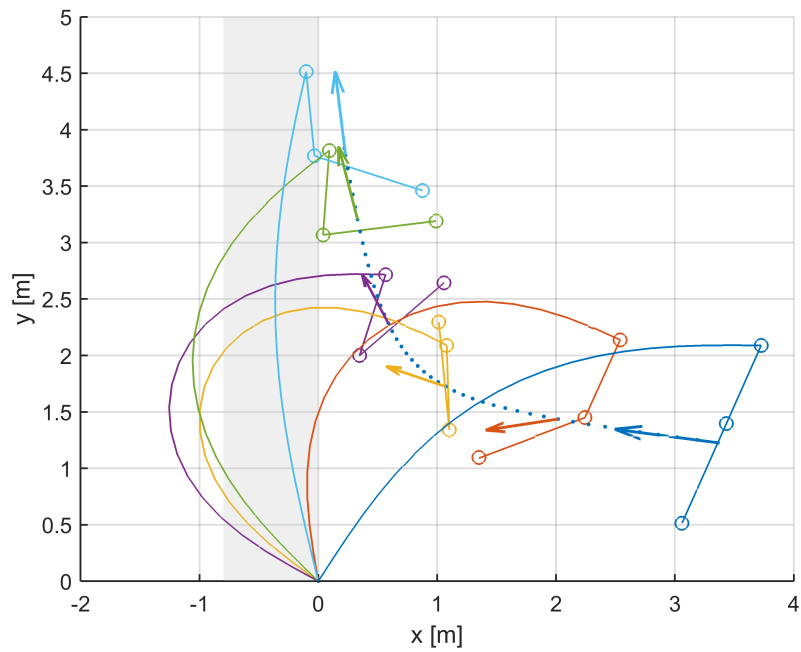


Figure 8.4: Trajectory of the pole vault for the control torques shown in figure 8.5.

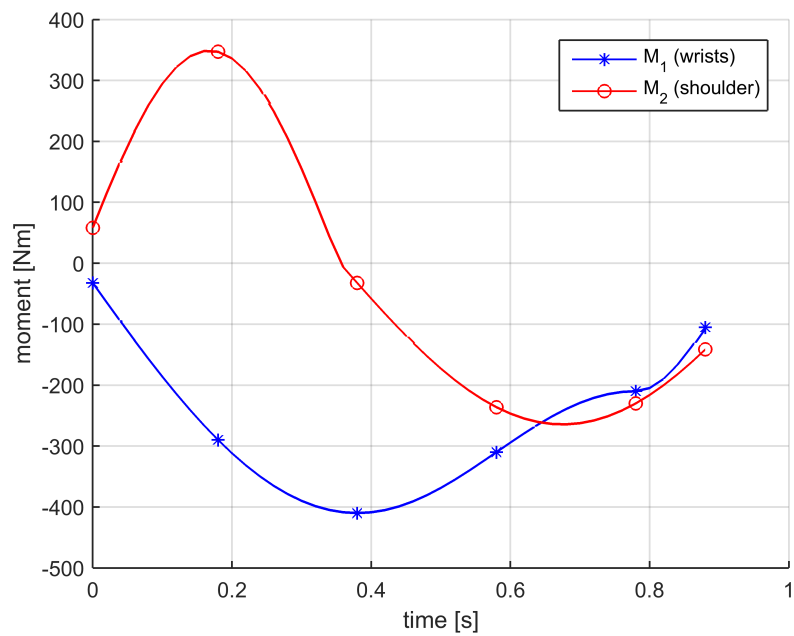


Figure 8.5: The control torques M_1 (wrists) and M_2 (shoulder) for the vault shown in figure 8.4.

Or equivalently, the maximum potential energy of the athlete. The constraints for the optimization problem are

- The x location for which the maximum height is achieved.
- The maximum torque the athlete can deliver.
- The maximum forces the pole can withstand.
- The maximum rotational velocity the athlete can withstand/achieve.
- The athlete has to have a forward velocity at pole release.²
- The y location of the top end of the pole cannot be lower than zero.³

Further work has to be performed to solve this problem. The model developed in chapter 4 can be used for the optimization. The computational time to simulate one vault is approximately seventeen seconds using a standard computer.

8.4 Summary

In this chapter the optimization problem of the pole vault is examined. It was demonstrated that the pole vaulting performance is influenced by three sets: the system properties, the initial conditions at take-off and the motion coordination during the vault. The optimum values of the initial conditions can be reasonably estimated at first such that only the system properties and motion coordination have to be optimized. An optimization problem was formulated and it was demonstrated that the mechanical model developed in this thesis can be used for the optimization. The optimized motion coordination can help the athlete to improve his technique and choose the optimal pole stiffness and length. Small variations for these parameters already resulted in significant differences in pole vaulting performance indicating the high potential of this solution to improve pole vaulting performance.

²To ensure that the athlete crosses the bar from the correct side.

³In the model there is no contact constraint between the ground and the athlete or pole. Therefore, in theory the pole vault motion could go below the ground. In reality, this is of course not possible and has therefore to be constrained.

Conclusions and Recommendations

In this MSc thesis report a model based exploration of the pole vault event is presented that identifies and assesses innovations from an engineering point of view that can improve pole vaulting performance of the top Dutch decathletes at the Tokyo Summer Olympics of 2020. Three steps are followed.

The first step consists out of a literature study. The following conclusions can be drawn from the results of the literature study. The current pole vaulting performance has reached a limit at approximately 6.00 [m]. The velocity at take-off and the maximum pole bend are important parameters that determine the pole vaulting performance. The current approach to improve pole vaulting performance tries to increase the take-off velocity by reducing the mass of the pole. However, current initial velocity is no longer limited by the mass of the pole but by the arm swing restriction. Another approach tries to improve the pole stiffness and pole length selection. Also here a limit is reached as the athlete currently use poles close to the optimum values. Innovations are required to improve pole vaulting performance. In the literature study two innovations are identified. The first innovation reduces the energy loss when the pole impacts with the planting box by adding a spring to the bottom end of the pole. The second innovation aims at optimizing the pole vault motion. Both innovations are evaluated in step three.

In the second step a mechanical model is developed that can describe the pole vault motion. The pole vault motion is simplified to a two dimensional motion neglecting the impact of the pole with the take-off box and the pull-up actions of the athlete. The model consists out of a massless pole and a two segment athlete. The motion coordination of the athlete is modeled using control torques. The control torque profile is determined from a starting value that prescribed the body orientation of the athlete. The pole deformation and forces are calculated using a numerical iterative solution that is based on the elastica solution of a slender rod loaded by a compressive force. The equations of motion are derived using the TMT-method. Results of the model are comparable with results available in literature for both magnitude and profile. The model is highly sensitive to multiple inputs. This decreases the robustness of the model and makes it difficult to compare individual parameters.

In the third step the two innovations identified in step one are evaluated using the mechanical model developed in step two. The evaluation of adding a linear elastic spring to the bottom end of the pole demonstrates that the motion of the athlete remains similar to a vault when the athlete uses a regular pole. This indicates that it should be feasible for an athlete to jump with such a pole using a similar technique and that the athlete can adapt to this in time for the Summer Olympics of 2020 in Tokyo. The increase in pole return force does not seem to have a significant influence on pole vaulting performance, while the reduction in impact force cannot be measured by the model. Results of the literature study suggest that the energy loss is equivalent to a decrease in height of 50 [cm]. A critical remark has to be placed at these results. The linear elastic spring compresses almost one meter and the choice of aligning the spring with the pole chord axis results in a significant different deformation.

The evaluation of the optimization of the pole vault motion demonstrates the sensitivity of the motion coordination of the athlete on pole vaulting performance. Tiny adaptations in to the technique of the athlete can result increases of 15 [cm] in vault height. The evaluation shows that optimizing the pole vault motion can significantly improve the pole vaulting of the top Dutch decathletes at the Summer Olympics of 2020. The optimization is also formulated for which the mechanical model developed in step two can be used.

To conclude, both innovations have the potential to improve pole vaulting performance of the top Dutch decathletes at the Summer Olympics of 2020 in Tokyo. The improvement in pole vaulting performance for the pole with spring cannot be determined accurately yet, but the improvement in pole vaulting performance by optimizing the pole vault motion can be significant and in the order of the required 15 [cm].

Several recommendations can be made for future work. The recommendations are on how the quality of the model can be improved and on how the two innovations can be implemented.

First it is recommended to develop a better strategy to determine the control torques. The current approach is not only time consuming but it is also difficult to analyze individual parameters using this strategy. When one parameter is varied, multiple other parameters have to be updated as well to obtain a realistic vault. A better approach would be to only update the control torque profile when one parameter of the system properties or initial conditions is varied. If the control torques are then optimized the effect of varying one parameter of the system properties or initial conditions on pole vaulting performance can be determined.

The second recommendation is to validate the model with an experiment that measures the specific input for the mechanical model¹ and desired outputs for a real vault. For the first validation done in chapter 6, the results of the mechanical model are compared to the results of the experiments that had been done for different purposes. Hence a direct comparison could not be made. This can be improved by performing a experiment specifically to validate the model. This will give a more accurate indication of the quality of the model.

For the further work on implementing the pole with spring it is recommended to improve the model with an impact sub-model and align the spring with the tangent at the lower

¹system properties, initial conditions and control torques

end of the pole. With these modifications the effect of inserting a spring on pole vaulting performance can be assessed more accurately. It is also recommended to examine a non-linear spring such that the compression can be reduced. It is also already recommended to investigate how the pole with spring can be designed and produced.

The future work of the optimization of the pole vault motion includes the development of the optimization itself. However, it is also recommended to increase the number of segments of the athlete, preferably a segment for the arms, torso, upper legs and lower legs. This will add additional control torques at the hips and knees, but the motion of the athlete can be described in more detail. This will increase the feedback that can be given to the athlete to adapt his technique.

References

- Abram, E., Dam, M., & Dinkelberg, T. (2013). *Pole vault - research and design report*.
- Adamczewski, H., & Perl, B. (1997). Run-up velocities of female and male pole vaulting and some technical aspects of women's pole vault. *New studies in athletics*, 12, 63–76.
- Angulo-Kinzler, R. M., Kinzler, S. B., Balias, X., Turro, C., Caubet, J. M., Escoda, J., & Prat, J. A. (1994). Biomechanical analysis of the pole vault event. *Journal of Applied Biomechanics*, 10(2), 147–165.
- Arampatzis, A., Schade, F., & Brüggemann, G.-P. (2004). Effect of the pole–human body interaction on pole vaulting performance. *Journal of biomechanics*, 37(9), 1353–1360.
- Boyce, W. E., DiPrima, R. C., & Haines, C. W. (1969). *Elementary differential equations and boundary value problems* (Vol. 9). Wiley New York.
- Burgess, S. (1998). The modern olympic vaulting pole. *Materials & design*, 19(5), 197–204.
- Davis, C., Kukureka, S., Hubbard, M., Mehta, R., & Pallis, J. (2004). Effect of materials and manufacturing on the bending stiffness of vaulting poles. *The Engineering of Sport*, 5, 245–252.
- Dempster, W. T. (1955). Space requirements of the seated operator: geometrical, kinematic, and mechanical aspects of the body, with special reference to the limbs.
- Dillman, C. J., & Nelson, R. C. (1968). The mechanical energy transformations of pole vaulting with a fiberglass pole. *Journal of Biomechanics*, 1(3), 175–183.
- Ekevad, M., & Lundberg, B. (1995). Simulation of smartpole vaulting. *Journal of Biomechanics*, 28(9), 1079–1090.
- Ekevad, M., & Lundberg, B. (1997). Influence of pole length and stiffness on the energy conversion in pole-vaulting. *Journal of biomechanics*, 30(3), 259–264.
- Fletcher, J., Lewis, H., & Wilkie, D. (1960). Human power output: the mechanics of pole vaulting. *Ergonomics*, 3(1), 30–34.
- Frère, J., Chollet, D., & Tourny-Chollet, C. (2009). Assessment of the influence of pole carriage on sprint kinematics: A case study of novice athletes. *International Journal of Sports Science and Engineering*, 3(1), 3–10.
- Frère, J., Göpfert, B., Hug, F., Slawinski, J., & Tourny-Chollet, C. (2012). Catapult effect in pole vaulting: Is muscle coordination determinant? *Journal of Electromyography and Kinesiology*, 22(1), 145–152.
- Frère, J., L'hermette, M., Slawinski, J., & Tourny-Chollet, C. (2010). Mechanics of pole vaulting: a review. *Sports biomechanics*, 9(2), 123–138.
- Gudelj, I., Zagorac, N., & Babić, V. (2013). Influence of kinematic parameters on pole vault results in top juniors. *Collegium antropologicum*, 37(2), 25–30.
- Hay, J. G. (1968). Mechanical energy in pole vaulting. *Track Technique*, 33, 1047–1051.
- Hubbard, M. (1980a). Dynamics of the pole vault. *Journal of Biomechanics*, 13(11), 965–976.
- Hubbard, M. (1980b). An iterative numerical solution for the elastica with causally mixed inputs. *Journal of Applied Mechanics*, 47(1), 200–202.
- Johnson, W., Al-Hassani, S., & Lloyd, R. (1975). Aspects of pole vaulting mechanics. *Proceedings of the Institution of Mechanical Engineers*, 189(1), 507–518.

- Linthorne, N. P. (2000). Energy loss in the pole vault take-off and the advantage of the flexible pole. *Sports Engineering*, 3(4), 205–218.
- Linthorne, N. P., & Weetman, A. G. (2012). Effects of run-up velocity on performance, kinematics, and energy exchanges in the pole vault. *Journal of sports science & medicine*, 11(2), 245.
- Love, A. E. H. (1944). *A treatise on the mathematical theory of elasticity* (Vol. 1). Cambridge University Press.
- McGinnis, P., & Bergman, L. (1983). A dynamic finite element model of pole vaulting. *Journal of Biomechanics*, 16(4), 287–288.
- Moore, J. K., Hubbard, M., Kooijman, J., & Schwab, A. (2009). A method for estimating physical properties of a combined bicycle and rider. In *Asme 2009 international design engineering technical conferences and computers and information in engineering conference* (pp. 2011–2020).
- Morlier, J., & Cid, M. (1996). Three-dimensional analysis of the angular momentum of a pole-vaulter. *Journal of biomechanics*, 29(8), 1085–1090.
- Morlier, J., & Mesnard, M. (2007). Influence of the moment exerted by the athlete on the pole in pole-vaulting performance. *Journal of biomechanics*, 40(10), 2261–2267.
- Morlier, J., Mesnard, M., & Cid, M. (2008, may). Pole-vaulting: Identification of the pole local bending rigidities by an updating technique. *Journal of Applied Biomechanics*, 24(2), 140–148.
- Ohshima, S., Nashida, Y., & Ohtsuki, A. (2010). Optimization of pole characteristic in pole vaulting using three-dimensional vaulter model. *Procedia Engineering*, 2(2), 3191–3196.
- Pikulsky, T. T. (1964). *Cinematographical and mechanical analysis of pole vaulting with the fibre glass pole*. Unpublished doctoral dissertation.
- Ropret, R., Kukulj, M., Ugarkovic, D., Matavulj, D., & Jaric, S. (1998). Effects of arm and leg loading on sprint performance. *European journal of applied physiology and occupational physiology*, 77(6), 547–550.
- Schade, F., Arampatzis, A., & Brüggemann, G.-P. (2000). Influence of different approaches for calculating the athlete's mechanical energy on energetic parameters in the pole vault. *Journal of Biomechanics*, 33(10), 1263–1268.
- Schade, F., Arampatzis, A., & Brüggemann, G.-P. (2006). Reproducibility of energy parameters in the pole vault. *Journal of biomechanics*, 39(8), 1464–1471.
- Schwab, A., & van der Linde, R. (1997). *Multibody dynamics b*. (Available: <http://bicycle.tudelft.nl/schwab/>)
- Southwell, R. V., et al. (1941). *Introduction to the theory of elasticity for engineers and physicists*. Oxford University Press.
- Walker, H., & Kirmser, P. (1973). Computer modeling of pole vaulting. *Mechanics and Sport, AMD*, 4, 131–141.
- Zagorac, N. (2013). Influence of kinematic parameters on pole vault result in top junior athletes. *Collegium antropologicum*, 37(2), 19-24.
- Zagorac, N., Retelj, E., & Katić, R. (2008). Successful pole vault influenced by certain kinematical parameters. *Collegium antropologicum*, 32(4), 1133–1139.

Appendix A

Convective Acceleration

In this appendix the complete expression for the convective acceleration h_i is given.

$$h_i = \begin{bmatrix} 0 \\ 0 \\ 0 \\ h_4 \\ h_5 \\ 0 \end{bmatrix} \quad (\text{A.1})$$

where h_4 is

$$h_4 = l_3 \dot{\phi}^2 \sin(\phi + \theta) + l_3 \dot{\theta}^2 \sin(\phi + \theta) + l_2 \dot{\phi}^2 \sin(\phi) + 2l_3 \dot{\phi} \dot{\theta} \sin(\phi + \theta) \quad (\text{A.2})$$

and h_5 is

$$h_5 = l_3 \dot{\phi}^2 \cos(\phi + \theta) + l_3 \dot{\theta}^2 \cos(\phi + \theta) + l_2 \dot{\phi}^2 \cos(\phi) + 2l_3 \dot{\phi} \dot{\theta} \cos(\phi + \theta) \quad (\text{A.3})$$

Appendix B

Trigonometry

Double Angle Formulae

$$\sin \phi = 2 \cos \left(\frac{1}{2} \phi \right) \sin \left(\frac{1}{2} \phi \right)$$

$$\cos(2\phi) = 1 - 2 \sin^2 \phi$$

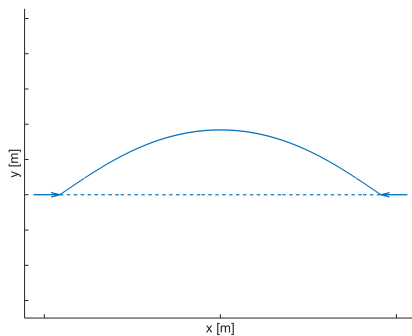
Pythagorean Identities

$$\cos^2 \phi + \sin^2 \phi = 1$$

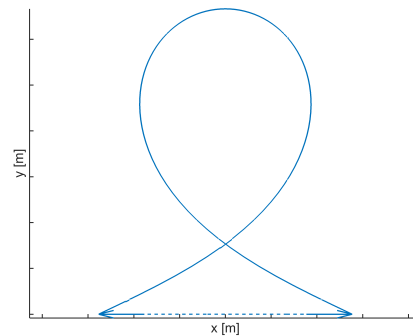
Appendix C

Elastica Shapes

The elastica solution presented in chapter 4 can describe various forms of the pole as the slope γ increases. This is illustrated in figure C.0. Figure (a) shows the deflection of the pole that usually takes place during the jump. However, in theory different different forms are also possible. If the force is increased the pole can form a loop as shown in figure (b). In reality this is not possible as the pole will contact itself (if the pole has not broken yet). Other shapes can be derived if ϕ is increased past $\pi/2$. Various shapes for this case are shown in figures (c)-(f). A special theoretical case is when the pole endpoints coincide. This is shown in figure (h) and occurs for an angle γ of approximately 130 degrees. The pole consist of several loops lying one over another. When γ increases the top end proceeds in the negative x -direction, this is shown in figure (i). (Love, 1944)



(a)



(b)

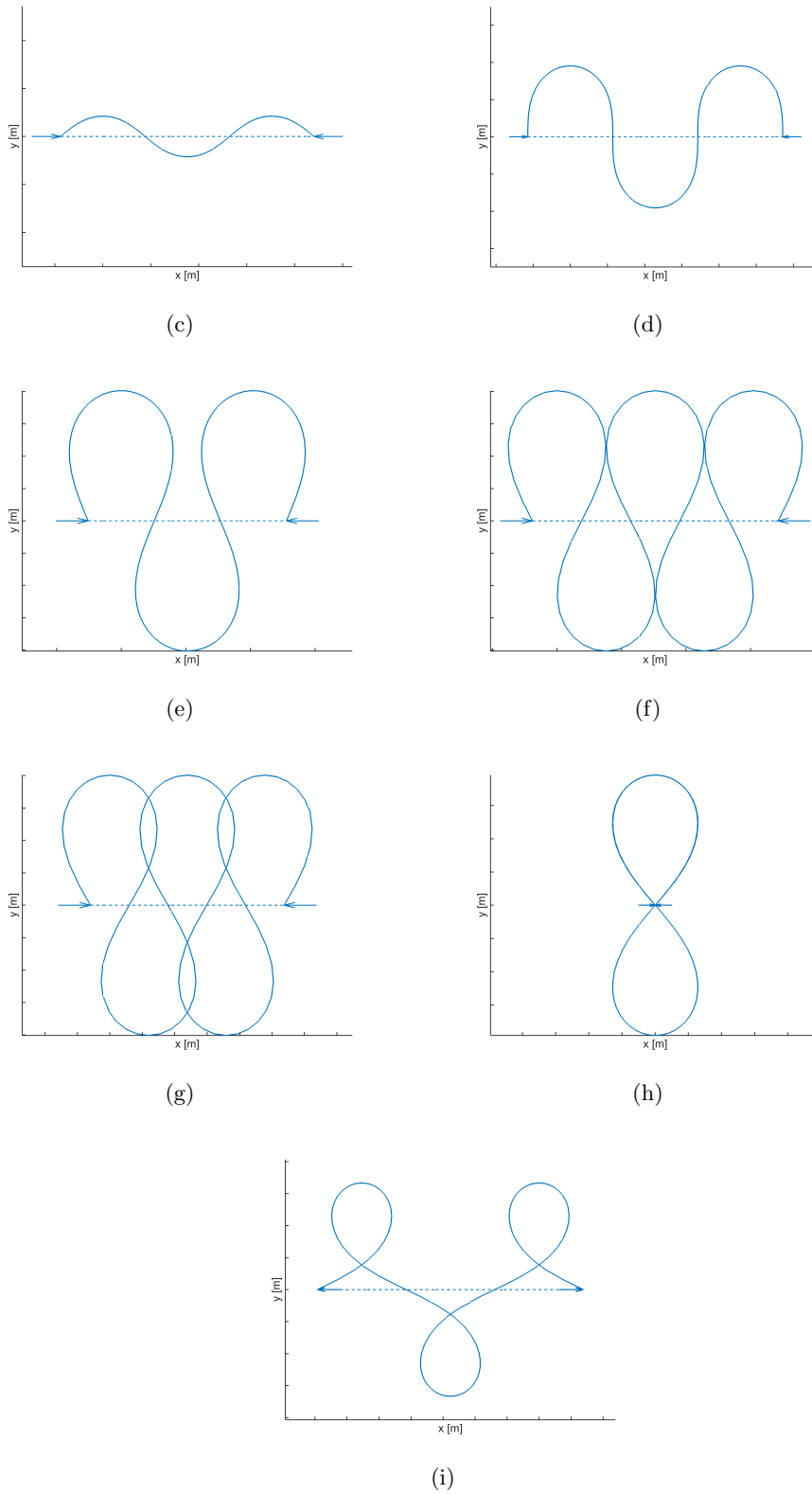


Figure C.0: Various deformed shapes of the pole for huge deflections.

Appendix D

MATLAB Script

The mechanical model developed in chapter 4 was solved using the computer program MATLAB 2013. In this appendix the functions used for the iterative numerical solution of the non-linear system of equations and the function used to determine the elliptic integrals are presented. Also the problems encountered using these functions are discussed.

To solve the non-linear system of equations to determine the pole forces the built-in solver 'fsolve' was used. This solver uses a trust-region-dogleg algorithm by the default but can also use a trust-region-reflective and Levenberg-Marquardt algorithm.

The elliptic integrals of the first and second kind were also determined with built-in functions. For the first kind this was 'ellipticF' and for the second kind 'ellipticE'. For the complete elliptic integrals the built-in function 'ellipke' was used. Note that all these built-in functions use k^2 as input for the elliptic integrals instead of k (as we defined as inputs for the elliptic integrals in chapter 4).

The MATLAB profiler was used to measure the execution time of the script. The results indicated that eighty percent of the execution time was spent in the functions 'ellipticF' and 'ellipticE'. The reason for this is that these function use a symbolic toolbox, which requires a lot of computational time. Igor Moiseev developed a function 'elliptic12' that calculates the value of the elliptic integrals of the first and second kind using a method of the arithmetic-geometric mean and descending Landen transformation (his function can be retrieved from: <https://wspr.wordpress.com/2011/02/03/elliptic-integrals-in-matlab/>). This function has the same accuracy as 'ellipticF' and 'ellipticE' but the computational effort is thirty times less. Hence using this function results in a significant reduction in execution time.

Appendix E

Small Angle Theorem Solutions for Pole Forces

In this appendix the small angle theorem solution will be given to determine the pole shape and forces when the deflection is small. The pole is loaded by a compressive force R and an applied moment M_0 at one end. The pole is assumed to be simply supported. The schematic diagram for this system is shown in figure E.1. It is assumed that the deflections are small: $y' \ll 1$.

First an equation for the shape of the pole is derived. This equation can then be used to determine the compressive pole force.

The linear elastic beam deflection can be described with the following equation.

$$EIy'' = -M \quad (\text{E.1})$$

where EI is the bending stiffness of the pole. The applied moment M can be defined as:

$$M = Ry + M_0 \frac{x}{l} \quad (\text{E.2})$$

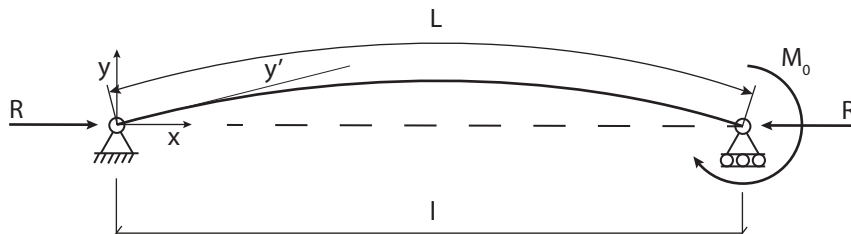


Figure E.1: Schematic diagram of a simply supported beam subjected to a compressive force and an applied moment at one end.

where l is the compressed chord length. This expression can be substituted in the equation of the beam deflection.

$$y'' + \frac{R}{EI}y = -\frac{M_o}{EI} \left(\frac{x}{l}\right) \quad (\text{E.3})$$

This is a non-homogeneous second order differential equation. It can be solved by determining the homogeneous and particular solution. The assumed homogeneous solution is

$$y = a \cos(\mu x) + b \sin(\mu x) \quad (\text{E.4})$$

where μ is defined as

$$\mu = \sqrt{\frac{R}{EI}} \quad (\text{E.5})$$

and a and b are unknown constants that have to be derived from the boundary conditions.

The assumed particular solution is defined as

$$y = a + bx + cx^2 + dx^3 \quad (\text{E.6})$$

where a , b , c and d are unknowns that have to be solved. Note that a and b are other unknown constants than the a and b for the homogeneous solution. The first and second order derivative of this assumed particular solution are

$$y' = b + 2cx + 3dx^2 \quad (\text{E.7})$$

$$y'' = 2c + 6dx \quad (\text{E.8})$$

Substitute the expression found for y and y'' into equation E.3.

$$EI(2c + 6dx) + R(a + bx + cx^2 + dx^3) = -\frac{M_o}{l}x \quad (\text{E.9})$$

The four unknown constants of the particular solution can now be solved at the location $x = 0$ and solving the first, second and third order derivative of equations E.9. Starting with the third order derivative.

$$6Rd = 0 \quad (\text{E.10})$$

As R is not equal to zero, $d = 0$. Next the second order derivative can be solved for c . The value for d is already substituted.

$$2Rc = 0 \quad (\text{E.11})$$

Hence $c = 0$. Then the first order derivative can be solved for b . The values for d and c are already substituted.

$$Rb = -\frac{M_0}{l} \quad (\text{E.12})$$

So $b = -\frac{M_0}{Rl}$. Finally, equation E.9 can be solved for a .

$$Ra = 0 \quad (\text{E.13})$$

So $a = 0$. The constants can be substituted in the particular solution shown in equation E.6. The solution for the differential equation now looks as follows.

$$y = a \cos(\mu x) + b \cos(\mu x) - \frac{M_0}{Rl} x \quad (\text{E.14})$$

The constants a and b of the assumed homogeneous solution can be determined by substituting the boundary conditions: $y(0) = 0$ and $y(L) = 0$. The results are

$$a = 0 \quad (\text{E.15})$$

and

$$b = \frac{M_0}{R \sin(\mu l)} \quad (\text{E.16})$$

Substituting these expression results in the following expression for y

$$y = \frac{M_0}{R} \left(\frac{\sin(\mu x)}{\sin(\mu l)} - \frac{x}{l} \right) \quad (\text{E.17})$$

This can be rewritten to include the ratio between the compressive force and the Euler buckling load R_{crit} as follows. The Euler buckling load is defined as

$$R_{cr} = \pi^2 \frac{EI}{l^2} \quad (\text{E.18})$$

A new variable λ is introduced that is the square root of the ratio of the compressive force and the Euler buckling load.

$$\lambda = \sqrt{\frac{R}{R_{crit}}} \quad (\text{E.19})$$

Substitute the expression of R_{crit}

$$\lambda = \sqrt{\frac{Rl^2}{\pi^2 EI}} \quad (\text{E.20})$$

The expression for μ given in equation E.5 can be substituted in this equation.

$$\lambda = \frac{l}{\pi}\mu \quad (\text{E.21})$$

and can be rewritten to

$$\mu x = \lambda\pi \frac{x}{l} \quad (\text{E.22})$$

This expression can then be substituted in the solution of the differential equation given in equation E.17. The results is

$$y = \frac{M_0}{R} \left(\frac{\sin(\lambda\pi(\frac{x}{l}))}{\sin(\lambda\pi)} - \frac{x}{l} \right) \quad (\text{E.23})$$

This expression can be used to determine the shape of the pole for small deflections. However, the compressive force R is still unknown. The compressive force can be determined from the compressed length, which is given as an input for the pole sub-model. The shape of the pole was derived first as equation E.23 is required to determine R . The derivation to determine R starts with the following expression for the total length of the pole L .

$$L = \int_0^l ds \quad (\text{E.24})$$

where the arclength ds is defined as

$$ds = \sqrt{1 - y'^2} dx \quad (\text{E.25})$$

where y' can be derived from equation E.23 and is

$$y' = \frac{M_0}{Rl} \left(\frac{\lambda\pi \cos(\lambda\pi\frac{x}{l})}{\sin(\lambda\pi)} - 1 \right) \quad (\text{E.26})$$

Assuming small displacements $y' \ll 1$ the expression for ds can be approximated with the following Taylor series.

$$\sqrt{1 + y'^2} = \sqrt{1 + \epsilon} \approx 1 + \frac{1}{2}\epsilon - \frac{1}{8}\epsilon^2 + \frac{1}{16}\epsilon^2 - \frac{5}{128}\epsilon^4 + \dots \quad (\text{E.27})$$

where $\epsilon = y'^2$.

This expression can be substituted in equation E.24

$$L = \int_0^l (1 + \frac{1}{2}\epsilon - \frac{1}{8}\epsilon^2 + \frac{1}{16}\epsilon^2 \dots) dx \quad (\text{E.28})$$

The upper limit l of the integral is unknown and has to be rewritten. This can be done by introducing the variable ϕ .

$$\phi = \pi \frac{x}{l} \quad (\text{E.29})$$

Then dx is

$$dx = \frac{l}{\pi} d\phi \quad (\text{E.30})$$

Substitute this expression for dx in equation E.28.

$$L = \int_0^\pi \frac{l}{\pi} \left(1 + \frac{1}{2}\epsilon - \frac{1}{8}\epsilon^2 + \frac{1}{16}\epsilon^2 \dots\right) d\phi \quad (\text{E.31})$$

If this expression is integrated for the first two terms the result is

$$\delta = \frac{l - L}{l} = -\mu^2 \left(\frac{2\pi^2 \lambda^2 - 4 \sin(\pi\lambda)^2 + \pi\lambda \sin(2\pi\lambda)}{8 \sin(\pi\lambda)^2} \right) \quad (\text{E.32})$$

which can be rewritten using the double angle formula to

$$\delta = \mu^2 \left(\frac{2\pi^2 \lambda^2 \sin(2\pi\lambda) + 2 \cos(2\pi\lambda) - 2}{4 (\cos(2\pi\lambda) - 1)} \right) \quad (\text{E.33})$$

This equation can be solved for R . The shape can then be determined with equation E.23.

Reversed Inputs Pole Sub-Model

In this appendix the solution is presented that can determine the applied moment M to the top end of the pole and the compressed chord length h from the normal component of the compressive force R_n and the slope θ at the top end of the pole relative to the R -direction (as shown in figure F.1).

This is not exactly the reverse process of the pole sub-model as that uses M and l as input to determine R and γ . However, R and γ can be determined from R_n and θ as follows.

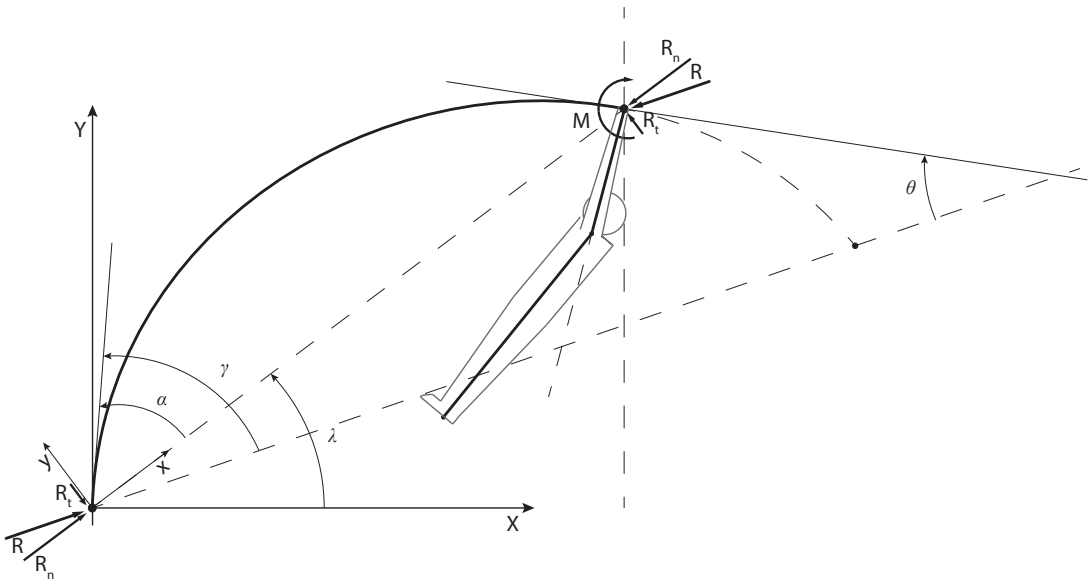


Figure F.1: Schematic diagram of the pole

$$R_n = R \cos(\lambda) \quad (\text{F.1})$$

$$k \sin(\varphi) = \sin\left(\frac{\theta - \lambda}{2}\right) \quad (\text{F.2})$$

The variables k , λ and ϕ are all a function of only R and γ .¹ The variable k is the elliptic modulus and given by

$$k = \sin\left(\frac{1}{2}\gamma\right) \quad (\text{F.3})$$

The variable φ is the value at an arclength $s = L$ and is defined as follows.

$$\varphi = \pi \frac{L}{L'} - \frac{\pi}{2} \quad (\text{F.4})$$

where the fictitious pole length L' is defined as

$$L' = \sqrt{\frac{B}{R}} 2K(k, \pi/2) \quad (\text{F.5})$$

and where K is the elliptic integral of the first kind. The variable λ is the slope between the pole chord and the pole chord axis of the fictitious rod (as shown in figure 4.5) and can be calculated as follows.

$$\lambda = \tan^{-1}\left(\frac{y(\varphi, k)}{x(\varphi, k)}\right) \quad (\text{F.6})$$

where the x' and y' coordinates can be determined using the following two equations and substituting the values for k and ϕ defined above.

$$x'(\varphi, k) = \sqrt{\frac{B}{R}} (2E(\varphi, k) - K(k, \varphi)) \quad (\text{F.7})$$

$$y'(\varphi, k) = -\sqrt{\frac{B}{R}} 2k \cos \varphi \quad (\text{F.8})$$

and E is the elliptic integral of the second kind. Note that all these equations are already derived in chapter 4.

The system of two equations defined above (equation F.1 and equation F.2) is solved using an iterative numerical method. An initial value is chosen for R and γ . The pre-programmed non-linear system solver 'fsolve' in MATLAB 2013 is then used to solve the system of two equations. This will yield the correct values for R and γ .

¹The detailed definition of all the variables can be found in chapter 4.

Now the problem is an exact reverse input problem. The system of two equations derived for the pole sub-model in chapter 4 can now be used to determine M and l for the determined values of R and γ . This system is again shown below.

$$M = Ry'(\varphi, k) \tag{F.9}$$

$$l = \sqrt{x'(\varphi, k)^2 + y(\varphi, k)^2} \tag{F.10}$$

Also, this system is solved using the pre-programmed non-linear system solver 'fsolve' in MATLAB 2013.

The value of the applied moment M is determined for a range of values for R_n and θ to examine the bending stiffness as a function of deflection. The results are shown in figure 5.2 in chapter 4.

Inertia Properties of the Athlete

Numerous methods are available to estimate the moments of inertia and the center of mass for the human body, among others cadaver measurements, photogrammetry, ray scanning techniques, water displacement, and mathematical geometrical estimation of the body segments. The method used to determine the inertia properties of the athlete for the illustrative example shown in chapter 6 is the mathematical geometrical estimation method of [Moore et al. \(2009\)](#).

The human body of the athlete is modeled using simple geometric shapes. The name tin man is derived from tin cans that can be used to model human body. The arms and legs are divided into a lower and upper segment. The shape of the arms and legs are defined as cylinders. The torso is defined as a cuboid and the head as a sphere. The athlete is positioned as shown in figure [G.1](#). His legs are straight and his arms are stretched upward. Using this discretization, the body position can be described by fifteen grid points in a two dimensional space. The grid points mark the center of the sphere or the end points of the cylinders and the cuboid. The principle axes of the segments are orientated along the lines connecting the corresponding gridpoints. The grid points are also shown in figure [G.1](#). The global origin is chosen at the center of the line connecting both lower gridpoints of the lower leg segments.

The required anthropomorphic parameters to determine the physical properties of each segment have been measured by [Moore et al. \(2009\)](#) and are presented in table [G.1](#). All but one of the anthropomorphic parameters were measured when the test subject was standing casually on flat ground. The measurements were performed using basic tools. No special attention was paid to higher accuracy as the basic geometric shapes are already a large simplification. The definition of the segment lengths is also shown in figure [G.1](#). The circumferences were measured at the cross section where the circumference was maximum, for example around the biceps for the arms and over the nipples for the chest ([Moore et al., 2009](#)).

[Moore et al. \(2009\)](#) used the data from the cadaver study of [Dempster \(1955\)](#) for the mass of each segment. These are shown in table [G.2](#).

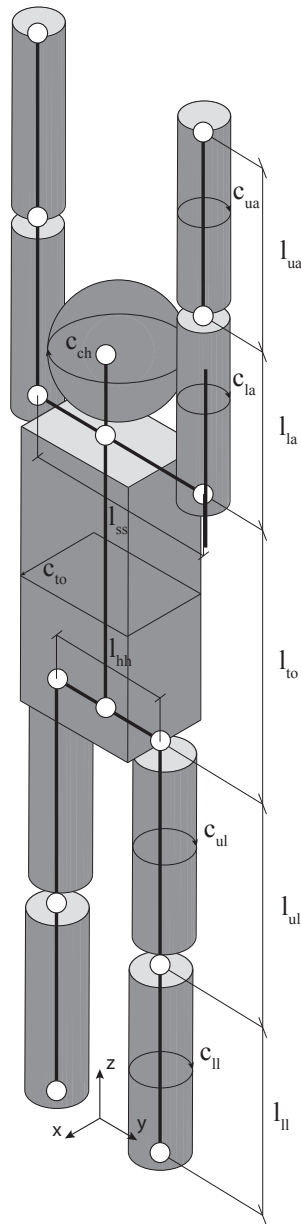


Figure G.1: Tin man

It is assumed that the mass is uniformly distributed over the segments such that the geometrical center is aligned with the center of mass. The center of mass of each segment is then located at the midpoint and can be calculated using the midpoint formula for the corresponding geometric shape. The center of mass for the whole body can be calculated using the following formula.

$$r_{Br} = \frac{\sum m_i r_i}{m_{Br}} \quad (\text{G.1})$$

Table G.1: Athlete Anthropomorphic Measurements (Moore, 2009)

Description	Symbol	Value	Unit
chest circumference	c_{ch}	0.94	m
head circumference	c_{ch}	0.58	m
hip joint to hip joint	l_{hh}	0.26	m
lower arm circumference	c_{la}	0.23	m
lower arm length	l_{la}	0.33	m
lower leg circumference	c_c	0.38	m
lower leg length	l_{ll}	0.46	m
shoulder to shoulder	l_{ss}	0.44	m
torso length	l_{to}	0.48	m
upper arm circumference	c_{ua}	0.30	m
upper arm length	l_{ua}	0.28	m
upper leg circumference	c_{ul}	0.50	m
upper leg length	l_{ul}	0.46	m

where r_i is the position vector to the centroid of each segment and m_i is the mass of each segment.

The local moment of inertia of each segment can be calculated using the moments of inertia equations for the corresponding geometrical shape. For a cylinder the moments of inertia are defined as follows.

$$\begin{bmatrix} I_x \\ I_y \\ I_z \end{bmatrix} = \begin{bmatrix} \frac{1}{2}m \left(\frac{3c^2}{4\pi^2} + l^2 \right) & 0 & 0 \\ 0 & \frac{1}{2}m \left(\frac{3c^2}{4\pi^2} + l^2 \right) & 0 \\ 0 & 0 & \frac{mc^2}{8\pi^2} \end{bmatrix} \quad (\text{G.2})$$

For a sphere the moments of inertia are defined as shown in the equation below.

$$\begin{bmatrix} I_x \\ I_y \\ I_z \end{bmatrix} = \begin{bmatrix} \frac{mc^2}{10\pi^2} & 0 & 0 \\ 0 & \frac{mc^2}{10\pi^2} & 0 \\ 0 & 0 & \frac{mc^2}{10\pi^2} \end{bmatrix} \quad (\text{G.3})$$

Table G.2: Body Mass and Segment Mass (Moore, 2009)

Segment	Symbol	Equation	Value	Unit
mass of athlete body	m_{Br}	N/A	72.0	kg
head	m_h	$0.068m_{Br}$	4.90	kg
lower arm	m_{la}	$0.022m_{Br}$	1.58	kg
lower leg	m_{ll}	$0.061m_{Br}$	4.39	kg
torso	m_{to}	$0.510m_{Br}$	36.72	kg
upper arm	m_{ua}	$0.028m_{Br}$	2.02	kg
upper leg	m_{ul}	$0.100m_{Br}$	7.20	kg

and for a cuboid the moment of inertia tensor is defined as shown below.

$$\begin{bmatrix} I_x \\ I_y \\ I_z \end{bmatrix} = \frac{1}{12}m \begin{bmatrix} l_y^2 + l_z^2 & 0 & 0 \\ 0 & l_x^2 + l_z^2 & 0 \\ 0 & 0 & l_x^2 + l_y^2 \end{bmatrix} \quad (\text{G.4})$$

Moore et al. (2009) defines the width of the cuboid for the torso as the shoulder width subtracted by the radius of the left and right upper arm.

$$l_y = l_{ss} - \frac{c_{ua}}{\pi} \quad (\text{G.5})$$

Furthermore, Moore et al. (2009) defines the cuboid thickness using the chest circumference and assuming the cross section of the chest is a stadium shape. This can be described by the equation below.

$$l_x = \frac{c_{ch} - 2l_y}{\pi - 2} \quad (\text{G.6})$$

Next, the parallel axis theorem can be applied to translate the local moments of inertia to the center of mass of the entire body.

$$I_i^* = I_i + m_i \begin{bmatrix} d_y^2 + d_z^2 & -d_x d_y & -d_x d_z \\ -d_x d_y & d_z^2 + d_x^2 & -d_y d_z \\ -d_x d_z & -d_y d_z & d_x^2 + d_y^2 \end{bmatrix} \quad (\text{G.7})$$

where d_x , d_y and d_z are the distances along the x , y , z axes between the segment center of mass and the center of mass of the whole body. The total moment of inertia \mathbf{I}_{Br} of the athlete is calculated by the summation of all the local translated moments of inertia.

$$\mathbf{I}_{Br} = \Sigma \mathbf{I}^* \quad (\text{G.8})$$

Appendix H

Maximum Internal Stress

In this appendix a first value of the maximum stress is calculated to determine if the pole can sustain the deformations happening during the vault as predicted by the mechanical model. The trajectory shown in figure 6.4 in chapter 6 is taken as an example.

Only considering bending the stress can be determined with the following equation.

$$\sigma = \frac{My}{I} \quad (\text{H.1})$$

The maximum stress occurs for the maximum internal moment M during the vault and for the distance furthest from the neutral axis. The maximum internal moment is achieved during the maximum curvature of the pole and is calculated in chapter 5. The maximum value is equal to 2700e3 [Nmm]. Pole vaulting poles typically have a symmetric circular cross-section with a wall thickness t of approximately 2 [mm]. Hence the neutral line lies in the middle and the furthest distance is equal to r . Hence $y = r$. The bending stiffness is 2522e6 [Nmm²]. Assuming a Young's modulus of 70 [GPa] for a carbon fibre pole, the area moment of inertia is equal

$$I = \frac{B}{E} \quad (\text{H.2})$$

Using the geometrical definition of the moment of inertia

$$I = \frac{\pi}{4}(r^4 - (r - t)^4); \quad (\text{H.3})$$

and substituting the values given above, the pole used in the illustrative example will have a radius of 18.8 [mm]. This is a realistic value. Most poles have an outer diameter of approximately 40 [mm].

Substituting the values into equation H.1 results in a maximum tensile stress of 1.2 [GPa] and a maximum compressive stress of 1.2 [GPa]. This is a high value and the pole will

most likely fail for this curvature. However, the ratio EI offers some room to reduce the maximum stress. Substituting a Young's modulus of glass-fibre of approximately 20 [Gpa] results in a maximum stress of 300 [MPa]. This is a feasible load the pole can sustain. The radius of the pole is then equal to 28 [mm] which is also still realistic. One can vary E and I accordingly to obtain the best design of the pole.

Appendix I

Inputs for Spring Added to Pole Results

The system properties for the results shown in chapter 7 for the pole where a spring is added to the length are shown in table I.1. The initial conditions used are shown in table I.2. The control torques are shown in figure I.1.

Table I.1: Athlete and Pole Properties

Symbol	Value	Unit	Symbol	Value	Unit
m_1	20	kg	K_{sp}	2100	N/m ²
m_2	50	kg	$l_{0,sp}$	0.7	m
I_1	2.96	kgm ²	L	4.57	m
I_2	5.67	kgm ²	B	2522	Nm ²
l_1	0.4	m	l_3	0.4	m
l_2	0.35	m			

Table I.2: Initial Conditions

Symbol	Value	Unit	Symbol	Value	Unit
x_{cm}	3.95	m	ϕ	0.4	rad
y_{cm}	1.75	m	θ	0	rad
\dot{x}_{cm}	-9.32	m/s	$\dot{\phi}$	0.2	rad/s
\dot{y}_{cm}	1.2	m/s	$\dot{\theta}$	0	rad/s

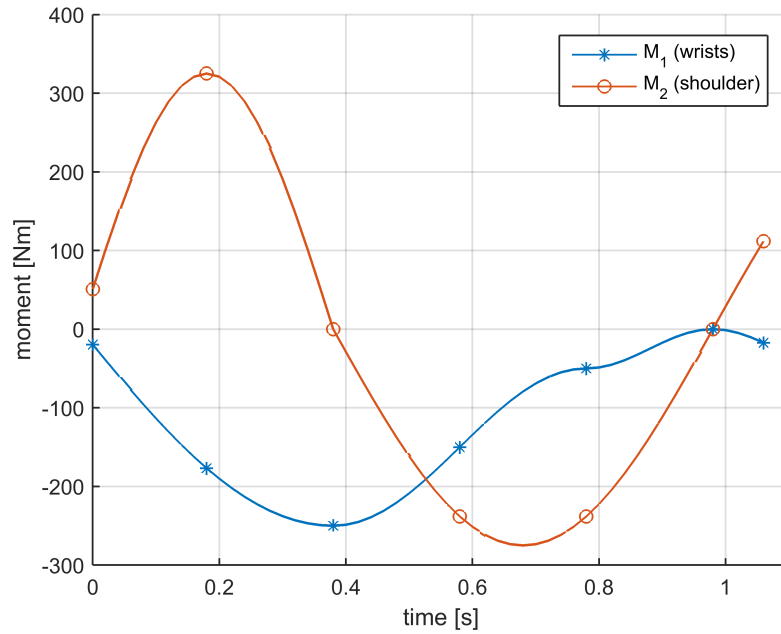


Figure I.1: The control torques M_1 (wrists) and M_2 (shoulder) during a vault for the results of a vault using a pole to which a spring is added that resulted in a realistic vault for the mechanical model of a massless pole and two-segment athlete. The time is defined from take-off until pole release.